Department of Applied Physics

# Universal relations in ultracold polarized Fermi gases

Elmer V. H. Doggen

Aalto University

DOCTORAL DISSERTATIONS

Aalto University publication series
**DOCTORAL DISSERTATIONS** 72/2015

# Universal relations in ultracold polarized Fermi gases

**Elmer V. H. Doggen**

A doctoral dissertation completed for the degree of Doctor of Science (Technology) to be defended, with the permission of the Aalto University School of Science, at a public examination held at the lecture hall M1 (Otakaari 1, Espoo) of the school on the 10th of July 2015 at 12 o'clock noon.

**Aalto University**
**School of Science**
**Department of Applied Physics**
**Quantum Dynamics**

**Supervising professor**
Prof. Päivi Törmä

**Thesis advisor**
dr. Jami J. Kinnunen

**Preliminary examiners**
Prof. Robert van Leeuwen, University of Jyväskylä, Finland
dr. Pietro A. Massignan, ICFO - The Institute of Photonic Sciences, Spain

**Opponent**
dr. Carlos Lobo, University of Southampton, United Kingdom

Aalto University publication series
**DOCTORAL DISSERTATIONS** 72/2015



ISBN 978-952-60-6215-0 (printed)
ISBN 978-952-60-6216-7 (pdf)
ISSN-L 1799-4934
ISSN 1799-4934 (printed)
ISSN 1799-4942 (pdf)
http://urn.fi/URN:ISBN:978-952-60-6216-7

Unigrafia Oy
Helsinki 2015

Finland

441 697
Printed matter

Aalto University

# Abstract

Aalto University, P.O. Box 11000, FI-00076 Aalto www.aalto.fi

**Author**
Elmer V. H. Doggen

**Name of the doctoral dissertation**
Universal relations in ultracold polarized Fermi gases

**Publisher** School of Science

**Unit** Department of Applied Physics

**Series** Aalto University publication series DOCTORAL DISSERTATIONS 72/2015

**Field of research** Engineering Physics

**Manuscript submitted** 11 March 2015 **Date of the defence** 10 July 2015

**Permission to publish granted (date)** 28 April 2015 **Language** English

☐ **Monograph** ☒ **Article dissertation (summary + original articles)**

**Abstract**

Ultracold quantum gases are an ideal toolbox for simulating complex condensed or nuclear matter systems and to investigate fundamental quantum properties of matter. In this thesis, we will investigate universal properties connecting the high-momentum tail of the momentum distribution, the short-range correlations and the thermodynamics, encapsulated in Tan's relations. These relations are especially useful in the strongly interacting case, where perturbative approaches usually fail. With the aid of Tan's universal relations, we can still come to general conclusions about strongly interacting quantum gases. In particular, the momentum distribution exhibits a characteristic algebraic decay, unlike the exponential decay of the non-interacting case.

The main focus in this thesis is on the one-dimensional, fermionic case, where we study the highly polarized case (the one-dimensional Fermi polaron), verifying Tan's relations using a variety of theoretical tools. In addition, we show that localized systems exhibit a universal, dynamical instability to delocalization when a short-range interaction between particles is switched off rapidly. This delocalization process relies on the algebraic decay of the momentum distribution, which guarantees that at least some of the delocalized single-particle states are occupied with a finite probability. Finally, we investigate the Bardeen-Cooper-Schrieffer (BCS) to Bose-Einstein condensation (BEC) crossover for the three-dimensional Fermi gas and develop a novel method to describe the breakdown of the Fermi liquid description in the vicinity of the critical temperature for superfluidity, in good agreement with a recent experiment.

**Keywords** ultracold atoms, quantum gases, one-dimensional systems, Tan relations, Fermi polaron, quench dynamics, disordered systems, localization properties, BCS/BEC crossover, Brueckner-Goldstone theory

**ISBN (printed)** 978-952-60-6215-0 **ISBN (pdf)** 978-952-60-6216-7

**ISSN-L** 1799-4934 **ISSN (printed)** 1799-4934 **ISSN (pdf)** 1799-4942

**Location of publisher** Helsinki **Location of printing** Helsinki **Year** 2015

**Pages** 160 **urn** http://urn.fi/URN:ISBN:978-952-60-6216-7

# Preface

If you have reached this point in my thesis, congratulations! You have come further than most. This thesis is the culmination of work spanning the period of September 2011 to May 2015. Many people who hold doctoral degrees themselves have often told me how stressful they found their time as a PhD student. I am not certain whether it is due to my pathologically stoic character, the relaxed atmosphere in the research group of prof. Päivi Törmä or the easy-going leadership style of my supervisor dr. Jami Kinnunen, but I do not recall any moment of stress during my studies and research at all. While my research has not culminated in the Nobel Prize that we were aiming for, I suppose I just enjoy doing research.

At this point I believe it is customary[1] to acknowledge everyone who contributed to my research and the working atmosphere in general. So as not to risk hurting anyone's feelings, I will just thank everyone who would like to be thanked, with a special thanks for those who deserve to be thanked. In particular, I am thankful to my girlfriend for putting up with me. I should also thank Jami, who always had time for some relaxing death metal concerts after work. Finally, I am grateful to my parents for providing a non-traumatic childhood and to my cats for inspirational meowing.

In this thesis, I have tried to focus mainly on the relevant physics, and less so on the details of mathematical derivations or the numerical methods employed. Nevertheless, I have included some detailed calculations in cases where I felt this added to physical insight. There is a variety of topics discussed; I have attempted (and most likely failed) to create a coherent whole, connecting the different parts through the basic, fundamental physics.

[1] Defying J. S. Mill's advice.

Espoo, Finland, May 8, 2015,

Elmer V. H. Doggen

# Contents

# List of Publications

This thesis consists of an overview and of the following publications which are referred to in the text by their Roman numerals.

**I** Elmer V. H. Doggen and Jami J. Kinnunen. Energy and contact of the one-dimensional Fermi polaron at zero and finite temperature. *Physical Review Letters*, 111, 025302, July 2013.

**II** Elmer V. H. Doggen, Anna Korolyuk, Päivi Törmä and Jami J. Kinnunen. One-dimensional Fermi polaron in a combined harmonic and periodic potential. *Physical Review A*, 89, 053621, May 2014.

**III** Elmer V. H. Doggen and Jami J. Kinnunen. Quench-induced delocalization. *New Journal of Physics*, 16, 113051, November 2014.

**IV** Elmer V. H. Doggen and Jami J. Kinnunen. Momentum-resolved spectroscopy of a Fermi liquid. *Scientific Reports*, 5, 9539, May 2015.

# Author's Contribution

**Publication I: "Energy and contact of the one-dimensional Fermi polaron at zero and finite temperature"**

The author performed a significant part of the analytical calculations, most of the numerical calculations and was the main author of the manuscript.

**Publication II: "One-dimensional Fermi polaron in a combined harmonic and periodic potential"**

The author performed a significant part of the analytical calculations pertaining to the variational method, wrote the code to calculate the solution for the variational method and was the main author of the manuscript.

**Publication III: "Quench-induced delocalization"**

The author conceived the idea, performed the numerical simulations and most of the calculations and was the main author of the manuscript.

**Publication IV: "Momentum-resolved spectroscopy of a Fermi liquid"**

The author contributed to numerical and analytical calculations and wrote a significant part of the manuscript.

# 1. Ultracold quantum gases

This thesis will discuss ultracold quantum gases. What's an ultracold quantum gas[1]? First of all, it's ultracold. Furthermore, it's quantum. Finally, it's a gas.

If that doesn't explain everything, let us take a closer look at *ultracold*. The temperature is connected to the *quantum* part in the sense that, generally speaking, the size of the region where a particle is likely to be found increases as the temperature decreases. This means that very cold particles cannot be accurately described as (classical) point particles, and we must employ the tools of quantum physics to describe such particles. We can quantify this transition from "classical" to "quantum" behaviour for a massive particle in terms of the thermal de Broglie wavelength $\Lambda_T$:

$$\Lambda_T = \frac{h}{\sqrt{2\pi m k_B T}}. \tag{1.1}$$

Here $h \approx 6.62 \times 10^{-34}$ Js is the Planck constant, $m$ is the mass of a particle, $k_B \approx 1.38 \times 10^{-23}$ JK$^{-1}$ is the Boltzmann constant and $T$ is the temperature. The important aspect of this formula is that as $T$ is reduced, the de Broglie wavelength $\Lambda_T$ increases. Therefore, at very low temperatures a group of particles (e.g., a cloud of atoms) will tend to overlap in the sense that the average inter-particle distance of the particles $d$ is of the same order or smaller than $\Lambda_T$. When this happens (for sufficiently high density and/or sufficiently low temperature), various interesting phenomena occur, provided the particles are indistinguishable.

The density brings us to the "gas"-aspect of quantum gases. In this context, we simply mean that the density of our cloud of atoms is low (that is, $d$ is large) compared to usual solids or liquids and more comparable to that of a gas. At this point, a hypothetical astute reader might remark

[1] I have tried writing a more or less non-technical introduction to the general topic. The reader who is familiar with quantum gases might want to consider skipping this chapter and continuing in the next chapter.

that we have just said that $d$ must be *small* compared to $\Lambda_T$. The reason why we are interested in quantum *gases* is that most types of matter will tend to solidify if you cool them down. That's nice if you want some ice cubes, but not what we are looking for in the experiment. Solids are much more complicated and much less controllable than gases, and what we would like to do is investigate the fundamental properties of matter in systems which are as simple and controllable as possible. The trade-off between requiring on the one hand low densities in order to avoid solidification, and on the other hand sufficiently high densities in order to reach the "quantum" regime, is precisely why it is extremely difficult to create such ultracold quantum gases. This is why we need *ultracold* temperatures to create a quantum gas. How cold is ultracold? It turns out that we need temperatures on the order of about a millionth of a degree above absolute zero.

## 1.1 A brief history of quantum gases

Historically, the first realization of a situation where the thermal de Broglie wavelength becomes sufficiently large in the laboratory was the - rather unexpected, at the time - discovery of superconductivity of mercury by Kamerlingh Onnes in 1911 [1]. Superconductivity is, simply speaking, the disappearance of resistance to the conduction of electrical current in a material. Many different metals are superconducting below a certain *critical temperature*, which varies from metal to metal. For instance, mercury has a critical temperature of about 4.2K. Currently, the highest critical temperature observed for superconductors is approximately 138K, significantly above absolute zero, but still far below the freezing point of water. These *high-temperature superconductors* are not made of metals, but of so-called "cuprates", a certain class of ceramic materials. The theoretical description of superconductivity eluded scientists for a long time, but a major breakthrough was achieved in 1957 by Bardeen, Cooper and Schrieffer, who published the now-famous BCS-theory of superconductivity [2]. Unfortunately, while BCS theory adequately describes "simple" low-temperature (on the order of 5-10K) superconductors, it fails to explain superconductivity in cuprates. A comprehensive theory that successfully explains high-temperature superconductivity is, to date, still lacking.

Incidentally, Kamerlingh Onnes also produced *superfluid* helium, al-

though he did not realize its significance at the time, and it was not until 1937 that the properties of the superfluid phase were characterized by Kapitsa [3], Allen and Misener [4]. A superfluid is similar to a superconductor in some ways, but whereas a superconductor has zero electrical resistance, a superfluid has zero resistance to *mechanical* flow, i.e. zero viscosity.

While superconductors and superfluid helium are essentially *quantum* systems not adequately described by classical physics, they are not quantum *gases*. To see how they are connected, we go back a small step in time to predictions made by Einstein and Bose in 1924-25 [5, 6, 7]. Empirically, we know that there are two kinds of particles in the universe, which we call *bosons* and *fermions* (they aren't all the same, but they all go in one of the two categories). At high temperatures (in the sense discussed above, i.e. at inter-particle distances much larger than $\Lambda_T$) the two are essentially indistinguishable and we can describe both of them using Maxwell-Boltzmann statistics developed in the 19$^{\text{th}}$ Century. As the temperature is reduced, the quantum nature of matter becomes evident, and one must forgo classical physics and the associated Maxwell-Boltzmann statistics. Instead, we must use *Bose-Einstein* statistics for bosons, and *Fermi-Dirac* statistics for fermions. What Bose and Einstein showed is that if you take some bosons and cool them down sufficiently, they will form a new phase of matter, a *Bose-Einstein condensate*. In this state, (almost) all of the particles occupy the lowest energy state of the system. By this time, the astute reader realizes what kind of temperature we need: a temperature such that $\Lambda_T$ is larger than the average distance between the bosons.

In turns out that it is pretty difficult to achieve such low temperatures with "ordinary" matter (i.e. atoms). In fact, it took about 70 years before this feat was finally achieved in 1995 with the Bose-Einstein condensation of rubidium [8] and sodium [9] atoms, for which Cornell, Wieman and Ketterle received the 2001 Nobel Prize in physics. The cloud of atoms is placed in a vacuum chamber (so the atoms don't just stick to oxygen or nitrogen molecules in the air) and held in place using lasers. At the same time, the lasers are also used to cool down the atoms (we won't go into the details of how this works; the interested reader is referred to Ref. [10]).

In the case of fermions, one can perform similar tricks and achieve an ultracold gas of fermions. Although this kind of system is also very interesting, it lacks the fancy name and is just called a *degenerate Fermi*

*gas* [11]. The crucial difference between a degenerate Fermi gas and a Bose-Einstein condensate is that in the case of fermions, the Pauli exclusion principle prevents the accumulation of particles in the lowest energy state of the system. So instead of (almost) all of the particles occupying the lowest energy state, there can be only one particle for each energy state.

## 1.2 So... what can one do with quantum gases?

Creating such a trapped cloud of ultracold atoms is not just impressive, but also useful. The key point is that while these ultracold atoms have an internal structure (they consist of quarks, electrons, etc.), their internal structure is not all that important when describing them in the context of quantum gases. The de Broglie wavelength $\Lambda_T$ of the atoms and the inter-particle spacing $d$ are much larger than the internal features of the atoms, so that in many respects, the atoms can be regarded as idealized, point-like bosons and fermions. This makes quantum gases an ideal testbed for investigating fundamental physics, because it allows us to say something general about nature using the (rather artificial) setting of atoms surrounded by tubes and mirrors.

On the other hand, while the internal structure of the atoms is not important for the quantum statistics of the ensemble, it can be exploited by correctly tuning the lasers to not only cool down the atoms, but also to change the interactions between the atoms using Feshbach resonances [12]. In addition, we can not only tune the magnitude of the inter-particle interactions, but we can tune the character of inter-particle interactions. For instance, it is possible to use atoms with a permanent dipole moment, such as chromium [13], and recently it has even become possible to use polar molecules with a tunable dipolar moment in the quantum regime [14].

In addition to using different kinds of atoms for our experiments, we can tune the lasers that trap the atoms so that we create effective potentials that can be changed almost at will. This allows us to use harmonic potentials, but one can also create periodic potentials that mimic lattices in solid state materials – *optical lattices* [15]. These optical lattices can be used to recreate simple models such as the Hubbard model in the laboratory, allowing for instance the observation of the Mott insulator state [16]. By using random potentials we can mimic the appearance of disorder in

nature [17], leading to the observation of Anderson localization [18] in an ultracold atomic gas [19, 20]. We can also change the dimensionality of the system by "squeezing" the cloud of atoms in one or more directions, thus obtaining (quasi-) two- or one-dimensional systems. In addition, we can also look at *polarized* systems, i.e. systems consisting of two components where one component greatly outnumbers the other [21].

The broad scope of what we can do with quantum gases also means that theoretical methods and models will vary greatly depending on the particular thing we might be interested in. In this thesis, we will (for the most part) focus on fermions (for the most part) interacting through short-range interactions in (for the most part) one dimension. We will consider various types of trapping potentials, from none at all to harmonic traps, square traps, periodic traps and disordered systems.

# 2. Tan's universal relations

In this chapter, we will consider whether or not we can say something general about interacting quantum systems. By interacting we mean that the particles "feel" each other in some way beyond the effects of quantum statistics (the particles being either fermions or bosons). In other words, there is some kind of force between the particles, such as gravity[1], Coulomb forces due to the effects of electric charges, van der Waals forces, and so on.

Now, let us consider some cloud of non-interacting fermions. From elementary quantum physics we know that the fermions, due to the Pauli exclusion principle, cannot occupy the same state. We obtain the Fermi-Dirac distribution, depicted in Figure 2.1 for zero as well as finite temperature as a function of the momentum of a particle. At zero temperature, the system is found in the state with the lowest energy, which just consists of $N$ particles occupying the $N$ lowest available energy states, which then all have unity probability of being occupied. The highest energy state is occupied at some momentum $k_F = (6\pi^2 N/V)^{1/3}$ (the Fermi momentum), which depends on the density $N/V$ of the system with volume $V$. At non-zero temperature, some of the states beyond the Fermi momentum are occupied, and the total energy increases.

Now it would be useful if we could extend this idea to a system with arbitrary inter-particle interactions. Consider a cloud of fermions that can exist in two "spin"[2] states $\uparrow$ and $\downarrow$. The $\uparrow$ and $\downarrow$-particles do not interact with themselves (apart from the Pauli exclusion principle), but there is some interaction $V_{\text{int}}$ between the particles that depends on the distance

[1] In most cases, however, the effects of gravity can be neglected in the context of an ultracold atom experiment.

[2] These states don't actually have to be different spin states. Here the notation is used to signify that the $\uparrow$ and $\downarrow$-particles are distinguishable. Usually, these states are different hyperfine states of a certain atomic species.

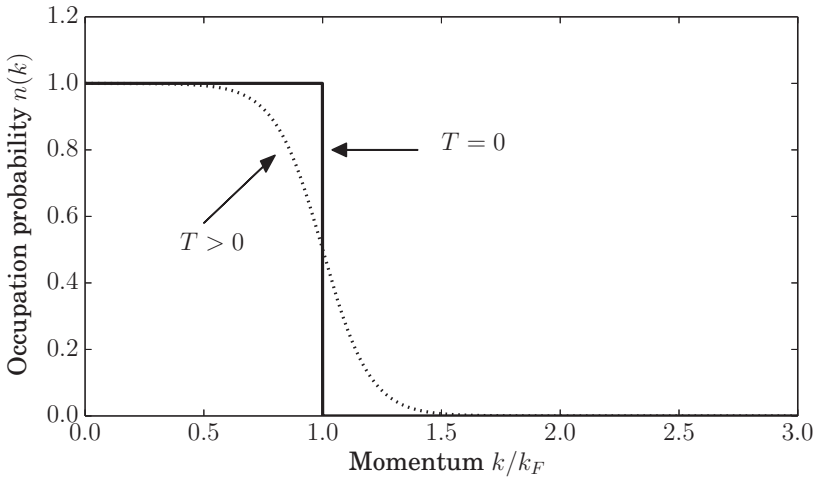


**Figure 2.1.** The momentum distribution of a non-interacting Fermi gas for zero temperature $T$ and at some finite temperature, as a function of the momentum $k$ normalized by the Fermi momentum $k_F$.

between them:

$$V_{\text{int}} = V_{\text{int}}(|\mathbf{r} - \mathbf{r}'|), \tag{2.1}$$

where $\mathbf{r}$ and $\mathbf{r}'$ indicate the respective positions of the particles.

Unfortunately, there isn't a great deal we can say about such an arbitrarily interacting system. The interactions might take a myriad of different forms, affecting the momentum distribution of the Fermi gas in potentially unexpected ways. However, as it turns out, we can say something about the *asymptote* of the momentum distribution for high momenta, under the condition that the inter-particle interactions are *short-ranged*. By short-ranged we mean that there is some distance, say $r_0$, beyond which the interaction between the particles is effectively negligible. The distance $r_0$ must be "short" in the sense that it is much smaller than other relevant length scales in the problem under consideration. For systems described by short-ranged interactions, we can introduce the (s-wave) *scattering length* $a$, which is a measure of the strength of the inter-particle interactions. Tan showed in a series of papers written in 2005 and published in 2008 [22, 23, 24] that the asymptote of the momentum distribution is then given by:

$$n(k) \to \frac{C}{k^4}, \quad (k \to \infty) \tag{2.2}$$

where the quantity $C$ is called the *contact parameter* or simply *contact*. Given our short-range interactions, we thus obtain a momentum distribution looking more like the one depicted in Figure 2.2. Note that the actual

strength of the tail in the momentum distribution (given by the contact parameter $C$) as well as the momentum for which the asymptotic regime is reached depend on the specifics of the system. However, the asymptotic behaviour is otherwise completely general and only breaks down for momenta on the order of the inverse range of the interactions $r_0^{-1}$. We can therefore identify the following regime where the asymptotic relation (2.2) holds:

$$\mathcal{L}^{-1} \ll k \ll r_0^{-1}, \tag{2.3}$$

where $\mathcal{L}$ is any relevant length scale in the system. In many cases, such as for example homogeneous systems and strongly interacting systems (at unitarity), $\mathcal{L}^{-1}$ is simply equal to the aforementioned Fermi momentum $k_F$. The full momentum distribution for a homogeneous three-dimensional Fermi gas in the strongly interacting limit was computed in Publication IV.

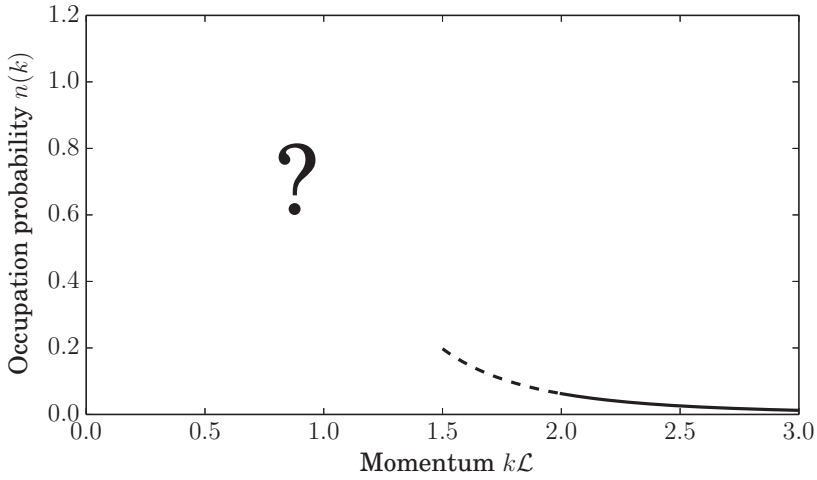


**Figure 2.2.** The momentum distribution of a short-range interacting Fermi gas, as a function of the momentum $k$ normalized by a characteristic length scale $\mathcal{L}$. The crossover to the asymptotic regime occurs when $k \gg \mathcal{L}^{-1}$, where $\mathcal{L}$ is any physically relevant length scale in the system.

Tan showed that the asymptotic momentum distribution (2.2) holds for a homogeneous (that is, untrapped) three-dimensional Fermi gas, and later extended his work to trapped fermionic systems [25]. It was actually already previously shown, in 2003, that interacting one-dimensional bosons have a similar asymptotic momentum distribution [26, 27]. Indeed, as it turns out, Eq. (2.2) is valid for *any* short-ranged interacting system. After Tan's set of seminal papers was published, the Tan relations were generalized to one-dimensional homogeneous Fermi gases [28] (the most relevant

case for the present discussion) and two-dimensional Fermi gases [29]. In the case of bosons, three-body collisions often play an important role, and one can introduce a *three-body contact* in analogy to Tan's two-body contact [30, 31], that decays according to a $1/k^5$ tail rather than the $1/k^4$ tail of the two-body contact (2.2).

The usefulness of the contact lies primarily in the fact that strongly interacting systems are very difficult to describe theoretically, yet are ubiquitous in nature. Therefore, Tan's contact gives us some grasp on these systems by providing exact results, albeit asymptotic ones. Tan's universal relations are valid at any polarization (relative population of the $\uparrow$ and $\downarrow$ states), at any phase (e.g. superfluid) and at any interaction strength. They are also valid at any temperature; the dependence of the contact on temperature has been investigated in for example Refs. [32, 33], and usage of the virial theorem provides results for the high-temperature asymptote of the contact [34, 35]. In our own work, we have determined the contact for the highly polarized one-dimensional Fermi gas in Publication I, where we also investigated the temperature dependence of the contact in this system. In Publication II and Publication III, we rely on the qualitative features of the contact in the sense that the existence of the slowly decaying high-momentum tail influences the physics of the systems considered in these publications. Furthermore, in Publication IV we compute the contact for a strongly interacting, spin-balanced three-dimensional system.

## 2.1 Physical meaning of the contact

As it turns out, the contact parameter $C$ has an intuitive interpretation [36]. To see this, consider the density-density correlator of the densities of the two different spin species ($n_\uparrow$ and $n_\downarrow$), separated by a distance $\mathbf{r}$ (we assume a homogeneous system):

$$\langle n_\uparrow(\mathbf{r}) n_\downarrow(0)\rangle \to \frac{\mathcal{C}}{16\pi^2 r^2}, \tag{2.4}$$

valid at small distances $\mathbf{r}$. Here $\mathcal{C}$ is the *contact density*, which is related to the contact as follows:

$$C = \int d^3\mathbf{r}\, \mathcal{C}(\mathbf{r}). \tag{2.5}$$

In a homogeneous system, the contact density does not depend on $\mathbf{r}$ and the contact and the contact density are related through a simple constant conversion factor. What the density-density correlator tells us is that the

probability that we find two particles at very *short* distances from each other is proportional to the contact. Thus, it is a measure of finding particles in close proximity as a result of the interactions between them. Indeed, for non-interacting systems the contact is always zero. Recently, the contact was also investigated theoretically near phase transitions [37].

## 2.2 Other Tan relations

In addition to the asymptote of the momentum distribution (2.2), Tan derived numerous other relations connecting the momentum decay to short-range correlations, energy, entropy and pressure [36]. In this thesis, we won't need most of these relations, but we will mention just one more.

*The adiabatic theorem* — a change in energy $E$ due to a change in the scattering length $a_{3\mathrm{D}}$ is related to the contact as:

$$\Big(\frac{dE}{da_{3\mathrm{D}}^{-1}}\Big)_S = -\frac{\hbar^2}{4\pi m}C, \tag{2.6}$$

where the derivative is determined with fixed entropy $S$ and the mass of a particle is $m$. The one-dimensional analog of this equation, with the one-dimensional scattering length $a$, is [28]:

$$\Big(\frac{dE}{da}\Big)_S = -\frac{\hbar^2}{4\pi m}C. \tag{2.7}$$

Note how the dependence on the scattering length is different from the three-dimensional case. This is because of effects related to the production of one-dimensional systems in the experiment [38]; in one dimension, the interactions become *weaker* as the one-dimensional scattering length $a$ is increased, while for three-dimensional systems a higher three-dimensional scattering length $a_{3\mathrm{D}}$ implies stronger interactions. To see how this follows, consider a three-dimensional system, where a strongly confining harmonic potential with oscillator length $a_\perp$ is applied in two of the three dimensions. If this confining potential is strong enough, we can to a good approximation assume that the particles are confined to the ground state of the harmonic oscillator in the perpendicular directions. One can now derive the one-dimensional scattering length [38]:

$$a = -\frac{a_\perp^2}{2a_{3\mathrm{D}}}\Big(1 - A\frac{a_{3\mathrm{D}}}{a_\perp}\Big), \tag{2.8}$$

where the constant $A \approx 1.4603...$. If the inter-particle interactions are of exactly zero range, we can write the inter-particle potential as:

$$V_{\mathrm{int}}(x - x') = g\delta(x - x'), \tag{2.9}$$

where $\delta(x - x')$ is the Dirac delta function, and the interaction parameter $g$ is related to $a$ as:

$$g = \frac{-2\hbar^2}{ma}. \tag{2.10}$$

Note that for a particular choice of the ratio $\frac{a_{3D}}{a_\perp}$ the scattering length $a$ vanishes, and consequently the interaction strength $g$ diverges. This is known as a *confinement-induced resonance* [39], in analogy with a Feshbach resonance.

## 2.3 Experimental determination of the contact

After Tan's publications, numerous experimental groups successfully verified the Tan relations in the experiment [40, 41]. In addition, researchers at JILA, Colorado measured the contact for a homogeneous Fermi gas [42] and for an atomic Bose-Einstein condensate [43]. Recently, researchers also succeeded in measuring the contact as a function of time in a dynamically changing system [44]. One of the uses of the experimental determination of the contact is that it allows experimental verification of different theories used in the strongly interacting regime. These theories tend to differ significantly in their predictions for the contact at unitarity (that is, when the scattering length diverges to infinity). However, the experiment [43] was not able to clearly identify a "best" theory. In Publication IV, we have developed a theory that predicts a contact parameter in good agreement with experimentally determined values.

Outside the field of ultracold atoms, the contact parameter has recently been found to be applicable to nuclear matter as well [45, 46]. This is a remarkable demonstration of the universality of Tan's relations, given that the density of nuclear matter and that of a dilute quantum gas differ by many orders of magnitude.

# 3. Fermi gases and the Fermi polaron

In this chapter, we will take a closer look at interacting fermions, the theoretical tools at our disposal to describe them, and the connection to Tan's contact parameter (2.2). We start by considering the highly spin-imbalanced Fermi gas, also referred to as the Fermi polaron or the "impurity problem." This means that we take just one particle (an impurity) of a certain kind (say $\downarrow$) and have it interact with many $\uparrow$-particles. It turns out that this system behaves, in certain respects, qualitatively differently from the spin-balanced case (where the number of $\downarrow$- and $\uparrow$-particles is equal).

Such highly spin-imbalanced systems are of interest because in nature one often encounters a small disturbance to a system, and it is then useful to investigate how this disturbance (the impurity) affects the system as a whole. Since the impurity $\downarrow$ may be interacting with all of the $\uparrow$ particles at the same time, this is not a trivial problem. Furthermore, spin-imbalanced systems are predicted to exhibit the so-called Fulde-Ferrell-Larkin-Ovchinnikov (FFLO) phase [47, 48], a novel superconducting phase that differs from "ordinary" superfluidity in that the fermion pairs that condense have finite momentum and the order parameter is spatially inhomogeneous.

In our work, we will focus on the one-dimensional case, that is, the particles are free to move only along a line, and movement in the other directions is suppressed. We consider interactions between the $\uparrow$ and $\downarrow$ particles that are described by the inter-particle potential $V_{\text{int}} = V_{\text{int}}(|x - x'|)$, where $x$ and $x'$ represent the positions of the particles. The Hamiltonian $\mathcal{H}$ of such a system is given by:

$$\begin{aligned}\mathcal{H} = &\sum_{\sigma} \int dx\, \psi_\sigma^\dagger(x) \Big[ -\frac{\hbar^2}{2m}\frac{d^2}{dx^2} + V_{\text{ext}}(x) \Big] \psi_\sigma(x) \\ &+ \iint dx dx'\, \psi_\uparrow^\dagger(x)\psi_\downarrow^\dagger(x') V_{\text{int}}(|x-x'|)\psi_\downarrow(x')\psi_\uparrow(x),\end{aligned} \tag{3.1}$$

Here $V_{\text{ext}}$ is the external trapping potential, the generalized spin $\sigma = \{\uparrow, \downarrow\}$ and we assume for simplicity that the mass $m$ is equal for both spin species. In the simplest possible case, the external potential $V_{\text{ext}} = 0$ and the inter-particle interactions take the following form:

$$V_{\text{int}}(x - x') = g\delta(x - x'), \tag{3.2}$$

where $g$, which is inversely proportional to the one-dimensional scattering length $a$, measures the strength of the interactions and $\delta(x - x')$ is the Dirac delta function. When the inter-particle potential is given by (3.2), we are said to have so-called *contact interactions*. In three dimensions, the delta function potential is not well-behaved and leads to an ultraviolet divergence, necessitating the use of a pseudopotential [49]. However, in one dimension, the delta function potential is properly defined. The use of such a potential is mathematically convenient, since it means that the double integral in (3.1) becomes a single integral. More importantly, it is also physically realistic in the case that the interactions are only of short range and the Fermi gas under consideration is dilute.

In the language of the previous chapter, the use of a contact potential means that the range $r_0$ of the inter-particle potential is exactly zero. This also means that the asymptotic momentum distribution (2.2) is valid for all $k \gg \mathcal{L}^{-1}$. Therefore, we should expect to find physics related to the contact parameter in systems described by such interactions. This is indeed the case, as we show in all the publications in this thesis.

Note that in the literature, a distinction is sometimes made between the Fermi polaron and the impurity problem in general, see for instance the review articles Refs. [50, 51, 52]. A *polaron* is a fermionic quasiparticle that occurs in higher (than one) dimensions, consisting of an impurity dressed by the interactions with the bath of majority component particles. For strongly attractive interactions, a transition occurs where the impurity forms a bosonic dressed molecule or *dimeron* with one of the particles from the bath [53, 54, 55, 56]. Strictly speaking, these quasiparticle descriptions break down in one dimension, as the quasiparticle residue vanishes due to the Anderson orthogonality catastrophe [57]. However, the same techniques employing the quasiparticle polaron description appear to work well even in one dimension. Hence, we will make no such distinction in this work and use the terms *Fermi polaron* and *impurity problem* (at arbitrary sign and strength of inter-particle interactions) interchangeably.

### 3.1 Chevy's variational Ansatz

A convenient and intuitive method to compute ground state properties of the Fermi polaron problem was developed by Chevy in a 2006 paper [58]. The idea, which was originally formulated for a homogeneous ($V_{\text{ext}} = 0$) three-dimensional system, goes as follows. Consider the non-interacting system at zero temperature. The fermions will now occupy the lowest $N$ states available, while the impurity occupies the lowest state. Now, if the impurity and the $N$ fermions are interacting, we cannot say *a priori* how the particles will be distributed. If we consider at most $M$ ($M > N$) states and place no further restriction on which states can be occupied by the particles, the Hilbert space spans $(M-N)!/N!$ states (assuming $N \gg 1$), which is usually a very large number.

Instead, we make the following assumption (which turns out to be a reasonable one): at most one particle from the sea of fermions can be excited to a different state. In other words, we restrict the number of particle-hole excitations to one. We can then write the Ansatz for the wave function $|\Psi\rangle$ in the following general form [59][1] (recall that the impurity is denoted by $\downarrow$ and the majority component fermions by $\uparrow$):

$$|\Psi\rangle = \sum_l \phi_l c_{\downarrow l}^\dagger |0\rangle + \sum_{mkn} \phi_{mkn} c_{\uparrow m}^\dagger c_{\uparrow k} c_{\downarrow n}^\dagger |0\rangle. \tag{3.3}$$

Here $|0\rangle$ denotes the undisturbed Fermi sea, i.e., the $N$ fermions located in the $N$ lowest available states, and the operator $c_{\sigma k}^{(\dagger)}$ destroys (creates) a particle in the state $k$ with spin $\sigma$. The coefficients $\phi_l$ and $\phi_{mkn}$ are variational coefficients, which are to be determined through a calculation, and depend on the specifics of the problem at hand, such as the strength of the inter-particle interactions $g$ and whether an external potential is present. The first term in equation (3.3) describes the impurity in one of the states $l$, while the majority component Fermi sea is undisturbed. Meanwhile, the second term describes a process where one of the fermions in one of the states $k$ (below the Fermi sea) is excited to a state $m$ (above the Fermi sea) and the $\downarrow$-particle is in a state $n$. We depict this schematically in Figure 3.1

In principle, any basis can be used for the states $l, m, k, n$. For a homo-

[1] Chevy's original form of the Ansatz considers a polaron in a fixed momentum state. This notation is convenient for a homogeneous system, where the interaction takes a simple constant form in momentum space, and the states with fixed momentum are eigenstates of the system. However, this is no longer the case if an external potential is present.

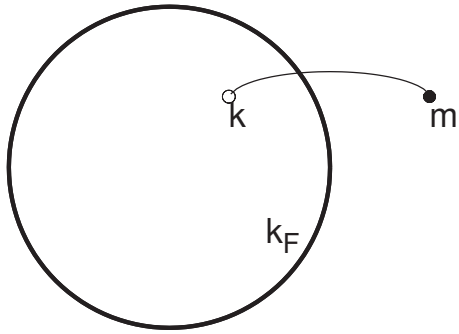


**Figure 3.1.** Schematic depiction of a particle-hole excitation. A particle in a state $k$, below the Fermi surface, is excited to a different state $m$ beyond the Fermi surface. This creates a hole in the state $k$. In the one-dimensional case, the "Fermi surface" consists of two points on a line located at $\pm k_F$.

geneous system, the momentum basis is a good choice, but in our work, Publication II and Publication III, an external potential is present. In this case, a more convenient choice is to use the single-particle eigenbasis of the system. When using the real-space single-particle eigenbasis of the system, we will also refer to the variational Ansatz as the real-space variational Ansatz (RSVA) to distinguish it from the momentum-space formulation. For an arbitrary external potential, the eigenbasis can be obtained numerically using for instance LAPACK [60].

The ground state properties of the Fermi polaron system can now be obtained by computing the expectation values of observables. For instance, the ground state energy follows from the expectation value $\langle\Psi|\mathcal{H}|\Psi\rangle$. Details of this calculation are given in the appendix of Publication II and are discussed further for a specific case in Chapter 5. Chevy's Ansatz has been applied to various highly polarized systems; the original work was extended to a systematic study of the homogeneous three-dimensional Fermi polaron [61]. Furthermore, it has been extended to a one-dimensional system, also taking into account the correction due to including two particle-hole excitations and showing that this correction is small [62]. Other applications include the study of two-dimensional [63] and mass-imbalanced [64] systems, the extension of the variational wave function to bound dimers in the attractive regime [53, 54, 55, 56], extensions to various external traps [59, 65], the behaviour of polarons near narrow Feshbach resonances [66, 67, 68] and the study of itinerant ferromagnetism [69]. Such a theoretical tool is useful, since it is possible to create and observe

the Fermi polaron in the experiment [70, 71, 72]. Highly polarized Fermi gases have also been studied using different approaches in the context of itinerant ferromagnetism [73], p-wave interactions [68], the collision of spin-polarized clouds [74], Efimov three-body physics [75], narrow Feshbach resonances [76], quasiparticle properties of the Fermi polaron [77], mixtures of different fermionic species [78] and in the strongly interacting (unitary) regime [79, 80].

## 3.2 The T-matrix approach: Green's functions and the self-energy

An alternative, and a more general method that can be used to describe interacting quantum particles[2] is the T-matrix formalism. Broadly speaking, the T-matrix approach is just the Schrödinger equation rewritten in a way to conveniently take into account the scattering of particles.

### 3.2.1 Green's functions

To see how this follows, we first introduce the concept of a Green's function[3]. The Green's function appears in mathematics as a tool to solve a certain set of differential equations, but here we are primarily concerned with its application in many-body physics as the *propagator*, which appears in quantum field theory in Feynman diagrams. Roughly speaking, the propagator or Green's function $G(x,t;x',t')$ indicates the probability amplitude that some particle, present at position $x$ and time $t$ is found at some other position $x'$ at some different time $t'$. It is called the Green's function, because it is closely related to the fundamental solution of the Schrödinger equation:

$$\left(i\hbar\frac{\partial}{\partial t} - H\right)\frac{1}{i\hbar}\theta(t-t')G(x,t;x',t') = \delta(x-x')\delta(t-t'), \tag{3.4}$$

where $H$ is the Hamiltonian written in $(x,t)$-space, $\theta$ is the step function which is zero for negative arguments and equal to one otherwise, and $\delta$ is the Dirac delta function. If the Green's function is known, then the "ordinary" wave function at $(x,t)$ is simply given by:

$$\psi(x,t) = \int_{-\infty}^{\infty}\int_{-\infty}^{\infty} dt'dx'\psi(x',t')G(x,t;x',t'). \tag{3.5}$$

[2] Actually, the T-matrix was originally formulated for classical waves as described by the Maxwell equations and can be used to describe light scattering processes.
[3] The concepts explained in this section are explained in greater detail in Fetter and Walecka [81] and other textbooks. I will attempt to give a broad overview of the concepts and refer the reader to textbooks for further (mathematical) details.

So far, we have just rewritten the Schrödinger equation. The point of this exercise is that for some problems, solving for the Green's function can be easier than solving the Schrödinger equation directly. The Green's function for a non-interacting particle (the so-called bare propagator) takes a very simple form in momentum space:

$$G_0(k,\omega) = \frac{1}{\omega - k^2 + i\eta}, \tag{3.6}$$

where $k$ is momentum, $\omega$ is the (Matsubara) frequency and $\eta \to 0$ is included to preserve the analytical structure of the equation. The imaginary part of the numerator in the Green's function has the purpose of representing a lifetime of (virtual) excitations; here $\eta \to 0$ simply represents a particle with infinite lifetime.

### 3.2.2 Self-energy: the Dyson equation and the ladder approximation

Suppose we have some interacting system, and we would like to describe the dynamics of this system. Given the bare Green's function for a non-interacting system of fermions, we can obtain the so-called *dressed* Green's functions for the interacting system through the Dyson equation [82] (we introduce the shorthand notation $K = (k, \omega)$):

$$G(K) = G_0(K) + G_0(K)\Sigma(K)G(K). \tag{3.7}$$

The quantity $\Sigma(K)$ is called the *self-energy* and contains the effect of interactions in the system on the bare Green's function. It is easy to verify that absent any interactions[4] the full Green's function $G(K)$ is equal to $G_0(K)$.

In general, solving a many-body problem without approximations is extremely difficult, although certain exact solutions are available. This is especially the case in the one-dimensional case, where the Bethe Ansatz enables various exact solutions [83]. Nevertheless, it is useful to consider approximative schemes in the case where exact solutions are not available.

One such approximative scheme is to determine the self-energy (3.7) through the *ladder approximation*:

$$\Sigma(P) = -i \int \frac{dK}{(2\pi)^{\mathrm{D}+1}} G_0(K)\Gamma(S). \tag{3.8}$$

Here the quantity $\Gamma(S)$ is the *many-body T-matrix* as a function of two-momentum $S = (1/2)(P + K)$ and D indicates the dimension. If we choose

[4] In that case, the self-energy is zero.

to take the non-interacting Green's function, then the approach is said to be *non-self-consistent*. On the other hand, a self-consistent approach yields an iterative procedure where the resulting self-energy determines a new Green's function, which in turn results in a new self-energy, etc. In the following, we will discuss how the many-body T-matrix can be obtained.

### 3.2.3 The scattering amplitude and the two-body T-matrix

Although the Dyson equation looks very simple, we haven't actually accomplished anything until we know how to calculate the self-energy $\Sigma(K)$. There is no general method for computing the self-energy; usually, approximations such as the ladder approximation mentioned in the previous section are required to obtain a solution. One type of problem where a momentum space representation is convenient is the scattering problem where we consider one particle bumping into another particle and interacting with it in some way. We assume that the first particle interacts with the second particle under the influence of a spherically symmetric and zero-range potential, an approximation that is usually justified in dilute systems and at low energies.

The scattering amplitude, which indicates the probability of a scattering event occurring, turns out to depend only on the incoming momentum $k$ of the particle [81, 82, 38], and is given in the limit that the interactions are zero-range by:

$$f(\mathbf{k}) = \frac{-a_{3\mathrm{D}}}{1 + ika_{3\mathrm{D}}} \quad (3D), \tag{3.9}$$

$$f(k) = \frac{-1}{1 + ika} \quad (1D). \tag{3.10}$$

Note in these equations that the definitions of $a$ and $a_{3\mathrm{D}}$ are different for different dimensions. Although the equations for one and three dimensions are similar, the physics that they represent are quite different. In $3$D, the scattering amplitude is zero as the scattering length goes to zero and reaches a finite value as $a_{3\mathrm{D}} \to \infty$. In $1$D, this situation is completely reversed and the scattering amplitude goes to zero as $a \to \infty$, which now represents the weakly interacting limit.

We now proceed to compute the two-body T-matrix $\Gamma_0(K)$ for a one-dimensional system. This object describes the interactions (scattering) between two particles, without the presence of the Fermi sea. Afterwards, we will see how we can obtain the full T-matrix $\Gamma(K)$ starting from the two-body T-matrix $\Gamma_0(K)$. The two-body T-matrix can be obtained using

the scattering amplitude or from the Lippman-Schwinger equation. Detailed derivations are given in Refs. [84, 85]; we will just state the main results[5]. If the inter-particle interactions are of the zero-range type, i.e.

$$V_{\text{int}}(x - x') = g\delta(x - x'), \tag{3.11}$$

where $g$ represents the strength of inter-particle interactions, then the momentum representation of this potential is very simple and independent of $k$: $V_{\text{int}}(k) = g$. The parameter $g$ depends on the one-dimensional scattering length $a$; $g = -2\hbar^2/ma$. Now the Lippman-Schwinger equation, which is an operator equation, can be solved *algebraically*, giving the following result (setting $\hbar = m = 1$ and assuming that both particles have equal mass):

$$\Gamma_0(K) = \frac{-g/2}{1 + \frac{ig}{2\sqrt{2\omega - k^2}}}. \tag{3.12}$$

So what does the two-body T-matrix *mean*? It is an object describing the scattering both "on the shell" ($\omega = k^2$) as well as "off-shell" ($\omega \neq k^2$, which incorporates virtual excitations), all in one neat package. Moreover, it is formulated in a way that is mathematically well-behaved, unlike the direct solution to the Schrödinger equation, with its nasty delta function. Still, it is useful to remember that the two-body T-matrix is equivalent to the exact solution of the Schrödinger equation, at least in the limit of two particles interacting through a delta function potential. In a two-body collision, momentum is conserved, so the "off-shell" part of the T-matrix appears redundant. The point is, of course, that we want to extend this formalism to a many-body setup, where particles might exchange momentum, both with one another as well as with a possible external potential. We will discuss this extension in the following section. It is interesting to note that for an "on-shell" collision $\omega = k^2$, we obtain precisely $-ikf(k)$, which is equal to the scattering amplitude as defined according to Ref. [84].

### 3.2.4 The many-body T-matrix

The two-body T-matrix describes scattering processes involving two particles. Ideally, we would like to extend this formalism to a many-body system, where many particles interact with each other. To include the effects of the Fermi sea, we compute the so-called many-body (or "full") T-

[5]Note that the definition of the scattering amplitude in Ref. [84] is different from the one used in Ref. [38], although the resulting physics is obviously identical.

matrix $\Gamma(K)$. We will then show how it is related to the two-body T-matrix (3.12).

To compute the self-energy, we use the ladder approximation discussed in Section 3.2.2. The basic idea of the ladder approximation is as follows. When two particles meet, they are allowed to interact repeatedly, and we then sum up all of the contributions of these processes. In terms of the wave function, we can write this as [81]:

$$\begin{aligned}\psi_k(x) =& e^{ikx} - \int dy\, G(x-y)V_{\text{int}}(y)e^{iky} \\ &+ \iint dydz\, G(x-y)V_{\text{int}}(y)G(y-z)V_{\text{int}}(z)e^{ikz} + \dots\end{aligned} \tag{3.13}$$

What are the processes that we are *neglecting* in this approximation? Not included are the processes involving the interactions of other particles while the two particles are interacting. Therefore, the ladder approximation is appropriate only for *dilute* systems, where the time interval between two-particle collisions is relatively long. Also, we are neglecting *collective excitations*. The latter reason is why the ladder approximation fails in the spin-balanced one-dimensional case [86], which is called a Luttinger liquid. The ladder approximation is actually remarkably similar to the single particle-hole excitation limitation in Chevy's variational approach (see Section 3.1), and indeed they can give similar or identical results [61], as also discussed in Publication I.

What remains is just the minor matter of determining the many-body T-matrix $\Gamma(S)$. A detailed derivation for the three-dimensional case is presented in Ref. [82], we will just give the result here. Given the two-body T-matrix $\Gamma_0(P)$, the many-body T-matrix in the ladder approximation is given by:

$$\Gamma(P) = \frac{\Gamma_0(P)}{1 - \Gamma_0(P)\int \frac{dq}{2\pi}\tilde{\chi}(q;P)}. \tag{3.14}$$

The quantity $\tilde{\chi}(q;P)$ is called the *regularized pair susceptibility* and is given by:

$$\tilde{\chi}(q;P) = -\frac{1}{E_P - q^2} + i\int \frac{d\omega_0}{2\pi} G(p+q,\omega-\omega_0)G(p-q,\omega+\omega_0). \tag{3.15}$$

Here the term with the product of Green's functions takes into account the effect of Pauli blocking into the many-body problem.

### 3.2.5 Obtaining the contact parameter from the T-matrix

One of the nice by-products of the T-matrix formalism is that it provides us with a means to compute the contact parameter discussed in Chapter

2. The momentum distribution $n_k$ is related to the Green's function as follows [55]:

$$n_k = \int \frac{d\omega}{2\pi} G(k,\omega). \tag{3.16}$$

However, obtaining the momentum distribution this way requires knowledge of the full Green's function. In the weakly interacting limit, the asymptotic tail was obtained already in 1960 for the three-dimensional case [87], although it took more than forty years before it was realized that the asymptotic scaling proportional to $1/k^4$ is completely general. The result is:

$$n_{\mathbf{k}} = \Big(\frac{2}{3\pi} k_F a\Big)^2 \frac{k_F^4}{k^4}, \quad (k_F a \ll 1) \tag{3.17}$$

where as before $a$ is the scattering length, $k_F$ is the Fermi momentum and $k$ is momentum.

Since obtaining the full Green's function without approximations is generally not an easy task, we will outline a perturbative approach [88, 82]. Assume that only pair-wise correlations are relevant at high momenta. The T-matrix now provides us with the probability $\mathcal{P}$ that a pair of atoms, initially in momentum states $p$ and $k$, scatter to states $q$ and $p+k-q$:

$$\mathcal{P}(k,p;q) = \Big|\frac{\Gamma(P)}{\varepsilon^*_{p+k-q} + \varepsilon^*_q - \varepsilon_p - \varepsilon_k}\Big|^2 n_k n_p, \tag{3.18}$$

where $n_k$ and $n_p$ are the momentum distributions, $P$ is the two-momentum $(p,\omega)$ and $\varepsilon_p$ is the sum of the kinetic energy $\epsilon_p = \hbar^2 p^2/2m$ and the (Hartree) self-energy $\Sigma(p)$. If the momentum $q$ is very large (i.e. we restrict our analysis to high-energy scattering events), then the associated Hartree self-energy will vanish, and we can assume $\varepsilon_q \approx \epsilon_q$. Then we can simplify the above equation to obtain:

$$\mathcal{P}(k,p;q) = \Big|\frac{\Gamma(P)}{2\epsilon_q}\Big|^2 n_k n_p. \tag{3.19}$$

By summing over the possible initial values of $k$ and $p$ we now obtain the momentum distribution for high momenta:

$$n_q \approx \frac{1}{V^2} \sum_{k,p} n_k n_p \frac{|\Gamma(P)|^2}{4\epsilon_q^2}, \tag{3.20}$$

where $V$ is the volume of the system. Since the kinetic energy is proportional to $q^2$, this immediately gives us the expected $1/q^4$ scaling of the momentum distribution, and with it the contact parameter:

$$C = \Big(\frac{m}{\hbar^2}\Big)^2 \frac{1}{V^2} \sum_{k,p} |\Gamma(P)|^2 n_k n_p, \tag{3.21}$$

where in the case of spin imbalance (unequal population of the two fermionic species) the momentum distributions $n_k$ and $n_p$ might differ. In the weakly interacting limit (in 3D), the T-matrix is constant and given by the simple expression $\Gamma = 4\pi\hbar^2 a/m$, where $a$ is the scattering length. This reproduces the limit (3.17) exactly. However, even beyond the weakly interacting limit, the simple perturbative calculation leading to Equation (3.21) works remarkably well, as we shall see in the next chapter.

# 4. The one-dimensional Fermi polaron: homogeneous case

We can use the methods outlined in the previous chapter to study highly polarized Fermi gases. For now, we are primarily interested in describing the ground state properties of interacting systems. We consider the impurity problem as discussed in the previous chapter, as formulated for one dimension.

First, we consider the homogeneous case, that is, the case where the external potential $V_{\text{ext}}$ is zero (as discussed in Publication I). We also assume contact interactions, which are of zero range, so that:

$$V_{\text{int}}(x - x') = g\delta(x - x'), \tag{4.1}$$

and $g$ indicates the strength of the inter-particle interactions, which depends on the 1D scattering length as $g = -2\hbar^2/ma$. For simplicity, we also assume that there is no mass imbalance, i.e. both the impurity particle $\downarrow$ and the majority component fermions $\uparrow$ have the same mass[1]. We can now write the Hamiltonian in the following simple form:

$$\begin{aligned}\mathcal{H} = &\sum_{\sigma} \int dx\, \psi_{\sigma}^{\dagger}(x)\Big[ -\frac{\hbar^2}{2m}\frac{d^2}{dx^2}\Big]\psi_{\sigma}(x) \\ &+ g\int dx\, \psi_{\uparrow}^{\dagger}(x)\psi_{\downarrow}^{\dagger}(x)\psi_{\downarrow}(x)\psi_{\uparrow}(x).\end{aligned} \tag{4.2}$$

The ground state energy of the homogeneous Fermi polaron at zero temperature ($T = 0$) was obtained by McGuire in the 1960s [89, 90], through the Bethe Ansatz method[2]. What we would like to do, then, is extend these results to finite temperature. Moreover, we analyze the behaviour of the contact parameter for this system.

In fact, we can already obtain the correct expression for the contact at zero temperature from McGuire's expression for the ground state energy,

[1] For a study of mass imbalance in the one-dimensional case, see Ref. [62].

[2] We will not discuss the Bethe Ansatz in this thesis. For a review of the Bethe Ansatz method and recent applications, the reader is referred to e.g. Ref. [83].

expressed in the convenient dimensionless interaction parameter $k_F a$ (we set $\hbar = m = 1$):

$$E = \frac{k_F^2}{\pi}\Big[\frac{1}{k_F a} + \arctan\Big(\frac{1}{k_F a}\Big) - \Big(\frac{1}{k_F a}\Big)^2\Big(\frac{\pi}{2} - \arctan\Big(\frac{1}{k_F a}\Big)\Big)\Big]. \tag{4.3}$$

We can derive the contact from this expression using the Tan adiabatic theorem (2.6). First, we define a dimensionless contact density for the one-dimensional system as $\mathcal{C} = C/(Lk_F^4)$. We obtain:

$$\mathcal{C} = \frac{4}{\pi^2(k_F a)^3}\Big[k_F a + \arctan\Big(\frac{1}{k_F a}\Big) + \frac{\pi}{2}\Big], \tag{4.4}$$

where an extra factor of two arises because the reduced mass $m_r = m/2$. This equation is valid for all values of $k_F a$. An interesting case is the infinitely repulsively interacting limit $k_F a \to 0^-$. Here, the contact density takes the value $4/3\pi^2$, which is exactly the same as the contact density for a Tonks-Girardeau gas[3] of infinitely repulsive one-dimensional bosons [27]! The result for the homogeneous spin-balanced fermionic system in the infinitely repulsive limit, $\mathcal{C} \approx 0.749...$ [28], however, is quite different. For weakly interacting systems, where $k_F a \to \pm\infty$, Equation (4.4) yields:

$$\mathcal{C} \propto \Big(\frac{1}{k_F a}\Big)^2 \propto g^2. \tag{4.5}$$

This scaling of the contact with the square of the coupling constant $g$ for weak interactions also occurs in the spin-balanced case, and is generally valid also for higher dimensions [55], as can also be elegantly shown using the Operator Product Expansion (OPE) method [95]. In this picture, the contact is *defined* as:

$$C = g^2 \int d^3r \langle \psi_\downarrow^\dagger \psi_\uparrow^\dagger \psi_\downarrow \psi_\uparrow(\mathbf{r})\rangle. \tag{4.6}$$

Note that the integrand times $g^2$ is precisely the contact density (2.5). As we shall see in the next chapter, the $g^2$ scaling is also valid for the case where an external potential is present. This universal behaviour of the contact for weak interactions is understandable, because in the limit that the interactions are very weak, the interaction can be regarded as a small perturbation that otherwise leaves the system undisturbed; in other words: the expectation value in Equation (4.6) remains unchanged.

[3]The Tonks-Girardeau gas of 1D bosons with infinitely strong repulsive interparticle interactions, proposed in the early 1960s [91, 92], was finally observed in 2004 [93, 94].

### 4.1 Polaron energy

We will use the T-matrix formalism in the following. Suppose that we have successfully determined the many-body T-matrix (see Section 3.2.4). Now the self-energy $\Sigma(P)$ at $1+1$-momentum $(p, p_0)$ is given in the ladder approximation according to the Galitskii integral approach as:

$$\Sigma(P) = -i \int \frac{dK}{(2\pi)^2} G_0(K)\Gamma(S), \tag{4.7}$$

where $S = (1/2)(P+K)$, and the non-interacting Green's function at finite temperature is given by:

$$G_0(k,\omega) = \frac{n_k(T)}{\omega - \epsilon_k - i\eta} + \frac{1-n_k(T)}{\omega - \epsilon_k + i\eta}, \tag{4.8}$$

where $\epsilon_k = \hbar^2 k^2/2m$ is the kinetic energy. Here we do not take the actual momentum distribution $n_k$, but take the non-interacting Fermi-Dirac distribution at a temperature $T$. We now determine the polaron energy $E_p$ at fixed momentum $p$, which can be determined from the self-energy (4.7). To do so, we start with a guess for $E_p$ and iterate Equation (4.7) using $E_p = \epsilon_p + \Sigma(p, E_p)$. During the iteration, we keep the Green's function unchanged. This approach is known as the *non-self-consistent* (NSC) method. A self-consistent approach would include the self-energy into the Green's function, which in turn influences the self-energy.

Let us first benchmark our approach using the exact zero-temperature energy as obtained by McGuire [89, 90], using the Bethe Ansatz. We compute the polaron energy for zero momentum (the ground state) using the NSC method, as well as using the Brueckner-Goldstone approach (see Chapter 8). The result is depicted in Figure 4.1. As was also shown in Ref. [61], the T-matrix approach yields good agreement with exact results. Note that on the attractive side ($k_F a > 0$), the polaron energy diverges to minus infinity. This is because the impurity binds with one of the majority component particles. The strength of this bond depends on the strength of the interactions and goes to infinity as the 1D interaction strength goes to infinity ($k_F a \to 0^+$). The Brueckner-Goldstone approach (explained in detail in Chapter 8) adds a self-consistency requirement to the T-matrix iteration. It is then perhaps surprising that the prediction from this theory is *worse*, even though we are including *more* diagrams in our description! The reason for this is a so-called *sign blessing* [54] – in a particle-hole expansion, each successive term contains two leading contributions that almost exactly cancel each other [96]. Adding some ad-

ditional processes to the description, while leaving out others, can thus lead to a less accurate description.

In the infinitely repulsive limit, $k_F a \to 0^-$, the energy approaches a finite value. This energy is actually easy to determine analytically on physical grounds. At infinite repulsion, the penalty for having any finite overlap with the majority component particles is also infinite, so the overlap must be zero. Since the energy levels of the majority component are filled up to the Fermi energy $E_F$, the lowest energy state one can place the impurity while having no overlap with the majority component fermions is at the Fermi level. Therefore, the ground state energy of the polaron at infinite repulsion is exactly equal to $E_F$. The T-matrix calculation gives a polaron energy of $E \approx 1.24 E_F$, reasonably close to the exact result, especially considering that we are attempting to describe an infinitely strongly interacting system using an approximative approach. Meanwhile, a calculation using Chevy's variational Ansatz [62] yields $E \approx 1.39 E_F$, so the T-matrix does a bit better in this case, despite it being argued that the T-matrix in the ladder approximation and Chevy's Ansatz restricting the excitations to a single particle-hole excitation are equivalent [61].

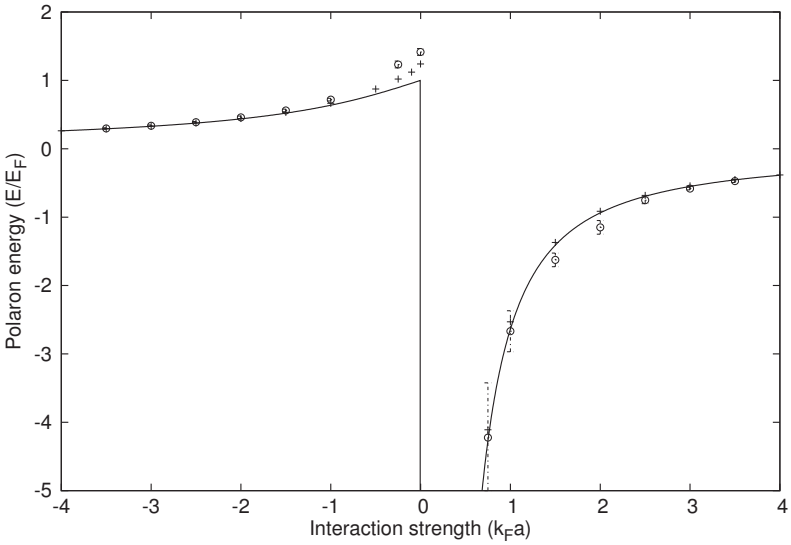


**Figure 4.1.** Polaron ground state energy $\Sigma(0,0)$ as computed using the non-self-consistent T-matrix approach (4.7), as a function of the inverse interaction strength $k_F a$. Solid line shows the exact result, plus symbols indicate the T-matrix result and circles indicate the result of the Brueckner-Goldstone approximation (see Chapter 8). Image adapted from Publication I. Copyright (2013) by the American Physical Society.

We now extend the result to finite temperature. We express temper-

atures in terms of the Fermi temperature $T_F = E_F/k_B$, where $E_F = \hbar^2 k_F^2/2m$ is the Fermi energy and $k_B$ is Boltzmann's constant. The result is shown in Figure 4.2, where we plot the temperature dependence of the energy as a function of inverse temperature. Note that the magnitude of the energy $|E_p|$ does not depend on the sign of the interaction in the high-temperature (mean-field) regime. In the inset, we have plotted the normalized energy $E'$ given by:

$$E' = \frac{E - E_{\text{ex}}}{E_{\text{MF}} - E_{\text{ex}}}. \tag{4.9}$$

Here $E_{\text{ex}}$ is the exact result for the energy at zero temperature, and $E_{\text{MF}}$ is the mean-field limit, exact at infinite temperature:

$$E_{\text{MF}} = -\frac{2\hbar^2 k_F^2}{m\pi k_F a}. \tag{4.10}$$

The value of $E'$ thus goes from $0$ at zero temperature to $1$ in the high-temperature limit. However, the crossover depends on the interaction, and in general occurs at higher temperatures for higher interactions. In the spin-balanced, attractive one-dimensional case (the Gaudin-Yang model), a similar crossover was recently reported [97]. The inset also gives an indication of the relative error of the T-matrix method compared to the Bethe Ansatz result at zero temperature, since $E'$ does not exactly approach 0 in the numerical results.

## 4.2 Contact

In the following, we will use the T-matrix approach to determine the contact as a function of temperature. Recall that the exact dimensionless contact density is given by (4.4). We use the perturbative approach outlined in Section 3.2.5. In a way similar to the depiction of the energy in Figure 4.1, we can compare to the exact result as depicted in Figure 4.3, where we plot the inverse contact density[4].

Note that, unlike the three-dimensional case [53, 54, 55, 56], there is no phase transition at finite $k_F a$. The step of the contact density at $1/k_F a = 0$ is not a phase transition, since the infinitely attractive and infinitely repulsive regimes are not adiabatically connected. We use three distinct methods to approximate the contact:

[4]We show the inverse contact density because the contact density diverges for strongly attractive interactions, so it is more difficult to plot it together with the contact density for repulsive interactions, which approaches a constant value at infinite repulsion.

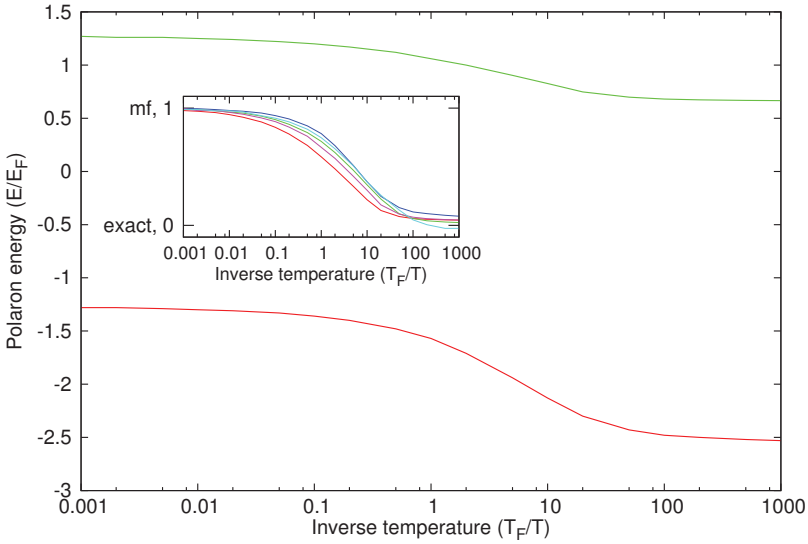


**Figure 4.2.** Polaron ground state energy $\Sigma(0,0)$ as computed using the non-self-consistent T-matrix approach (4.7), as a function of inverse temperature $T_F/T$, for $k_F a = -1$ (green) and $k_F a = 1$ (red). Inset: normalized energy $E'$ (see main text) for various values of the interaction strength $k_F a = -0.5, -1, -2, -10, 1$. Image adapted from Publication I. Copyright (2013) by the American Physical Society.

1. *Perturbation theory*. — The plus symbols in Figure 4.3 show the result (3.21) as obtained using the perturbative method of Ref. [82]. The generalization to the one-dimensional case is fairly straightforward, see Section 3.2.5.

2. *The Tan adiabatic theorem*. — Using Tan's adiabatic theorem (2.6), we can directly compute the derivative with respect to the scattering length, where we use the energies obtained from the T-matrix for different values of the scattering length, as shown by the stars in Figure 4.3.

3. *Modified perturbation theory*. — We can extend the aforementioned perturbation theory, taking into account the depletion of the ground state in order to obtain a better result at stronger interactions. This method will be described in more detail below.

Observe that the modified theory gives approximately the same result as a direct computation using Tan's adiabatic theorem. The perturbation theory itself significantly overestimates the contact at strong repulsion.

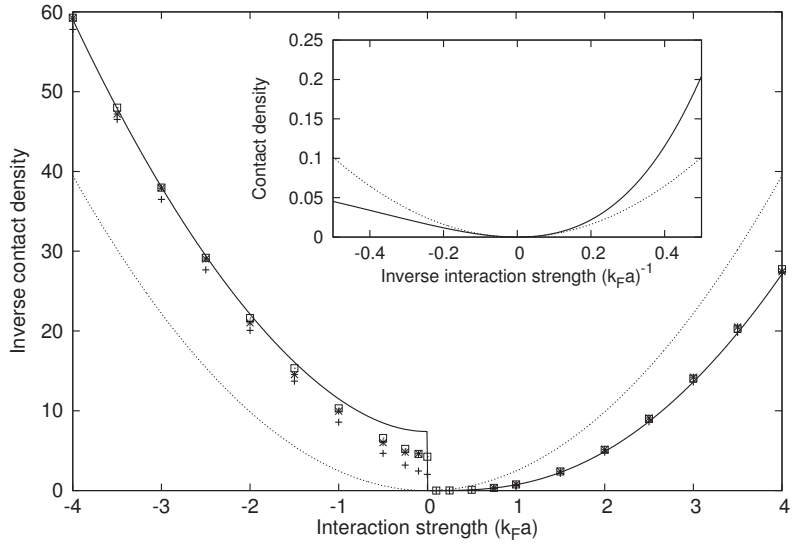


**Figure 4.3.** Inverse contact density $1/\mathcal{C}$ as a function of interaction strength for $T = 0$. Plus symbols show the perturbative result. Squares use a modified perturbation theory (see main text) and stars use the Tan adiabatic theorem (2.6). The solid line shows the exact zero-temperature result (4.4) and the dashed line shows the weakly interacting limit. Inset: contact density as a function of $1/k_F a$, showing the crossover to the weakly interacting regime. Image adapted from Publication I. Copyright (2013) by the American Physical Society.

The reason for this is that the perturbation theory does not take into account the depletion of the lowest momentum state. This depletion is significant for a strongly interacting system. Let us denote the result from the modified theory as $C_{\mathrm{m}}$. It is related to the perturbative result $C_{\mathrm{pert}}$ as[5]:

$$C_{\mathrm{m}} = \frac{C_{\mathrm{pert}}}{1 + \sum_{p \neq 0} \nu_p}, \tag{4.11}$$

where $\nu_p$ is the occupation probability of the momentum state $p$. From this equation it is immediately clear that the perturbation theory and the modified theory give approximately the same result for weak interactions, where the occupation probability $\nu_0 \approx 1$.

In the following, we will derive the result (4.11). We can determine the occupation probability $\nu_p$ using an approach based on Chevy's Ansatz [58], combined with the Tan adiabatic theorem. According to this approach[6],

[5] See also the supplementary material to Publication I.

[6] Note that the way the Ansatz is written down here, it is restricted to the homogeneous case, unlike in our more general discussion of Section 3.1.

the polaron energy is given as a function of the scattering length by:

$$E(a) = \sum_{q<k_F} \frac{g}{1 - g\sum_{k>k_F} \frac{1}{E(a)+\epsilon_q-\epsilon_k-\epsilon_{q-k}}} = \sum_{q<k_F} \frac{g}{1 - g\chi(E(a), q)}, \quad (4.12)$$

where the coupling constant (in units where $\hbar = m = 1$) is $g = -2/a$, $\epsilon_q$ is the kinetic energy $(1/2)q^2$ and we introduce the auxiliary function $\chi(E(a), q)$. Here the summation is restricted to $k > k_F$ and $q < k_F$, which implicitly incorporates the step function momentum distribution at zero temperature (we will generalize our result to finite temperatures at the end of the calculation). Now we can use the 1D analog of Tan's adiabatic theorem to obtain:

$$\frac{\partial E}{\partial a} = -\frac{1}{a}E(a) - \sum_{q<k_F} \frac{g}{\left[1 - g\chi(E(a), q)\right]^2} \frac{\partial}{\partial a}\left[1 - g\chi(E(a), q)\right], \quad (4.13)$$

using $\partial g/\partial a = -g/a$. We can rewrite this using:

$$\frac{\partial}{\partial a}\left[1 - g\chi(E(a), q)\right] = \frac{g}{a}\chi(E(a), q) - g\frac{\partial \chi}{\partial a}, \quad (4.14)$$

which, upon substitution, yields

$$\frac{\partial E}{\partial a} = -\frac{1}{a}E(a) - \sum_{q<k_F} \frac{g}{\left[1 - g\chi(E(a), q)\right]^2} \left[\frac{g}{a}\chi(E(a), q) - g\frac{\partial \chi}{\partial a}\right]. \quad (4.15)$$

Combining the first and second terms on the right yields

$$\frac{\partial E}{\partial a} = \frac{2}{m}\sum_{q<k_F} \left(\frac{g}{1 - g\chi(E(a), q)}\right)^2 + \sum_{q<k_F} \frac{g^2\frac{\partial \chi}{\partial a}}{\left[1 - g\chi(E(a), q)\right]^2}. \quad (4.16)$$

Recall that the first term in this equation is precisely the perturbative contact as obtained from the T-matrix calculation in Section 3.2.5. The second term is a correction to this result. We can rewrite this correction using:

$$\frac{\partial \chi(E(a), q)}{\partial a} = \sum_{k>k_F} \frac{\frac{-\partial E(a)}{\partial a}}{\left[E(a) + \epsilon_q - \epsilon_k - \epsilon_{q-k}\right]^2}. \quad (4.17)$$

Thus we now obtain, using Tan's adiabatic theorem $C = (1/2)\frac{\partial E}{\partial a}$,

$$C = C_{\text{pert}} - C\sum_{q<k_F} \frac{g^2}{\left[1 - g\chi(E(a), q)\right]^2} \sum_{k>k_F} \frac{1}{\left[E(a) + \epsilon_q - \epsilon_k - \epsilon_{q-k}\right]^2}. \quad (4.18)$$

This yields, replacing the restricted summation at $T = 0$ to the more general result incorporating the (non-interacting) finite temperature distributions $n_q(T)$:

$$C = C_{\text{pert}} - C\sum_{p\neq 0}\sum_{q} \left[\frac{n_q(1 - n_{q-p})g^2}{\left[1 - g\chi(E(a), q)\right]^2} \frac{1}{\left[E(a) + \epsilon_q - \epsilon_{q-p} - \epsilon_p\right]^2}\right], \quad (4.19)$$

which gives us the modified perturbative result (4.11). Note that the correction term has all the expected properties: it scales with the interactions as $g^2$ for weak interactions, where we can approximate $1 - g\chi(E(a), q) \approx 1$, and the high-$p$ tail gives us the correct momentum tail since:

$$\lim_{p\to\infty} (E(a) + \epsilon_q - \epsilon_{q-p} - \epsilon_p)^2 \propto \frac{1}{p^4}. \tag{4.20}$$

However, the approach is not fully self-consistent since we are using the non-interacting momentum distributions at finite $T$ and the NSC T-matrix. This explains why we do not obtain the exact result, and since we are making the same approximations as when we are using the Tan adiabatic theorem directly, both approaches give the same result. The small deviation that is visible in Figure 4.3 is just due to the small discretization error when approximating the derivative, which we do by computing the energy at different scattering lengths $a_1$ and $a_2$ ($a_2 > a_1$) and computing the first order approximation:

$$\frac{\partial E}{\partial a} \approx \frac{E(a_2) - E(a_1)}{a_2 - a_1} \tag{4.21}$$

Now we are ready to compute the contact at finite temperature. The result is shown in Figure 4.4. As before, we compute a normalized contact density $\mathcal{C}'$ as depicted in the inset of Figure 4.4:

$$\mathcal{C}' = \frac{\mathcal{C} - \mathcal{C}_{\text{ex}}}{\mathcal{C}_{\text{MF}} - \mathcal{C}_{\text{ex}}}, \tag{4.22}$$

where $\mathcal{C}_{\text{MF}}$ is the weakly interacting (mean-field) value of the contact density, acquired from the limit that $k_F a \to \infty$ in Equation (4.4). We will use the values as computed using the perturbative theory.

The behaviour of the contact density has some interesting features. For instance, for the repulsive polaron the contact is monotonically *increasing* with increased temperature, a peculiar feature that in the spin-balanced three dimensional system is only visible in limited temperature ranges [32]. Furthermore, the contact approaches a constant value in the high-temperature limit rather than approaching zero. This indicates that interactions remain significant at any temperature for one-dimensional systems (or at least this particular one). An alternative way to view this difference is through the two-body T-matrix[7] $\Gamma_0$ (or the product of the scattering amplitude and $ik$), which in 1D remains finite even for momenta $k \to \infty$, while it vanishes in the 3D-case. As the temperature

[7] In the high-temperature limit, the effect of quantum statistics is negligible, so we can approximate $\Gamma(P) \approx \Gamma_0(P)$.

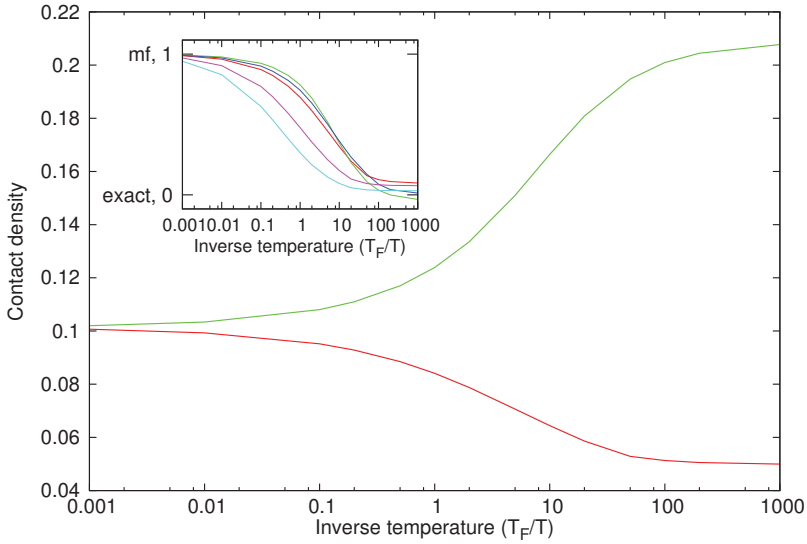


**Figure 4.4.** Contact density as a function of inverse temperature $T_F/T$ for the attractive polaron with interaction strength $k_F a = 2$ (top, green) and the repulsive polaron $k_F a = -2$ (bottom, red). Inset: normalized contact density showing crossover from the zero-temperature to the mean-field regime for various values $k_F a = -0.25, -0.5, -2, 2, -10$. Image adapted from Publication I. Copyright (2013) by the American Physical Society.

increases, the momentum distribution becomes more and more weighted towards high momenta, which means that in 3D particles which are ever more weakly interacting make the dominant contribution. In other words, as the temperature is increased, particles become more and more like point particles, so that the scattering cross-section approaches zero in the higher-dimensional case, where the probability that a particle hits another particle has measure zero in the $T \to \infty$ limit. However, in the one-dimensional case, particles must meet when they are moving along the axis to which movement is confined no matter how "small" the particles are. In the spin-balanced case, a similar mechanism results in an instability to spin density waves for one-dimensional Fermi liquids [98, 86]. This leads to the breakdown of the Fermi liquid description in one dimension.

# 5. The one-dimensional Fermi polaron: inhomogeneous case

In the case where the external potential $V_{\text{ext}}$ is non-zero, the T-matrix formalism is less suitable, because the external potential does not conserve momentum. Instead, we will in this section use an alternative method to describe in detail the inhomogeneous case for an arbitrary external potential, as applied to the one-dimensional Fermi polaron system (see Publication II).

The Hamiltonian of this system, including the external potential, is given by:

$$\begin{aligned}\mathcal{H} = &\sum_{\sigma} \int dx\, \psi_{\sigma}^{\dagger}(x)\Big[-\frac{\hbar^2}{2m}\frac{d^2}{dx^2} + V_{\text{ext}}(x)\Big]\psi_{\sigma}(x) \\ &+ g\int dx\, \psi_{\uparrow}^{\dagger}(x)\psi_{\downarrow}^{\dagger}(x)\psi_{\downarrow}(x)\psi_{\uparrow}(x).\end{aligned} \tag{5.1}$$

As before, we will assume short-range contact interactions as described by the delta function potential, and we consider many $\uparrow$ fermions interacting with a single $\downarrow$ impurity. We will attempt to compute the ground state energy of the system using Chevy's variational Ansatz, as discussed in Section 3.1. That is, we take the following educated guess for the wave function:

$$|\Psi\rangle = \sum_{l} \phi_l c_{\downarrow l}^{\dagger}|0\rangle + \sum_{mkn} \phi_{mkn} c_{\uparrow m}^{\dagger} c_{\uparrow k} c_{\downarrow n}^{\dagger}|0\rangle, \tag{5.2}$$

where $c_{\sigma i}^{(\dagger)}$ destroys (creates) a particle of the type $\sigma \in \{\uparrow,\downarrow\}$ in the state $i$, and the variational coefficients $\phi_l$ and $\phi_{mkn}$ are to be determined. The state $|0\rangle$ refers to the non-interacting Fermi sea of the $\uparrow$-particles at zero temperature. We refer to this generalization of Chevy's Ansatz to a system with an arbitrary external potential as the real-space variational Ansatz (RSVA).

## 5.1 Determination of ground state properties

### 5.1.1 Ground state energy and variational coefficients

The expectation value of an observable $\mathcal{O}$ is given by $\langle\Psi|\mathcal{O}|\Psi\rangle$. Therefore, the ground state energy of the system can be computed by minimizing the quantity $\langle\Psi|\mathcal{H}|\Psi\rangle$. Let us first separate the non-interacting and interacting parts of the Hamiltonian, so that $\mathcal{H} = \mathcal{H}_0 + \mathcal{H}_{\text{int}}$, where

$$\mathcal{H}_{\text{int}} = g \int dx\, \psi_\uparrow^\dagger(x)\psi_\downarrow^\dagger(x)\psi_\downarrow(x)\psi_\uparrow(x). \tag{5.3}$$

We choose as a basis the eigenstates of the non-interacting part of the Hamiltonian $\mathcal{H}_0$ and expand the creation and annihilation operators as follows:

$$\psi_\sigma(x) = \sum_i \alpha_i(x) a_{\sigma i}, \quad \psi_\sigma^\dagger(x) = \sum_i \alpha_i^*(x) a_{\sigma i}^\dagger, \tag{5.4}$$

where the operators $a_{\sigma i}^{(\dagger)}$ destroy (create) a particle of the kind $\sigma \in \{\uparrow, \downarrow\}$ in the state $i$ described by the eigenfunction $\alpha_i(x)$. If we are interested in a closed system with fixed boundary conditions (that is, the wave function vanishes at the boundary), then without loss of generality we can assume that the eigenfunctions $\alpha(x)$ as well as the variational coefficients $\phi_l, \phi_{mkn}$ are real.

Suppose that we have computed the full eigenbasis of the non-interacting system, so that we have knowledge of the functions $\alpha_i(x)$ and their corresponding eigenenergies $E_i$ (we sort the energies $E_i$ in ascending order and assume the spectrum is non-degenerate). The expectation value of the non-interacting part of the Hamiltonian is now fairly easy to compute. It is simply given by:

$$\langle\mathcal{H}_0\rangle = \sum_l E_l |\phi_l|^2 + \sum_{mkn} \Delta E_{mkn} |\phi_{mkn}|^2, \tag{5.5}$$

where $\Delta E_{mkn} = E_n - E_k + E_m$. This expression can be understood as follows. Without interactions, the energy of the impurity is given by two parts. First, the sum over the energies $E_l$ times the weighted probability that it is in the state $l$, without any changes in the majority component particles. Second, the sum over the energies $E_n$ times the weighted probability that it is in the state $n$, with an additional contribution for the energy associated with the particle-hole excitation – one of the fermions in state $k$ going to state $m$. Note that the energy of a $\uparrow$-particle is always higher than the energy gained by creating a hole, so that this contribution is positive definite. It is now straightforward to see that the energy

of the non-interacting system is minimized by the wave function with the following variational coefficients:

$$|\phi_0|^2 = 1, |\phi_l|^2 = 0 (l > 0), |\phi_{mkn}|^2 = 0. \tag{5.6}$$

This configuration just puts the impurity in the ground state of the non-interacting system and leaves the majority component particles undisturbed, as we ought to expect.

Now let us add the interactions to the mix. The interacting part of the Hamiltonian is given in the chosen basis (no longer an eigenbasis of the full Hamiltonian):

$$\begin{aligned} &\mathcal{H}_{\text{int}} = g \sum_{ijpq} U_{ijpq} a^\dagger_{\uparrow i} a_{\uparrow j} a^\dagger_{\downarrow p} a_{\downarrow q}, \\ &\text{where} \;\; U_{ijpq} = \int dx \, \alpha_i(x) \alpha_j(x) \alpha_p(x) \alpha_q(x). \end{aligned} \tag{5.7}$$

It is also possible to take a different basis for the impurity than for the majority component. In this case the elements $U_{ijpq}$ will change accordingly; however, for simplicity we will take the same basis for both components. We can subdivide the expectation value $\langle \Psi | \mathcal{H}_{\text{int}} | \Psi \rangle = \langle \mathcal{H}_{\text{int}} \rangle$ into three terms:

$$H_1 = g \sum_{ijpqll'} \phi^*_l \phi_{l'} U_{ijpq} \langle 0 | a_{\downarrow l} a^\dagger_{\uparrow i} a_{\uparrow j} a^\dagger_{\downarrow p} a_{\downarrow q} a^\dagger_{\downarrow l'} | 0 \rangle \tag{5.8}$$

$$\begin{aligned} H_2 = g \sum_{\substack{ijpqmkn \\ m'k'n'}} &\phi^*_{m'k'n'} \phi_{mkn} U_{ijpq} \\ &\times \langle 0 | a_{\downarrow n'} a^\dagger_{\uparrow k'} a_{\uparrow m'} a^\dagger_{\uparrow i} a_{\uparrow j} a^\dagger_{\downarrow p} a_{\downarrow q} a^\dagger_{\uparrow m} a_{\uparrow k} a^\dagger_{\downarrow n} | 0 \rangle \end{aligned} \tag{5.9}$$

$$H_3 = g \sum_{mknlijpq} \phi^*_{mkn} \phi_l U_{ijpq} \langle 0 | a_{\downarrow n} a^\dagger_{\uparrow k} a_{\uparrow m} a^\dagger_{\uparrow i} a_{\uparrow j} a^\dagger_{\downarrow p} a_{\downarrow q} a^\dagger_{\downarrow l} | 0 \rangle + \text{H.c.} \tag{5.10}$$

Here H.c. indicates the Hermitian conjugate. These expressions can be greatly simplified because most of the terms in the inner product are zero, since the basis states are orthogonal. For the term $H_1$ we obtain that $i = j$, $q = l'$ and $p = l$, so that:

$$H_1 = g \sum_{ill'} U_{iill'} n_i \phi^*_l \phi_{l'}. \tag{5.11}$$

Note that here the summation over $i$ is restricted to $n_i \leq n_F$ because the destruction operator only gives a non-zero contribution if the majority component state is occupied. Here we denote by $n_i$ the occupation probability of the state $i$, for which we assume a Fermi-Dirac distribution, which is at $T = 0$ is just a step function. $n_F$ is the highest occupied state (corresponding to the Fermi surface), so that if there are $N$ majority component

particles, $n_F = N - 1$, $n_i = 0$ for $i \geq N$ and $n_i = 1$ otherwise. Therefore, we can rewrite the term $H_1$ as:

$$H_1 = g \sum_{ll'} U_{ll'} \phi_l^* \phi_{l'}, \quad U_{ll'} = \int dx\, n_\uparrow(x) \alpha_l(x) \alpha_{l'}(x), \tag{5.12}$$

where $n_\uparrow(x)$ is the total density of the majority component particles. This term can be interpreted as a Hartree-like energy shift.

The second term, $H_2$, is the most complicated one, containing a 10-tuple summation. However, also in this case we can greatly simplify the given expression. There are three ways to do so:

$$k = k', m = m', i = j, \tag{5.13}$$

$$k = i, m = m', k' = j, \tag{5.14}$$

$$k = k', m = j, i = m'. \tag{5.15}$$

Where in each of these cases we also have, as before, $n = q$ and $p = n'$. This gives us three separate summations:

$$\begin{aligned} H_2 = g &\sum_{mknn'} \phi^*_{mkn'} \phi_{mkn} U_{nn'} n_k (1 - n_m) \\ - g &\sum_{mkk'nn'} \phi^*_{mk'n'} \phi_{mkn} U_{kk'n'n} n_k n_{k'} (1 - n_m) \\ + g &\sum_{mm'knn'} \phi^*_{m'kn'} \phi_{mkn} U_{m'mn'n} n_k (1 - n_m)(1 - n_{m'}). \end{aligned} \tag{5.16}$$

The minus sign in the second term comes from the required rearrangement of the fermionic operators; we get a minus sign if an odd number of permutations are required. An analogous procedure yields the last term:

$$H_3 = 2g\Re \sum_{mknl} \phi^*_{mkn} \phi_l U_{mknl} n_k (1 - n_m). \tag{5.17}$$

Adding together all these terms, plus the contribution from the non-interacting part of the Hamiltonian, we now have an explicit expression for the expectation value of the Hamiltonian (i.e. the energy). To determine the ground state energy, we minimize this expression with respect to the coefficients $\phi_l$ and $\phi_{mkn}$. It follows that [58]:

$$\frac{\partial}{\partial \phi_l^*} \langle \mathcal{H} \rangle = \frac{\partial}{\partial \phi_l^*} E \langle \Psi | \Psi \rangle = E \phi_l. \tag{5.18}$$

The constant $E$ is a Lagrange multiplier, which can here be identified with the energy. Taking the derivative with respect to $\phi_{mkn}$ yields a similar expression:

$$\frac{\partial}{\partial \phi^*_{mkn}} \langle \mathcal{H} \rangle = \frac{\partial}{\partial \phi^*_{mkn}} E \langle \Psi | \Psi \rangle = E \phi_{mkn}. \tag{5.19}$$

Calculating the derivatives explicitly, we obtain:

$$\frac{\partial\langle\mathcal{H}\rangle}{\phi_l^*} = E_l\phi_l + g\phi_l\sum_{l'}U_{ll'} + g\sum_{mkn}\phi_{mkn}U_{kmln}n_k(1-n_m), \tag{5.20}$$

$$\begin{aligned}\frac{\partial\langle\mathcal{H}\rangle}{\phi_{mkn}^*} &= \Delta E_{mkn}\phi_{mkn} + g\phi_l U_{kmln}n_k(1-n_m)\\ &+ g\sum_{n'}\phi_{mkn'}U_{nn'}n_k(1-n_m)\\ &- g\sum_{k'n'}\phi_{mk'n'}U_{k'knn'}n_{k'}n_k(1-n_m)\\ &+ g\sum_{m'n'}\phi_{m'kn'}U_{mm'nn'}n_k(1-n_m)(1-n_{m'}).\end{aligned} \tag{5.21}$$

We introduce the following auxiliary quantity to shorten notations:

$$\begin{aligned}\Gamma_{mkn} &= \sum_{n'}\phi_{mkn'}U_{nn'}n_k(1-n_m)\\ &- \sum_{k'n'}\phi_{mk'n'}U_{k'knn'}n_{k'}n_k(1-n_m)\\ &+ \sum_{m'n'}\phi_{m'kn'}U_{mm'nn'}n_k(1-n_m)(1-n_{m'}).\end{aligned} \tag{5.22}$$

Now the ground state energy $E$ is the solution to the following set of equations:

$$E\phi_l = E_l\phi_l + g\phi_l\sum_{l'}U_{ll'} + g\sum_{mkn}\phi_{mkn}U_{kmln}n_k(1-n_m), \tag{5.23}$$

$$E\phi_{mkn} = \Delta E_{mkn}\phi_{mkn} + g\Gamma_{mkn} + g\sum_{l}\phi_l U_{mknl}. \tag{5.24}$$

Note that the variational coefficients $\phi_l$ and $\phi_{mkn}$ are themselves not determined yet. They can be determined simultaneously with the energy, using for instance an iterative procedure.

### 5.1.2 Number density

Now that we have obtained the ground state energy and the corresponding variational coefficients, we can determine other ground state properties with relative ease. A quantity of interest is the number density (the expectation value of the density operator) $n_\sigma(x) = \langle\psi_\sigma^\dagger(x)\psi_\sigma(x)\rangle$. Let us calculate the number density of the impurity $\downarrow$ as an example. We obtain:

$$n_\downarrow(x) = \sum_{ij}\langle\Psi|\alpha_i(x)\alpha_j(x)a_{\downarrow i}^\dagger a_{\downarrow j}|\Psi\rangle. \tag{5.25}$$

Recall that the variational wave function is given by Equation (3.3). An analogous calculation to the previous section now gives us two terms:

$$n_1 = \sum_{ijll'}\phi_{l'}^*\phi_l\alpha_i(x)\alpha_j(x)\langle 0|a_{\downarrow l'}a_{\downarrow i}^\dagger a_{\downarrow j}a_{\downarrow l}^\dagger|0\rangle. \tag{5.26}$$

Here it follows that $j = l$ and $i = l'$ so that:

$$n_1 = \sum_{ll'} \phi^*_{l'} \phi_l \alpha_{l'}(x) \alpha_l(x). \tag{5.27}$$

The term involving particle-hole excitations of the majority component is given by:

$$n_2 = \sum_{\substack{ijmkn \\ m'k'n'}} \phi^*_{m'k'n'} \phi_{mkn} \alpha_i(x) \alpha_j(x) \langle 0 | a_{\downarrow n'} a^\dagger_{\uparrow k'} a_{\uparrow m'} a^\dagger_{\downarrow i} a_{\downarrow j} a^\dagger_{\uparrow m} a_{\uparrow k} a^\dagger_{\downarrow n} | 0 \rangle, \tag{5.28}$$

which yields $j = n, i = n', m = m', k = k'$:

$$n_2 = \sum_{mknn'} \phi^*_{mkn'} \phi_{mkn} \alpha_{n'}(x) \alpha_n(x). \tag{5.29}$$

Note that terms which involve, e.g., $m = k$ are forbidden because the operators involving $m$ and $m'$ involve creating a particle beyond the Fermi surface, while the operators with indices $k$ and $k'$ create holes below the Fermi surface. For the same reason, the cross-terms involving coefficients $\phi_{l'}$ and $\phi_{mkn}$ give no contribution (unlike in the case of the ground state energy). To summarize, we obtain for the impurity density:

$$n_\downarrow(x) = \sum_{ll'} \phi^*_{l'} \phi_l \alpha_{l'}(x) \alpha_l(x) + \sum_{mknn'} \phi^*_{mkn'} \phi_{mkn} \alpha_{n'}(x) \alpha_n(x), \tag{5.30}$$

where we insert the variational coefficients as determined through the solution of Equations (5.23)-(5.24). A very similar calculation then yields the majority component density. It should be noted that since the variational Ansatz is approximative, so is the resulting density profile obtained through it. In the following section, we will more closely examine how well the Ansatz reproduces the actual energy and density in the case where we can benchmark the result using other methods.

## 5.2 The Fermi polaron in an optical lattice with additional harmonic trapping

In the following section, we will use the formalism described in the previous section to investigate the ground state properties of an impurity interacting with a majority sea of fermions in a specific realization. We take the external potential to be the sum of a periodic standing wave and an additional weak harmonic part. Optical lattices are of interest, because they can be used to model solid state systems, which tend to align atoms in regular lattices [15]. In addition, we can use quantum gases

in optical lattices to mimic various theoretical models, such as the Bose-Hubbard model, disordered models, the Heisenberg spin model, et cetera [99]. The problem of an impurity in harmonic external confinement was also considered in Ref. [100].

In one dimension, the potential is given by:

$$V_{\text{ext}}(x) = \frac{1}{2}m\omega^2 x^2 + \frac{V_0}{2}\Big(1 - \cos(2\pi k_{\text{L}} x)\Big), \tag{5.31}$$

where $\omega$ represents the strength of harmonic trapping, $m$ is the mass of a particle and $k_{\text{L}}$ is the periodicity of the optical lattice with a depth given by $V_0$. We depict the external potential we use schematically in Figure 5.1.

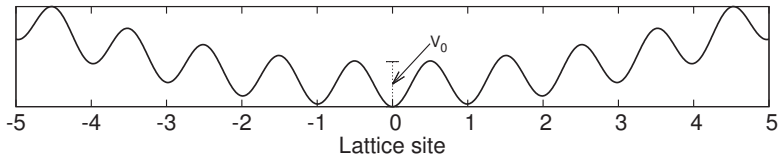


**Figure 5.1.** Schematic depiction of the potential (5.31). Particles are confined to lattice sites at the bottom of each well in the periodic lattice, where each well has a potential depth $V_0$. To ensure all particles are confined to a fixed region of space, a weak harmonic potential acts as an additional trapping potential.

One of the neat things we can now do is directly compare the results of the potential (5.31) to discrete lattice models, which only take into account confinement to lattice sites, without considering the details of the potential. The archetypal lattice model for fermions is the (Fermi-)Hubbard model[1], with a Hamiltonian given by [102]:

$$\mathcal{H}_{\text{Hubbard}} = -J\sum_{i\sigma} c^\dagger_{i\sigma}c_{i+1\sigma} + \text{H.c.} + U\sum_i c^\dagger_{i\uparrow}c_{i\uparrow}c^\dagger_{i\downarrow}c_{i\downarrow}. \tag{5.32}$$

Here $J$ is the so-called hopping parameter, which represents the kinetic energy cost for a particle to jump from one site to an adjacent one, $c^{(\dagger)}_{i\sigma}$ destroys (creates) a particle of the type $\sigma \in \{\uparrow,\downarrow\}$ on lattice site $i$, and $U$ represents the on-site interaction between particles of different spin. To compare with the continuum potential (5.31), we furthermore add an on-site potential, representing the weak harmonic part of the potential, resulting in the total lattice Hamiltonian $\mathcal{H}_{\text{lattice}}$:

$$\mathcal{H}_{\text{lattice}} = \mathcal{H}_{\text{Hubbard}} + V_h\sum_{i\sigma} c^\dagger_{i\sigma}c_{i\sigma}i^2, \tag{5.33}$$

[1]The original Hubbard model was used to describe fermions, but a bosonic analog also exists [101].

where $V_h$ represents the strength of the harmonic potential, which obviously depends on $\omega$.

To compute the ground state properties of the lattice Hamiltonian (5.33), we compare to the "numerically exact" method of time-evolving block decimation (TEBD) [103], which is closely related to the density matrix renormalization group (DMRG) method [104]. By numerically exact, we mean that the error compared to the exact solution is controllable and can be kept below a fixed, small tolerance. The TEBD method is suitable for the computation of static as well as dynamical properties of one-dimensional lattice models. It relies on the concept of *entanglement entropy*, in the sense that (under certain conditions, such as short-range interactions) correlations have a finite propagation speed within the system. TEBD exploits this slow growth of the entanglement entropy by appropriately restricting the Hilbert space, which yields it a significant speedup compared to the case where one diagonalizes the full interacting Hamiltonian. In the latter case, one is typically restricted to a dozen or so lattice sites, while with TEBD one can easily handle more than $100$ sites using contemporary computers. We will not give a detailed overview of the method here, and instead refer to some examples (beyond Publication II) of applications in Refs. [105, 106, 107].

Let us first compute the ground state energy and particle number densities for a system described by the lattice Hamiltonian (5.33), using both TEBD and the variational approach. The result is given, for various parameters, in Figure 5.2. We express the interaction in dimensionless units $U/J$, the trapping potential in units of $V_h/J$. The impurity (polaron) energy is expressed in units of the recoil energy $E_\mathrm{R} = \hbar^2 k_\mathrm{L}^2/2m$, and we scale length scales by the lattice spacing $k_\mathrm{L}/2\pi$ such that a length of $1$ corresponds to one lattice site. We fix the number of majority component particles $N = 20$. This may not seem like a "many-body" system, but in the case of the impurity problem, the many-body limit is approached surprisingly rapidly [108, 109], and 20 majority component particles turns out to be more than sufficient. We consider a fixed number of lattice sites $L$ with boundary conditions so that the wave function vanishes at the boundary of the system, i.e. we assume an infinite barrier outside our system.

*Ground state energy.* — The result of Figure 5.2 shows that the variational Ansatz provides excellent agreement with numerically exact results for the ground state energy, especially in the weakly interacting and attractive regimes. In the latter case, the polaron energy is dominated

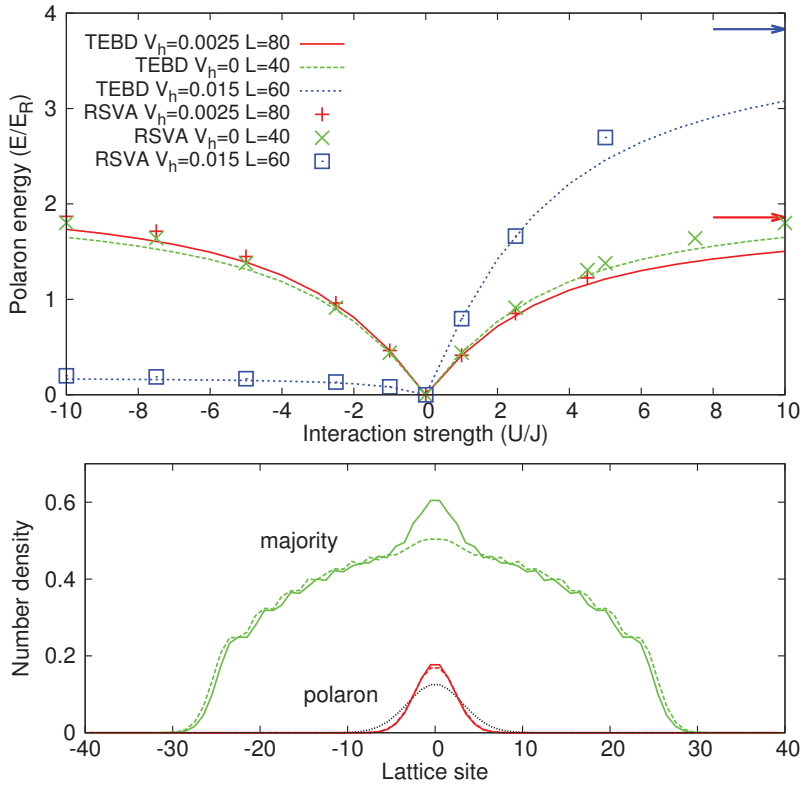


**Figure 5.2.** Top: ground state energy for an impurity immersed in a Fermi sea of $N = 20$ majority component fermions, for various harmonic trapping strengths $V_h$ and various system sizes with $L$ lattice sites. Lines show the TEBD result, while symbols show the result of the variational calculation. Arrows indicate the infinitely repulsive limit, computed using the single-particle spectrum. On the attractive side ($U < 0$), we have subtracted the maximum on-site interaction energy $U/J$. Bottom: number densities of the majority component and the impurity for fixed interaction strength $U/J = -10$ and $V_h/J = 0.0025$. The solid green line shows the TEBD prediction for the majority component density, while the dashed green line shows the variational result. The solid red and dashed red lines show the density for the impurity (polaron). For comparison, the number density for a single non-interacting particle is also shown as a dotted black line. Figure adapted from Publication II. Copyright (2014) by the American Physical Society.

by the on-site interaction of pairs, which takes a maximum value of $U/J$, which occurs when the impurity is guaranteed to be found with a majority component fermion at some site. In the figure, this contribution is subtracted, but even then the agreement is excellent. On the strongly repulsive side, the iterative procedure breaks down close to $U/J \approx 5$, but provides good agreement up to that point. It is interesting to note that the result for trapping $V_h = 0.0025$ and number of lattice sites $L = 80$ closely resembles that of the lattice-only case without harmonic trapping and $L = 40$. This is because the weighted average density (in the region where

the impurity density is significant) is approximately equal to the density over the entire lattice in the lattice-only case. This suggests that the approach employed in Ref. [109], employing a local density approximation (LDA) is valid to a good approximation. The excellent agreement on the attractive side is a peculiar feature of one-dimensional systems [62]. Note also that the Ansatz consistently *over*estimates the ground state energy. This must be the case, since the variational approach restricts the possible configurations of the system; the lowest energy-state it finds must therefore be an excited state for the system without any restrictions in the number of particle-hole excitations. In three dimensions, the Ansatz needs to be adjusted to properly take into account pairing [53, 54, 55, 56].

*Number density.* — The bottom panel of Figure 5.2 shows the prediction for the number density as computed using the variational coefficients. For the density of the polaron, we find good agreement with the TEBD prediction, with only a minor discrepancy. However, the majority component density profiles are significantly different, with the TEBD result showing a much stronger peak in the centre, where the impurity is localized due to the harmonic trapping potential. This suggests two things: the energy can change weakly with significant changes in the majority component density, and the variational method outlined above is not suitable for determining the majority component density in the impurity problem.

### 5.2.1 Incorporating higher lattice bands

The lattice model (5.33) is a so-called *lowest band approximation* (LBA). This means that the high-energy physics is explicitly neglected, an approximation that is justified if the lattice depth $V_0$ is sufficiently deep [49, 110]. The reason this approximation tends to work reasonably well is that the dispersion will show a *band gap* of order $V_0$ near the edge of the first band, which implies that scattering to higher bands is suppressed, since it takes a large amount of energy to access higher bands.

However, it is still of interest to carefully investigate when the LBA breaks down for an interacting system. To do so, we explicitly compute the ground state energy for a continuum system trapped by the external potential (5.31), using the variational approach. We take various values of the lattice depth $V_0$ (expressed in units of the recoil energy $E_\mathrm{R}$) and study the behaviour of the ground state energy for attractive interactions, for which we know that the Ansatz works well. The result is shown in the main panel of Figure 5.3. Since it is numerically more challenging to

consider the lattice-resolved case, we will consider a smaller system with $L = 16$ lattice sites, slightly stronger harmonic trapping with $V_h = 0.1$ and $N = 6$ majority component particles. The on-site interaction is now replaced by a zero-range contact interaction, with a strength chosen so that it is mapped onto the lattice model. Thus, we have the inter-particle potential described by:

$$V_{\text{int}}(x - x') = g\delta(x - x'). \tag{5.34}$$

We now simply scale the interaction parameter $g$ linearly such that it corresponds to the value of the energy predicted by the lattice model in the weakly interacting limit $|U/J| \ll 1$, an approach that is justified because the polaron energy scales linearly with $g$ in the weakly interacting limit in all systems where the local density approximation can be applied.

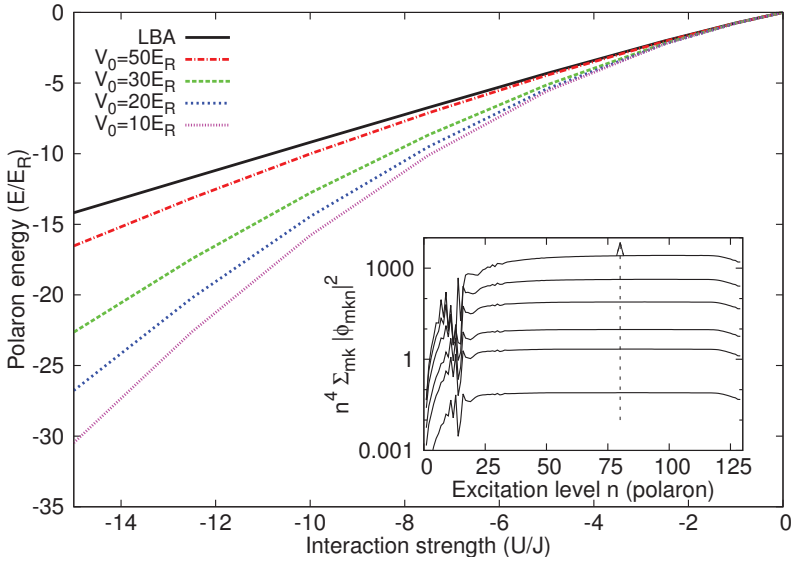


**Figure 5.3.** Ground state energy of an impurity interacting through attractive contact interactions. The black line shows the ground state energy as predicted using the single-band lowest band approximation (LBA), with a Hamiltonian described by Equation (5.33). Coloured lines show the energy obtained through a variational calculation in the continuum case (5.31). The chosen parameters are (see main text) $L = 16$, $V_h = 0.1$ and $N = 6$. Inset (note the log scale): occupation probability of highly excited states for various values of the interaction $-U/J = 0.1, 0.5, 1.0, 2.5, 5.0, 10.0$, showing universal scaling behaviour expected from Tan's universal relations. The lattice depth is taken to be $V_0 = 10E_{\text{R}}$, and parameters are otherwise the same as for the main figure. The arrow indicates increasing values of the magnitude of the interactions $|U/J|$. Figure adapted from Publication II. Copyright (2014) by the American Physical Society.

As is shown in Figure 5.3, the lowest band approximation appropriate for a lattice model works well for weak interactions $|U/J| \leq 1$. However,

for a realistic lattice depth of $V_0 = 10E_\mathrm{R}$ the LBA breaks down quickly, and even for very deep lattices we find significant deviations from the LBA. Here it appears that the additional harmonic trap implies that the LBA is not as good an approximation as in the case where only a (continuum) lattice is present, since in that case the LBA is known to be a decent approximation as long as $|U/J| \leq V_0/E_\mathrm{R}$ [49]. Indeed, by directly comparing to the case $V_h = 0$, we have determined that at $U/J = -10$ about two thirds of the deviation of the ground state energy compared to the LBA prediction is due to the additional harmonic trapping.

There is an additional interesting observation we are now able to make. Since we have zero-range contact interactions between the particles in the system, we know that the Tan relations discussed in Chapter 2 are valid. In particular, the momentum distribution $n(k)$ of the system obeys:

$$n(k) \to \frac{C}{k^4}, \quad (k \to \infty), \tag{5.35}$$

where $C$ is the contact parameter. This momentum tail decays only weakly, with a power law dependence on momentum $k$. Therefore, we must have finite occupation of the high-energy states beyond the band gap even for a weakly interacting system. The summed occupation probability $Q$ of the impurity in the state $n$ with arbitrary single particle-hole excitations is given by:

$$Q = \sum_{mk} |\phi_{mkn}|^2. \tag{5.36}$$

Since the highly excited states are approximately equal to standing waves with a dispersion $\propto k^2$, we should expect the quantity $Q$ to have a $1/n^4$ decay, analogous to the decay of the momentum distribution. The inset of Figure 5.3, where we have plotted the quantity $n^4 Q$, shows that this is indeed the case. At low energies, this quantity has features related to the details of the potential, with some sharp features around the edge of the first band[2], near $n = 16$. The occupation probability then gradually approaches the regime where it decays smoothly according to the expected $1/n^4$ decay. This is precisely what we would expect to happen according to Tan's analysis, because we expect the asymptotic regime to set in when momentum $k$ is much larger than any relevant inverse length scale. In this system, the relevant length scale is the lattice spacing, which in momentum space corresponds to the edge of the lowest band. Note that the contact tail is visible even for weak interactions, $U/J = -0.1$. Indeed,

[2]The observer with a keen eye may also notice less pronounced features near the edge of the second band, around $n = 32$.

we should expect the strength of this tail to scale as $U^2$ (see the discussion on the homogeneous polaron in Chapter 4 and Ref. [28]), which is in agreement with the plotted results.

Therefore, while the lattice model provides a decent approximation for the polaron energy at weak coupling, we must be careful when using it. Not only does the approximation break down earlier if an additional harmonic potential is added, but the lowest band approximation neglects physics related to Tan's universal relations as discussed in Chapter 2. In this particular system, throwing away the physics related to the contact is not necessarily a critical error, but in Chapter 7 we will investigate a situation where this is the case. This happens when the external potential is disordered. Such systems are often described using lattice models. In the following chapters we will show that such a description is, in certain respects, inadequate.

# 6. Quantum gases in disorder

In this chapter, we will consider the case where particles are under the influence of a potential that is (in some sense) *random*. This case is of interest because real materials are not perfect – a metal, for instance, contains randomly distributed impurities, lattice defects, etc. These disturbances can drastically alter the macroscopic features of materials. Disordered systems were investigated in Publication III.

Using ultracold atoms, we can mimic the appearance of disorder in solid state systems by using a trapping potential that is disordered [17, 111, 112, 113, 114]. There are several ways to do this. One method involves using a diffusive plate to create a so-called *speckle potential* [19]. This kind of potential has the property that the potential at two points sufficiently far from each other is completely uncorrelated, while at distances on the order of the *correlation length* correlations appear. Thus, the potential only appears random on distances sufficiently larger than the correlation length. A second method involves superimposing two standing waves [20]. Suppose that the standing waves have periodicities $k_a$ and $k_b$ and the amplitude of the first wave is much greater than that of the second one. Now, if one chooses the ratio $k_a/k_b$ such that it is close to (for instance) the golden ratio $(1+\sqrt{5})/2 \approx 1.618...$ then the resulting potential is said to be *quasi-periodic*. This means that while the resulting potential is periodic on very long length scales, the second standing wave causes a disturbance in the local minima of the first wave that approximates purely random behaviour. An alternative scenario involves so-called *binary disorder*, which can take only two possible values. Such a system can be realized through the use of impurities, which are randomly distributed throughout an optical lattice [115, 116, 117, 118].

## 6.1 Anderson localization

The first systematic study of disorder in quantum systems dates back to Anderson [18], who showed that in certain disordered systems, the eigenstates of the system become *localized* in the sense that the eigenstates have exponentially decaying tails. In fact, Anderson proved that in one dimension[1], *all* eigenstates are exponentially localized at *any* disorder strength! This remarkable result was obtained for the following lattice model:

$$\mathcal{H}_{\text{Anderson}} = -J \sum_i c_i^\dagger c_{i+1} + \text{H.c.} + \sum_i V_{\text{ext}}^i c_i^\dagger c_i, \tag{6.1}$$

where $J$ is the hopping parameter, which determines the kinetic energy required to jump from one site to an adjacent one, and $V_{\text{ext}}$ now indicates an on-site potential and takes a random value in the interval $[-W/2, W/2]$, where $W$ can be identified with the strength of the disorder. If $W = 0$, then we obtain a homogeneous lattice model with non-interacting particles, and all of the eigenstates are just extended states with some momentum. However, for non-zero $W$ the eigenstates are localized and exhibit exponential decay which is at least as strong as $\exp(-|x|/\xi_{\text{A}})$, where $x$ is a site sufficiently far from the peak of the density. The quantity $\xi_{\text{A}}$ is called the *Anderson localization length*, which depends only on $W/J$ [120].

Thus, if one takes an arbitrary wave packet, initially (at a time $t = 0$) centred about some lattice site $i$ then transport is suppressed at all times at least as strongly as $\exp(-|x|/\xi_{\text{A}})$ sufficiently far away from the lattice site $i$. This suppression of transport, or localization, is a general wave phenomenon and has been observed in the aforementioned ultracold atom experiments, but also for e.g. light waves [121, 122] and sound [123].

## 6.2 Realistic disordered potentials: the appearance of correlations

While the Anderson model (6.1) describes non-interacting disordered systems adequately, it does have some anomalous features. One of the features in particular is that in the Anderson model, the disorder at one lattice site does not depend on the disorder at other sites. While this can be a good approximation, it cannot be true in general for a continuum system, because the absence of correlations on *any* length scale implies that the Fourier spectrum of the potential is unbounded, and the energy density

[1] In three dimensions, there is a mobility edge [119], a certain energy below which the eigenstates are localized. Above the mobility edge, the states are extended.

of the potential then goes to infinity. Thus, correlations in the disordered potential must arise at some length scale, which we can identify with the aforementioned correlation length, denoted by $\sigma$. In the experiment, such correlations are generated from a speckle or quasiperiodic potential, but here we will consider Gaussian correlations[2]. The Gaussian disordered potential on a certain lattice site $x$ takes the following discretized form (in 1 spatial dimension):

$$V_{\mathrm{Gaussian},x} = \frac{1}{\sqrt{\pi\sigma}} \sum_y \mathcal{W}_y \exp\left[\frac{-(x-y)^2}{2\sigma^2}\right], \tag{6.2}$$

where $\mathcal{W}_y \in [-W/2, W/2]$. An example realization of such a potential is depicted in Figure 6.1.

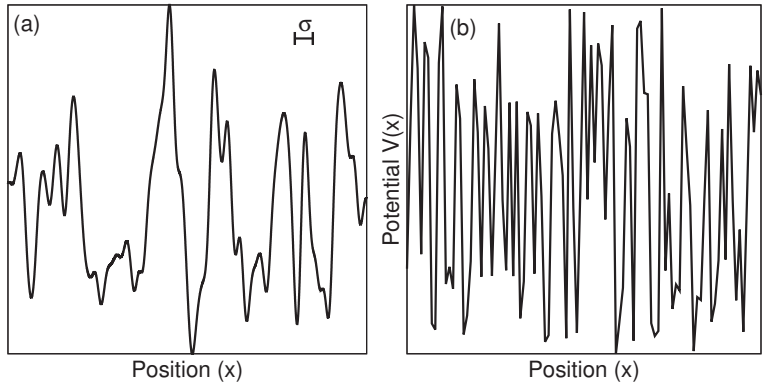


**Figure 6.1.** Schematic depiction of a Gaussian disordered potential and an uncorrelated potential. The correlation length is depicted in the left panel by $\sigma$. Figure from Publication III.

The Gaussian correlated potential (and correlated disordered potentials in general) has some properties which are similar to the case of uncorrelated disorder. At low energies, the single-particle wave functions are localized exponentially in both cases. However, when the energy approaches the value corresponding to the correlation length, that is $E_\sigma \approx \hbar^2/2m\sigma^2$, the localization length increases relative to the case of uncorrelated disorder. At high energies $E \gg E_\sigma$ the localization length diverges exponentially, so that for finite-sized systems transport from one side of the system to the other side is no longer suppressed [124].

[2]Gaussian correlated potentials are slightly easier to handle numerically.

# 7. Non-equilibrium dynamics; the interaction quench

Although it's nice to know what the static properties of a system are, nature is not static, and we would like to know how systems change over time. That is, we want to determine the *dynamic* properties of systems. This is relevant for quantum computing, the study of localization, quantum chaos and research into the thermalization of closed systems [125]. Furthermore, this touches on fundamental questions relating to the foundations of quantum mechanics; since wave function collapse is a *dynamical* phenomenon, we ideally would like to have a fully time-dependent description of it and be able to reproduce it from first principles. However, this turns out to be far from easy [126, 127].

In this thesis, our goal will be slightly less ambitious and we will study a so-called quantum *quench*. The idea is as follows. Suppose we have a system that is described by a Hamiltonian $\mathcal{H}$. At a time $t = 0$, we change the Hamiltonian in some way, so that we obtain a new Hamiltonian $\mathcal{H}'$. The change in the Hamiltonian (in the context of an ultracold atom experiment) might correspond to, for example, switching an external trap on or off [128, 129, 130] or suddenly changing the strength of the inter-particle interactions.

## 7.1 Quench-induced delocalization

We will here consider the following scenario (discussed in Publication III), which falls under the category of an *interaction quench*. Consider a short-range interacting system in the ground state of the Hamiltonian $\mathcal{H} = \mathcal{H}_0 + g\mathcal{H}_{\text{int}}$, where the interactions between the particles are contained in the part of the Hamiltonian described by $\mathcal{H}_{\text{int}}$. At a time $t = 0$, we turn off the interactions. Can we now say something general about the dynamics of the system after the quench? As it turns out, we can in fact

do so, with the aid of Tan's relations discussed in Chapter 2. Recall that the high-momentum tail of the momentum distribution $n(k)$ is given by (2.2):

$$n(k) \to \frac{C}{k^4}, \quad (k \to \infty). \tag{7.1}$$

This relation tells us that the initial system has an algebraically decaying high-momentum tail.

Now we consider the situation where the non-interacting part of the Hamiltonian $\mathcal{H}_0$ contains both bound states (restricted to some localized region) and scattering (delocalized) states. The former is often the case, especially in an ultracold atom experiment, where the cloud of atoms is held in place using optical devices. The latter is *always* the case for a continuum external potential which is bounded from above. This is because of the same reason as realistic disordered potentials must have short-correlations at least at some scale (however small), see Chapter 6. A particle with momentum $k$ does not "feel" changes in the potential occurring at length scales much larger than $k^{-1}$, but the external potential contained in the non-interacting Hamiltonian $\mathcal{H}_0$ cannot have significant variations at arbitrary length scales. So there must be some regime of high momentum where the corresponding variations in the external potential are weak, and the single-particle eigenstates corresponding to these momenta are scattering states. Now if the momentum distribution had been similar to the Fermi-Dirac distribution, with its exponentially decaying tail, then this conclusion would not necessarily be very meaningful. The Fermi-Dirac distribution decays rapidly, so the occupation of high-momentum states is negligible. However, the $1/k^4$-tail in the momentum distribution decays only algebraically, so its contribution cannot be neglected[1].

Suppose that the initial interacting state is localized and would remain so under the influence of the full Hamiltonian $\mathcal{H}$. In such a system, the high-momentum states are still occupied, but they are interfering destructively so that no delocalization occurs. What the interaction quench does is introduce a source of *dephasing* into the system[2]. The eigenstates of $\mathcal{H}$ are projected onto the new Hamiltonian $\mathcal{H}_0$. $\mathcal{H}_0$ describes a non-interacting system, and the phases of the different components will change as a function of time with varying frequencies. Then, in the limit

[1]Except in the limit where the temperature $T \to \infty$ and the dimensionality is larger than one. In this limit, the virial expansion based on the Maxwell-Boltzmann distribution is valid [34].

[2]Dephasing has also been associated with transport in a completely different system consisting of a chain of quantum dots [131] and in a Mott insulator [132].

$t \to \infty$, when to a good approximation all the phases are uncorrelated, all the initial correlations between the phases are lost, and the particles occupying the high-momentum states will propagate ballistically.

## 7.2 The diagonal ensemble

We will illustrate how the dephasing manifests itself by considering a simple example: two distinguishable interacting particles in one dimension, where we denote the particles by $\uparrow$ and $\downarrow$. We consider particles interacting through the contact potential $V_{\text{int}} = g\delta(x - x')$, and assume that there is some external potential $V_{\text{ext}}(x)$. In the language of the previous section, the full Hamiltonian $\mathcal{H}$ and its non-interacting and interacting parts ($\mathcal{H}_0$ and $\mathcal{H}_{\text{int}}$ respectively) are given by:

$$\begin{aligned}\mathcal{H} = \mathcal{H}_0 + \mathcal{H}_{\text{int}} = &\sum_\sigma \int dx\, \psi_\sigma^\dagger(x)\Big[ -\frac{\hbar^2}{2m}\frac{d^2}{dx^2} + V_{\text{ext}}(x)\Big]\psi_\sigma(x) \\ &+ g\int dx\, \psi_\uparrow^\dagger(x)\psi_\downarrow^\dagger(x)\psi_\downarrow(x)\psi_\uparrow(x),\end{aligned} \tag{7.2}$$

where $\psi_\sigma^{(\dagger)}(x)$ destroys (creates) a particle of the kind $\sigma \in \{\uparrow, \downarrow\}$ at position $x$. Analogous to Equation (3.3), we can write the wave function for this system as follows:

$$|\Psi\rangle = \sum_{mn} \phi_{mn} c_{\uparrow m}^\dagger c_{\downarrow n}^\dagger |0\rangle, \tag{7.3}$$

where $|0\rangle$ represents the vacuum and the operators $c_{\sigma k}^\dagger$ create a particle in the state $k$ and spin $\sigma$. Given an appropriate method to determine the coefficients $\phi_{mn}$, Equation (7.3) represents an *exact* solution to the two-body problem. As a choice for the states that the operators $c$ create, we can take the eigenstates of the non-interacting Hamiltonian $\mathcal{H}_0$, which can be determined analytically in certain cases such as the infinite well or the harmonic oscillator and can be straightforwardly determined numerically otherwise. Let us sort these eigenstates in ascending order of their corresponding eigenenergies so that they form a complete set $\alpha_0(x), \alpha_1(x), \ldots, \alpha_n(x), \ldots$, with corresponding eigenenergies $E_0, E_1, \ldots, E_n, \ldots$ (for simplicity, let us assume the spectrum is not degenerate).

Suppose that at a time $t = 0$, we have found the solution to the interacting two-body problem and have knowledge of the coefficients $\phi_{mn}$. We now turn off the interactions: $g = 0$. The density (of e.g. the $\uparrow$-component)

is given at a time $t > 0$ by (setting $\hbar = 2m = 1$):

$$\langle \psi_\uparrow^\dagger(x,t)\psi_\uparrow(x,t)\rangle = \sum_{mnj} \phi_{mn}^* \phi_{jn} \alpha_j^*(x)\alpha_m(x) e^{i(E_j - E_m)t}. \tag{7.4}$$

*Assumption* — after a long time, the different components propagate with different phase velocities $E_j - E_m$, which in principle are arbitrary. Therefore, it is reasonable to suppose that these components have significant destructive interference, i.e. we assume *dephasing*. Meanwhile, the components with $j = m$ are not affected by these interference effects. The time-averaged density is therefore to a good approximation (where the overbar denotes a time average over a sufficiently long interval):

$$\eta(x) = \lim_{t\to\infty} \overline{\langle \psi_\uparrow^\dagger(x,t)\psi_\uparrow(x,t)\rangle} = \sum_{mn} |\phi_{mn}|^2 |\alpha_m(x)|^2. \tag{7.5}$$

This equation represents the *diagonal ensemble* [133, 134, 135, 136] with respect to the density operator, first introduced in this context by Deutsch [137].

It turns out that the assumption of dephasing leading to the diagonal ensemble is a pretty good one, as we will show for two examples. In fact, since the one-dimensional two-particle system is sufficiently simple, we can explicitly verify that it works by comparing it to the exact result of Equation (7.4). First, we will consider the case where the two particles are trapped in a simple finite well. Then we will consider the case of disorder as discussed in Chapter 6.

## 7.3 The finite well

The finite well is an archetypical potential that one encounters almost immediately in an elementary quantum physics textbook. This is an interesting scenario, because it is one of the simplest systems where one encounters a single-particle spectrum consisting of both bound and scattering eigenstates. Suppose that our two particles are trapped in a finite well of width $\Delta X$ and depth $V_0$, as schematically depicted in Figure 7.1. The potential is thus given by:

$$V_{\text{ext}}(x) = \begin{cases} -V_0 & \text{if } |x| \leq \Delta X/2, \\ 0 & \text{otherwise.} \end{cases} \tag{7.6}$$

For sufficiently large values of $V_0$, this potential will admit at least one bound state. The lowest energy eigenstate of the non-interacting system, $\alpha_0(x)$, then has a corresponding eigenenergy $E_0 < 0$. There will be a

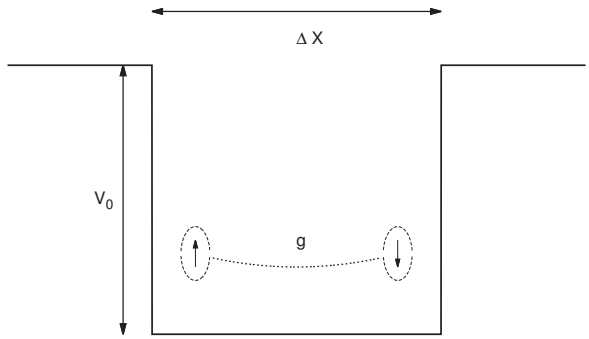


**Figure 7.1.** Schematic depiction of two distinguishable particles, denoted by $\uparrow$ and $\downarrow$, in a finite well of depth $V_0$ and width $\Delta X$. The inter-particle potential has strength $g$.

limited number of these localized eigenstates, and the remaining eigenstates (with higher energy) are delocalized scattering states, which can no longer be normalized. The ground state properties of the system were previously investigated in the limit that at most one particle escapes the well, using the Bethe Ansatz [138]. In addition, a general solution can be obtained for the infinite well and periodic boundary conditions [139]. However, obtaining the coefficients $\phi_{mn}$ from the Bethe Ansatz solution is not straightforward, so we opt for a numerical solution using a method analogous to the computation of the variational coefficients of Equation (3.3).

If the initial interaction strength $g = 0$, then the ground state of the system will simply have both particles in the eigenstate $\alpha_0(x)$. In this case, the coefficients $\phi_{mn}$ can be determined quite easily: $|\phi_{00}|^2 = 1$ and all the other coefficients are zero. For weak interactions, we can expect the coefficient $\phi_{00}$ to dominate, while the other coefficients will get some non-zero occupation.

Let us define the following dimensionless interaction parameter $\gamma = g/V_0\Delta X$. We compute the interacting ground state of a system with $V_0 = 30$ for a closed system of length $L/\Delta X = 8$, express time in units of $1/V_0$ and use fixed boundary conditions so that the wave function vanishes at the boundary. In principle, a closed system such as this permits only localized states since all wave functions vanish outside the boundaries $x = \pm 4\Delta X$. However, we can to a good approximation associate the states spread throughout the whole length of the system with the scattering con-

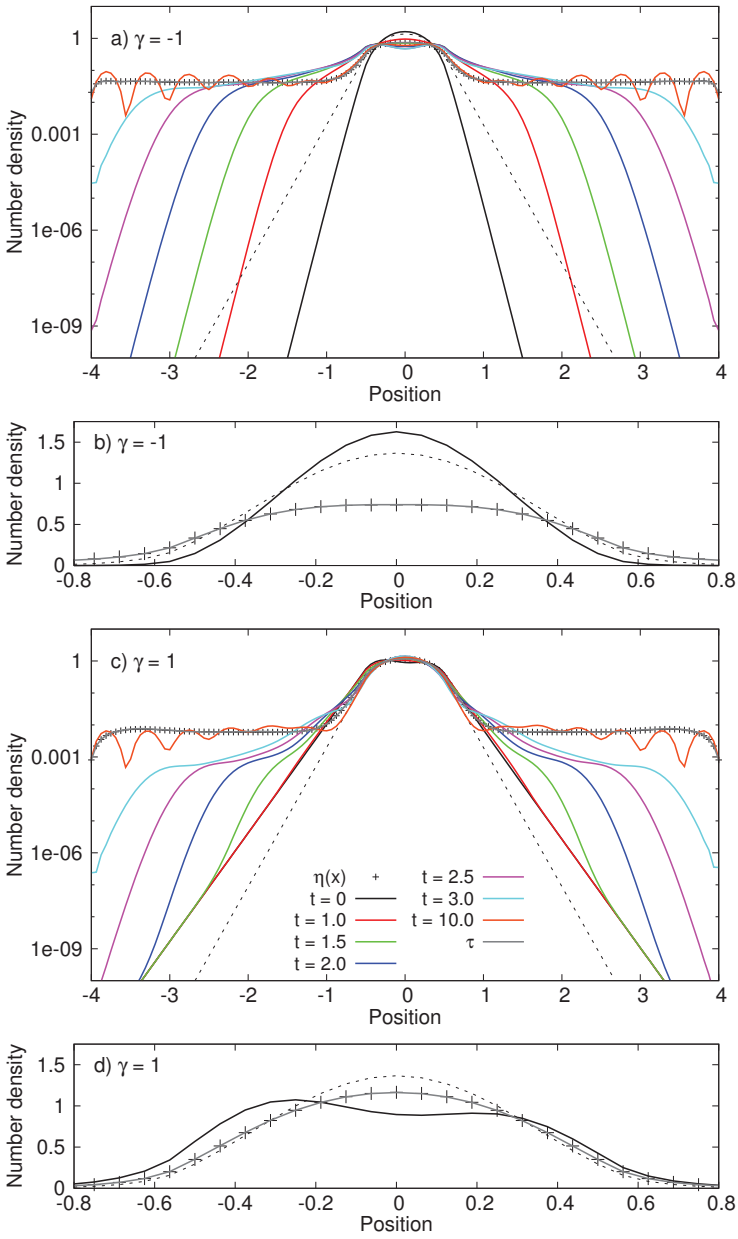


**Figure 7.2.** Number density of a particle after an interaction quench from $\gamma = -1$ (attractive, panel **(a)**) and $\gamma = 1$ (repulsive, panel **(c)**) to zero interactions $\gamma = 0$. Panels **(b)** and **(d)** show zoomed regions. Note the log scale, and that the $x$-coordinate represents position in units of $\Delta X$. Time-dependent densities are computed using Equation (7.4), while plus symbols indicate the result of the diagonal ensemble (7.5). The grey line indicates a time-averaged result of many densities in the interval $t \in [100, 200]$, the dashed line indicates the ground state of the non-interacting system. Figure adapted from Publication III.

tinuum of the open system. At a time $t = 0$ we switch off the interactions and we study the time evolution of the system according to Equation (7.4). We can then check explicitly whether the predictions of the diagonal ensemble are reproduced. The result is shown in Figure 7.2.

The result shows that the diagonal ensemble (7.5) is indeed in very good agreement with the time average obtained from (7.4), for both attractive ($\gamma = -1$) and repulsive ($\gamma = 1$) inter-particle contact interactions. Observe that the initial state at $t = 0$ is exponentially localized regardless of the sign of the interaction[3]. In the case of attractive interactions, the exponential decay is slightly stronger, as tunnelling is suppressed due to the negative interaction energy of the particles. Conversely, this makes the decay weaker for repulsive interactions. There is also a breaking of symmetry for repulsive interactions clearly visible in panel **(d)** of Figure 7.2. Note, however, that the total density of both particles remains symmetric – here, the algorithm "chooses" either the "left" or "right"-oriented density profile for one of the particles.

After the interactions are turned off at $t = 0$, a wave starts expanding in both the attractive and repulsive cases, with an identical propagation speed (numerically we have determined this speed to be approximately equal to $V_0 \Delta X$). This propagating wave represents the elements $\phi_{mn}$ corresponding to scattering states. The loss of coherence leading to dephasing is therefore clearly visible over time. After some time, the waves reach the boundary of the system, from where they will reflect. This leads to the interference pattern visible in the result for $t = 10$.

After a long time, there is an approximately constant density corresponding to the fraction of particles in scattering states. Let us define this density, $\eta_{\text{far}} = \eta(x = 2.5\Delta X)$, so that we can associate the fraction of delocalized particles with the quantity[4] $L\eta_{\text{far}}$. In Figure 7.3 we plot the density obtained from the diagonal ensemble as well as the value of $\eta_{\text{far}}$. Note how for weak interactions, the delocalized fraction is independent from the sign of the interaction, and scales as $\gamma^2$. In this limit, the long-time density $\eta(x)$ also does not depend on the sign of $\gamma$. This scaling behaviour is expected, because in the weakly interacting limit the contact

[3] In the limit of very strongly repulsive interactions, $g \to \infty$, the situation is not so clear-cut, but we will not consider this case here.

[4] As $L$ is increased, the waves behave the same but will be bouncing back and forth in a larger system, so that $\eta_{\text{far}}$ scales as $1/L$. In the limit that $L \to \infty$ we obtain an open system, and the waves will propagate outwards indefinitely; however, the fraction of particles delocalized remains the same.

depends in exactly the same way on the interactions [28], see also Publication I. The algebraic behaviour of the delocalized fraction as a function of interaction is noteworthy, because it shows that even a quench from small finite to zero interactions can produce significant delocalization.

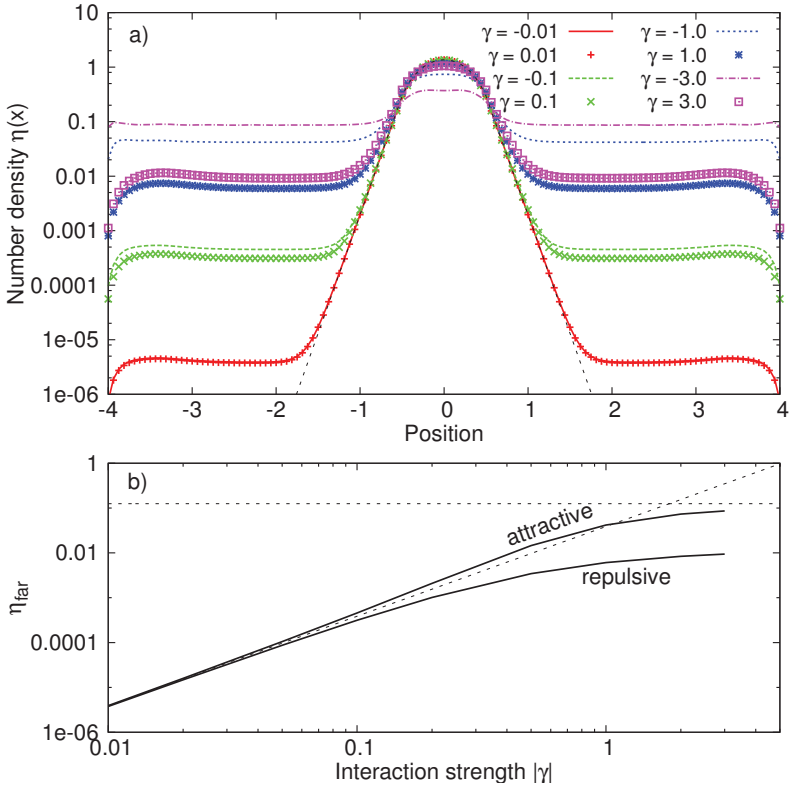


**Figure 7.3.** The long-time density after an interaction quench for two particles interacting through a contact potential, initially trapped in a finite well of depth $V_0$ and width $\Delta X = 1$. Panel **(a)** shows the value of $\eta(x)$ as computed using Equation (7.5) for various initial values of the inter-particle interaction $\gamma$, where the dashed line shows the non-interacting single-particle ground state. Panel **(b)** shows the value of $\eta_{\text{far}} = \eta(x = 2.5\Delta X)$ as a function of the initial interaction. The diagonal dashed line shows the weakly interacting limit with a slope $\kappa \approx 0.31$ (see main text), and the horizontal line shows the expected limit ($L\eta_{\text{far}} = 1$) for infinitely strongly attractive particles. Figure adapted from Publication III.

At strong interactions, the delocalized fraction $L\eta_{\text{far}}$ approaches 1 in the case of attractive interactions, cf. the divergence of the contact at infinitely attractive interactions. Meanwhile, for strongly repulsive interactions, the delocalized fraction approaches a fixed limit smaller than 1, analogous to the saturation of the contact at infinitely repulsive interactions [28]. The slope in the weakly interacting limit can be deduced from a simple perturbative calculation. Let us define this slope according to the

dimensionless constant $\kappa$, which obeys:

$$\eta_{\text{far}} = \frac{\kappa\gamma^2}{L}, \tag{7.7}$$

which is just another way of saying that the delocalized fraction of particles $L\eta_{\text{far}}$ is proportional to $\gamma^2$ with proportionality constant $\kappa$. The occupation probability $P$ for a scattering state with momentum $q$ is now:

$$P_q = \frac{(gn_0)^2}{(2E_q - 2E_0)^2}, \tag{7.8}$$

where $n_0$ is the density [82]. By integrating over the occupation probability of all scattering states we obtain the total number of particles in scattering states $N_{\text{s}}$:

$$N_{\text{s}} = \frac{1}{2\pi L}\int dq\, P_q = \frac{\kappa\gamma^2}{L}. \tag{7.9}$$

Now if we assume that the dispersion of the scattering states is given by the free particle dispersion $E_q \approx \hbar^2 q^2/2m$, $E_0 \approx V_0$ and $n_0 \approx 1/\Delta X$, then this calculation yields $\kappa \approx 0.31$, which is the same (to these two digits) as the value obtained by fitting the slope in Figure 7.3b.

### 7.3.1 The contact tail and finite-range interactions

Since the one-dimensional two-particle system is sufficiently simple, we can explicitly consider the influence of the range of the interactions. This case is of interest, because the zero-range contact potential is obviously only an approximation and real systems must have more complicated inter-particle potentials[5]. We do this by numerically simulating the system described by the following Hamiltonian:

$$\begin{aligned}\mathcal{H} = \mathcal{H}_0 + \mathcal{H}_{\text{int}} = \textstyle\sum_\sigma \int dx\, \psi^\dagger_\sigma(x)\Big[-\frac{\hbar^2}{2m}\frac{d^2}{dx^2} + V_{\text{ext}}(x)\Big]\psi_\sigma(x) \\ + \textstyle\int dx\, \psi^\dagger_\uparrow(x)\psi^\dagger_\downarrow(x')V_{\text{int}}(|x-x'|)\psi_\downarrow(x')\psi_\uparrow(x),\end{aligned} \tag{7.10}$$

which is the same as the Hamiltonian considered in the previous section, except for the interaction term.

We model the inter-particle interactions using a Gaussian potential described by:

$$V_{\text{int}}(|x-x'|) = \frac{g}{r_0\sqrt{2\pi}}\exp\Big(\frac{-(x-x')^2}{2r_0^2}\Big). \tag{7.11}$$

This potential has the feature that in the limit that the range of the interaction $r_0 \to 0$ we obtain the contact potential used in the previous section.

[5] For recent studies of systems with finite-range interactions, see e.g. [140, 141, 142, 143].

However, it is not a *long-range potential*[6] in the sense that we can cut off the interactions beyond some point (we choose $2r_0$) to a good approximation.

The high-momentum scattering states are, to a good approximation, standing waves inside the closed system (see also Publication II), with energy $E = \hbar^2 k^2/2m$. Therefore, we should expect that the high-momentum contact tail (2.2) is reflected in a $1/E^2 \propto 1/k^4$ decay of the occupation of states with fixed energy. We can show this decay by plotting the occupation of the states $\phi_{nn}$ as a function of the energy of the single-particle energy $E_n$, which we depict in Figure 7.4. We express energies in units of $\hbar^2/2m\Delta X^2$ and the range in units of the finite well width $\Delta X$. At low energies, we see some features related to the specifics of the potential (in this case, the finite well), which crosses over to a universal regime. For zero-range interactions, we obtain the expected $1/E^2$ scaling of the occupation numbers at all energies beyond this crossover regime. However, for finite-range interactions this contact regime breaks down near the energy scale $\hbar^2/2mr_0^2$, and the occupation probability $|\phi_{nn}|^2$ decreases much more rapidly than the scaling expected from Tan's asymptotic momentum distribution. This breaking down of universal behaviour is consistent with our treatment in Chapter 2, where we discussed the regime of validity of Tan's universal relations with respect to the range of the inter-particle potential $r_0$.

## 7.4 Delocalization in a disordered system

We can extend the analysis of the finite-well case to the case of a disordered potential (for related studies of two particles in disordered systems, see e.g. [144, 145]). As discussed in Chapter 6, if the disordered potential has short-range correlations, then there will be a crossover to extended single-particle states at high energies. Following the analysis in the previous sections, we should expect an interaction quench from finite to zero interactions to lead to delocalization through these single-particle states, as long as the range of the correlations (sufficiently) exceeds the range of the interactions. Here we will take for the sake of simplicity the range $r_0 = 0$, so that any non-zero correlation in the disordered potential will

[6]Examples of long-range potentials are the Coulomb potential and the gravitational potential.

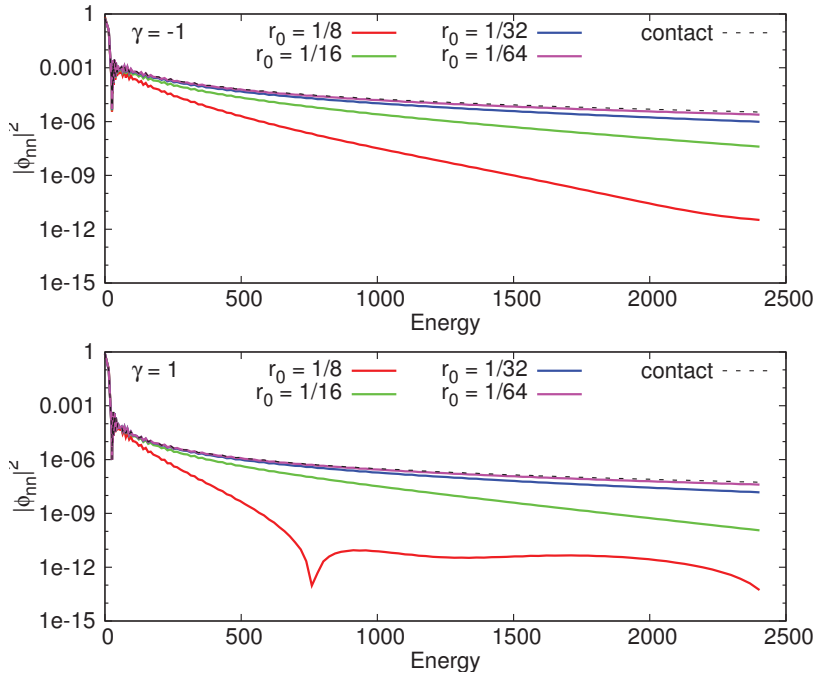


**Figure 7.4.** Occupation probability $|\phi_{nn}|^2$ of both particles occupying the $n$'th single-particle eigenstate as a function of the energy $E_n$ of the $n$'th state. The dashed line indicates the result from using zero-range contact interactions. The top figure shows the result for attractive ($\gamma = -1$) interactions and the bottom figure shows repulsive ($\gamma = 1$) interactions. Figure adapted from Publication III.

lead to delocalization. As a reminder, the potentials are then given by:

$$V_{\text{uncorrelated},x} = \mathcal{W}_x, \tag{7.12}$$

$$V_{\text{Gaussian},x} = \frac{1}{\sqrt{\pi\sigma}} \sum_y \mathcal{W}_y \exp\left[\frac{-(x-y)^2}{2\sigma^2}\right], \tag{7.13}$$

where $\mathcal{W}_x$ is a random number[7] in the interval $[-W/2, W/2]$ and the extra factor of $\sqrt{2\sigma}$ is to ensure the amplitude of the peaks and troughs is of the order of $W$ (otherwise an increased correlation length $\sigma$ would also reduce the average difference between the maxima and minima). We therefore use a Gaussian correlated external potential, not to be confused with the Gaussian inter-particle potential of section 7.3.1.

In the case of uncorrelated disorder, the Anderson localization length[8] can be computed to a good approximation for $W \approx 1$ using the following

[7] We use a pseudorandom number generator in the numerical implementation.
[8] We define this length as the maximum localization length, obtained at the band centre.

expression [120]:

$$\xi_{\mathrm{A}}^{-1} = \frac{1}{2}\ln\left(1+\frac{W^2}{16}\right) + \frac{4\arctan(W/4)}{W} - 1. \tag{7.14}$$

If we perform the interaction quench from finite to zero interactions for the uncorrelated case, we should therefore expect the long-time density to decay exponentially according to the Anderson localization length of Equation (7.14). This must be the case, since the momentum distribution (2.2) implies that all the high-momentum states are significantly occupied. For the case of correlated disorder, we should expect this decay to be much weaker, and for sufficiently large correlations we can expect a long-time density $\eta(x)$ (Equation (7.5)) that is a constant, similar to the finite well-case.

We perform numerical simulations in the same way as for the finite well, using contact interactions. However, the solution gives us only the coefficients $\phi_{mn}$ corresponding to one particular realization of the disorder. Therefore, we take the log-average[9] of many such realizations:

$$\langle\psi_\uparrow^\dagger(x,t)\psi_\uparrow(x,t)\rangle_{\mathrm{avg}} = \exp\left[\frac{1}{N}\sum_{i=1}^{N}\ln\left(\langle\psi_\uparrow^\dagger(x,t)\psi_\uparrow(x,t)\rangle_i\right)\right], \tag{7.15}$$

where we take the number of realizations $N = 250$. In addition, since for each different realization the maximum density will be at a different (almost random) site, we consider only the distance from the maximum density in the direction where the edge of the system is furthest away. We do this for a system with a number of sites $L = 151$, and use the same boundary conditions as before, with a vanishing wave function at the boundary.

For the strength of the disorder, we pick $W = 4$. Ideally, we would like to have as weak a disorder as possible, to prevent the "classical" trapping of particles in the randomly generated wells of the potential. However, for such weak disorder, the localization length becomes very large, which becomes increasingly difficult to simulate numerically, as the total length of the system must be much larger than the localization length in order to suppress finite size-effects. Our choice of $W$ yields $\xi_{\mathrm{A}} \approx 7.6$, such that this condition is adequately fulfilled. Nevertheless, the aforementioned trapping in the wells of the disordered potential now implies that the lowest (few) single-particle eigenstate(s) occupy the so-called Lifshits

[9]The log-average is better suited to this problem than the arithmetic average, because it attaches much less weight to large deviations from the average. In the limit that $N \to \infty$ both limits give identical results.

tail [146, 111]. Therefore, the lowest-energy single-particle eigenstate is strongly localized in the deepest well of the potential, and for sufficiently weak interactions, both particles will remain in the deepest well. However, this is not a serious issue, because the interaction quench also populates the states beyond the Lifshits tail, and it is these states that will be associated with quench-induced delocalization. We pick a correlation length $\sigma = 2$. Again, it would be better to be able to investigate greater correlation lengths, so that we have access to many states beyond the crossover to delocalized states. However, in addition to increasing finite-size effects, increasing the correlation length also increases the number of states in the Lifshits tail. The numerical result is shown in Figure 7.5.

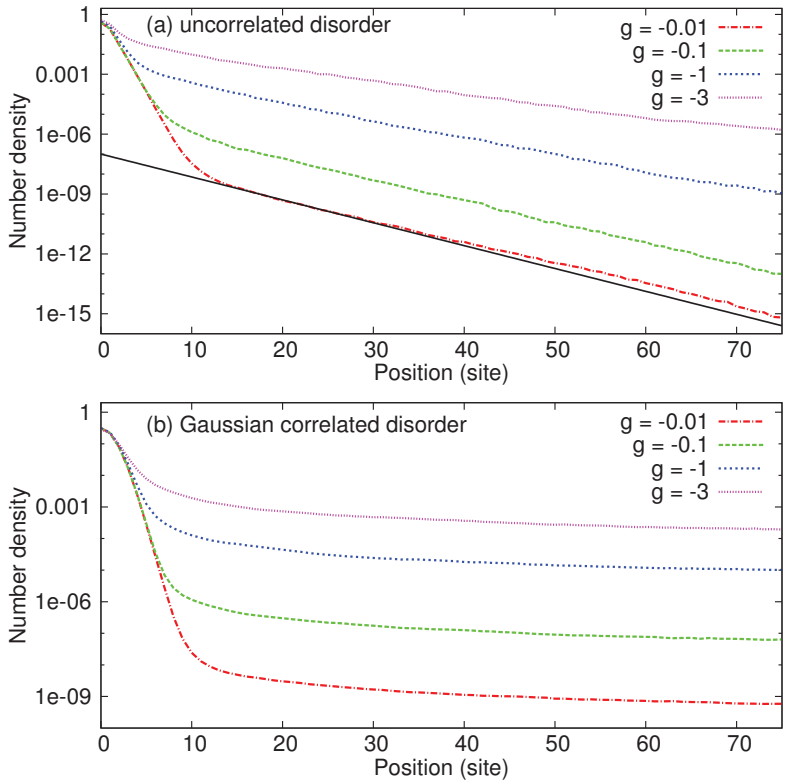


**Figure 7.5.** Logarithmic-averaged number density $\eta(x)$ of two particles a long time after an interaction quench to $g = 0$ as computed using Equation (7.5), for both an uncorrelated (top) and a Gaussian correlated (bottom) external potential. Values are shown for various initial interaction strengths, $\sigma = 2$ and the number of sites $L = 151$. The solid black line indicates exponential decay according to the localization length as computed using Equation (7.14). Figure adapted from Publication III.

The result shows that for the uncorrelated case (7.12), the quench indeed populates the least localized state with a localization length in good

agreement with the prediction from theory (7.14). However, since this result is approximative, a small deviation is to be expected. The result also indicates the surprising result that the localization length increases for stronger initial interactions; since the time evolution is determined by the single-particle states, we would expect the localization length to be bounded by the single-particle localization length. We have, however, not been able to verify whether this result is robust to increases in the system size.

In the case of correlated disorder (7.13), the long-time density shows a much weaker decay compared to the uncorrelated case, as expected. However, the density does not approach a constant as it does in the case of the finite well. This is because the high-momentum states in the correlated disorder are not far enough beyond states with energy corresponding to the correlation length $E_\sigma = \hbar^2/2m\sigma^2$. Such states with energy $E \gg E_\sigma$ cannot be resolved numerically, since this would require $\sigma \gg 1$. In fact, the localization length for Gaussian correlated disorder remains finite at all energies, although it diverges exponentially [124].

We can also compute the explicit time dependence of the density after the quench, which nicely illustrates the mechanism and the time scale associated with it. This results in a propagating wave much akin to what we saw in the finite well-case, shown in Figure 7.6. We express time $t \to tW/\hbar$. Note that delocalization in these units occurs at time scales of the order $t \approx 1$, as it also does in the case of the finite well. This is not surprising, given that $W$ is a measure of the depth of the wells. Also note that there is a slight difference between the prediction of the diagonal ensemble and the explicit time dependence. This difference was also observed using a similar method for a non-interacting wave packet [147]. The initial interacting state at $t = 0$ is also shown, indicating that it is indeed strongly localized at a fixed point in space.

It would also be of interest to look at the case where $N$ majority component fermions interact with an impurity. We have computed the interaction quench in this case, using the Chevy Ansatz approximation explained in detail in Section 3.1, and obtained qualitatively similar results (see Figure 9 in Publication III).

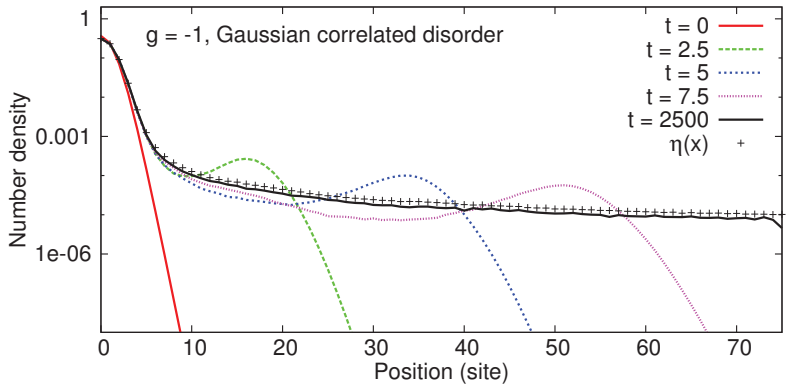


**Figure 7.6.** Logarithmic-averaged density of two particles a time $t$ after an interaction quench to $g = 0$ as computed using Equation (7.4), for the case of correlated disorder with $\sigma = 2$ and the number of sites $L = 151$. After the quench, a wave propagates outward from the lowest well in the disordered potential. Plus symbols indicate the result for the diagonal ensemble (7.5).

## 7.5 Some additional thoughts

In this chapter, we have discussed delocalization as a result of an interaction quench from a finite value of the interaction parameter $g$ to $g = 0$. What happens in an interaction quench from some value $g_1$ to some other arbitrary value $g_2$? This question is significantly more difficult to answer, because unlike the case where we quench to the non-interacting system, we no longer have (easy) access to the full eigenbasis of the post-quench Hamiltonian. In addition, the post-quench Hamiltonian is, in general, no longer integrable. This profoundly affects the dynamics, which are no longer ballistic as in the cases discussed above. Indeed, both an experiment [148] and numerical studies [149, 150, 151, 152] indicate that transport occurs *subdiffusively* for a disordered system with fixed interparticle interaction strength. This subdiffusive transport also leads to delocalization, albeit on longer time scales. However, other studies indicate a *many-body localized* phase that is stable for sufficiently small interactions [153]. The precise nature of this phase, and the connection to statistical ensembles[10], are the subject of current investigation [154, 155].

Consider the situation where we have the interacting system discussed above, and instead of quenching from $g_1$ to $g_2 = 0$, we quench the interactions to some *small* value $g_2 \ll g_1$, $g_2 \ll 1$. Now the post-quench dynamics

[10] A so-called *generalized Gibbs ensemble* has been proposed to make the link between the universal properties of the dynamics in closed quantum systems and the familiar ensembles of classical statistical mechanics.

is described [156] by the exact non-interacting Hamiltonian, perturbed by some small interacting part, say $\mathcal{H}_2$. Since the contribution from the interacting part $\mathcal{H}_2$ is small, we should expect the non-interacting part to dominate the immediate post-quench dynamics. Therefore, given a non-adiabatic interaction quench, I conjecture that the behaviour of the system will show initial ballistic expansion, with a crossover to the long-time behaviour – (sub)diffusive spreading – dominated by the interactions. The strength of the interactions $g_2$ will determine the time scale at which this crossover happens, which should go to infinity as $g_2 \to 0$.

# 8. The BCS-BEC crossover

In the final chapter of this thesis, we will deviate a bit off course in orthogonal directions and study a three-dimensional system (see Publication IV). Yet, we will encounter many of the same concepts and tools as we did in previous chapters, including but not limited to Tan's contact, momentum distributions, the T-matrix formalism and strongly interacting systems.

The system we will investigate is the homogeneous, spin-balanced, three-dimensional Fermi gas interacting through contact interactions, as described by the Hamiltonian:

$$\begin{aligned}\mathcal{H} &= -\sum_{\sigma}\int d\mathbf{r}\,\psi_{\sigma}^{\dagger}(\mathbf{r})\frac{\hbar^2}{2m}\nabla^2\psi_{\sigma}(\mathbf{r}) \\ &+ \frac{1}{2}\int d\mathbf{r}\int d\mathbf{r}'\psi_{\uparrow}^{\dagger}(\mathbf{r})\psi_{\downarrow}^{\dagger}(\mathbf{r}')V_{\mathrm{int}}(\mathbf{r}-\mathbf{r}')\psi_{\downarrow}(\mathbf{r}')\psi_{\uparrow}(\mathbf{r}).\end{aligned} \tag{8.1}$$

Here $\psi_{\sigma}^{(\dagger)}$ destroys (creates) a particle at (now three-dimensional) position $\mathbf{r}$ with generalized spin $\sigma \in \{\uparrow,\downarrow\}$, and $V_{\mathrm{int}}$ indicates the inter-particle potential as before. In this case, we can no longer use the delta function potential to describe short-range interactions, because this potential suffers from an ultraviolet divergence. Instead, we use the following *pseudopotential*:

$$V_{\mathrm{int}}(\mathbf{r}) = g\delta(\mathbf{r})\frac{d}{dr}\Big(r\,\cdot\,\Big), \tag{8.2}$$

where $g = 4\pi\hbar^2 a/m$ and $a$ denotes the three-dimensional scattering length[1].

This system can exist in various phases depending on the temperature and the sign and magnitude of the inter-particle interactions. At zero temperature and for weakly attractive interactions, the system is found in a superfluid phase as described by the Bardeen-Cooper-Schrieffer (BCS) theory [2]. Here the fermions form pairs of opposite momentum called

[1]The relation between the three- and one-dimensional scattering length is detailed in Ref. [38].

Cooper pairs. These pairs condense, creating a superfluid. At a certain temperature, the critical temperature $T_c$, the pairs are broken and the system is no longer superfluid. This phase has the rather boring name *normal phase*, in which case Fermi liquid theory works rather well [157, 158]. If the attraction between fermions is very strong (and at low temperatures), the fermions form tightly bound "point-like" bosonic pairs. These pairs are themselves weakly *repulsively* interacting, and can condense and form a Bose-Einstein condensate (BEC). The intermediate regime of strong interactions (attractive or repulsive) is called the *unitary* regime, where the size of the pairs is comparable to the inter-particle distance. In this regime, no obvious perturbative parameter exists to describe the interactions, so that more elaborate theoretical approaches are required. Since we are then in between the regimes where the BCS limit is valid and the one where the BEC limit holds, the regime of strong interactions is also called the BCS-BEC crossover [159, 160].

## 8.1 Properties of a Fermi liquid

The Fermi liquid briefly mentioned in the introduction to this chapter has some remarkably simple properties. It is very much like a non-interacting Fermi gas, in the sense that its momentum distribution has a step at the Fermi surface. The Fermi surface itself does not change for a Fermi liquid (for a fixed density), as guaranteed through Luttinger's theorem [161, 162]. However, the step is no longer of magnitude $1$, but has some smaller size, called the *quasiparticle weight* $Z$, as schematically depicted in Figure 8.1. The elementary excitations of a Fermi liquid are long-lived quasiparticles with a dispersion relation similar to non-interacting particles, but with an *effective mass* dressed by the interactions between the particles.

## 8.2 The unitary Fermi gas

The unitary Fermi gas is a strongly interacting Fermi gas at the BCS-BEC crossover. This state is difficult to describe, because a perturbative expansion in the interaction parameter $k_F a$ is likely to fail as $k_F a \to \infty$. On the other hand, since the scattering length diverges and no longer is a relevant length scale, the only remaining length scale in the system is

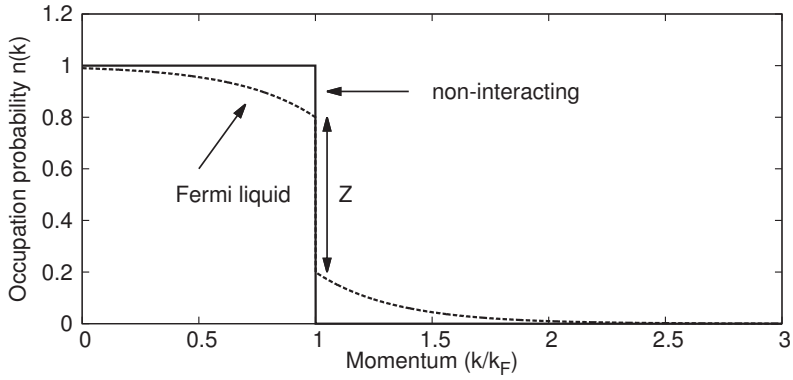


**Figure 8.1.** Schematic depiction of the zero-temperature momentum distribution of a Fermi liquid (dashed line), compared to a non-interacting Fermi gas (solid line). The momentum distribution for a Fermi liquid has a step of size $Z$, the quasiparticle weight, at the Fermi surface.

the inverse Fermi momentum $k_F^{-1}$. Therefore, the properties of strongly interacting Fermi gases are *universal* and depend only on the density (or equivalently, $k_F$) and the temperature. This makes the controlled environment of quantum gases particularly attractive to study the unitary Fermi gas [157, 40].

One topic of discussion is the nature of the Fermi liquid at and near unitarity. At zero temperature, it is found in the superfluid phase, which has a critical temperature of roughly $T_c \approx 0.2T_F$, where $T_F$ is the Fermi temperature. Above the critical temperature, a *pseudogap* phase has been proposed [163, 164, 165], which still exhibits Cooper pairing above $T_c$ that gradually becomes weaker until Fermi liquid behaviour is obtained at some higher temperature. In a recent experiment at JILA [166], the disappearance of Fermi liquid properties slightly on the repulsive side of the crossover was reported. This disappearance was measured through the vanishing of the quasiparticle weight $Z$.

A convenient experimental tool for studying strongly interacting Fermi gases is spectroscopy, which comes in various forms, e.g. (momentum-resolved) radio-frequency spectroscopy and Bragg spectroscopy. We will not discuss the details of these methods in this work and refer to Refs. [167, 168, 169, 170] for various examples of applications and theoretical descriptions. It is worthwhile to note that the contact parameter discussed in Chapter 2 can be directly measured using rf spectroscopy [40, 42, 36].

## 8.3 Brueckner-Goldstone theory

In this chapter, we will use the Brueckner-Goldstone theory [171, 172] previously mainly applied to the study of $^3$He. The main idea of the theory is to solve the Dyson equation (see Section 3.2.2) using an approximative method. The Dyson equation for either of the two components (they are the same in the spin-balanced case) is given by:

$$G(\mathbf{k},\omega)^{-1} = G_0(\mathbf{k},\omega)^{-1} - \Sigma(\mathbf{k},\omega). \tag{8.3}$$

We will consider the self-energy "on the energy shell" only, defining the Brueckner-Goldstone self-energy:

$$\Sigma_{\mathrm{BG}}(k) = \Sigma(k, \epsilon_k + \Sigma_{\mathrm{BG}}(k)), \tag{8.4}$$

where $\epsilon_k = \hbar^2 k^2/2m$ is the kinetic energy of a particle. The dressed Green's function takes a particularly simple form in this picture, even at finite temperature:

$$G_{\mathrm{BG}}(\mathbf{k},\omega) = \frac{n_k}{\omega - \epsilon_k - \Sigma_{\mathrm{BG}}(k) - i\eta} + \frac{1-n_k}{\omega - \epsilon_k - \Sigma_{\mathrm{BG}}(k) + i\eta}, \tag{8.5}$$

where $n_k$ is the non-interacting momentum distribution. This approach boils down to neglecting pairing between the fermions, since the pairing branch is located near $\omega = -\epsilon_k$. Therefore, the current approach can be regarded as valid only when pairing is not important (such as in the case of a Fermi liquid). The breakdown of the theory can then be associated with the increasing importance of (superfluid or pseudogap) pairing.

We will seek to obtain various quantities through the Brueckner-Goldstone theory: momentum distributions, Tan's contact, the Hartree self-energy and (momentum-resolved) radio-frequency spectra. However, as indicated in Equation (8.5), the standard Brueckner-Goldstone theory actually does not change the momentum distribution. We will therefore extend it using a first order perturbative approximation to the Dyson equation:

$$G(k,\omega) \approx G_{\mathrm{BG}}(k,\omega) + G_{\mathrm{BG}}(k,\omega)\Big[\Sigma(k,\omega) - \Sigma_{\mathrm{BG}}(k)\Big]G_{\mathrm{BG}}(k,\omega) =: G_{\mathrm{pert}}(k,\omega). \tag{8.6}$$

Here we determine $\Sigma(k,\omega)$ using the ladder approximation:

$$\Sigma_\uparrow(K) = \int \frac{dP}{i(2\pi)^4}\Gamma(K+P)G_\downarrow(P), \tag{8.7}$$

where $\Gamma(K+P)$ is the many-body T-matrix (see section 3.2.4 and the discussion for the three-dimensional case in Ref. [82]).

## 8.4 Numerical results

In this section, we will discuss the predictions of the perturbative BG theory through numerical calculations of various observables.

### 8.4.1 Momentum distribution

The perturbative extension to the Brueckner-Goldstone theory outlined above yields momentum distributions that behave appropriately in various limits. In particular, we obtain the correct $1/k^4$-asymptote in the limit that $k \to \infty$, in contrast to for example BCS theory. The result is depicted in Figure 8.2. Note how the low-momentum states are slightly depleted in the strongly interacting case, as a result of number conservation.

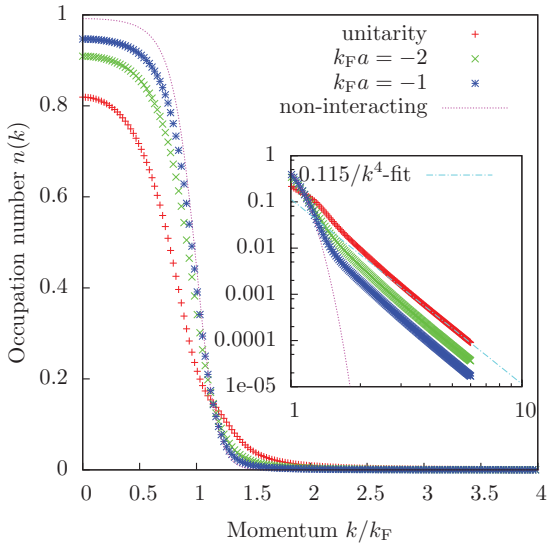


**Figure 8.2.** Momentum distribution as predicted using the perturbative extension to BG theory (8.6) for various values of the interaction strength $k_Fa$ at a temperature $T = 0.2T_F$. For comparison, the non-interacting case at this temperature is also shown. Inset: high-momentum asymptote of the momentum distribution (note the log scale). Figure adapted from Publication IV.

### 8.4.2 Quasiparticle weight

Another quantity of interest is the quasiparticle weight $Z$ (see Figure 8.1). As shown, in the zero-temperature limit, $Z$ is simply defined as the size of the step. However, at finite temperatures, the momentum distributions are broadened, so that there is no longer a discontinuity. Not wanting to abandon the concept of the quasiparticle weight, we introduce an alternative definition, which corresponds to $Z$ in the zero-temperature limit.

Define the deviation from the non-interacting momentum distribution $n_k$ at a fixed temperature: $\delta n_k = n(k) - n_k$, where $n(k)$ is the momentum distribution obtained using BG theory. The quasiparticle weight is now defined using:

$$Z = 1 - \delta n_{\text{max}} + \delta n_{\text{min}}, \tag{8.8}$$

where $\delta n_{\text{max}}$ and $\delta n_{\text{min}}$ are the maximum and minimum deviation from $n_k$ respectively. The result is shown in Figure 8.3.

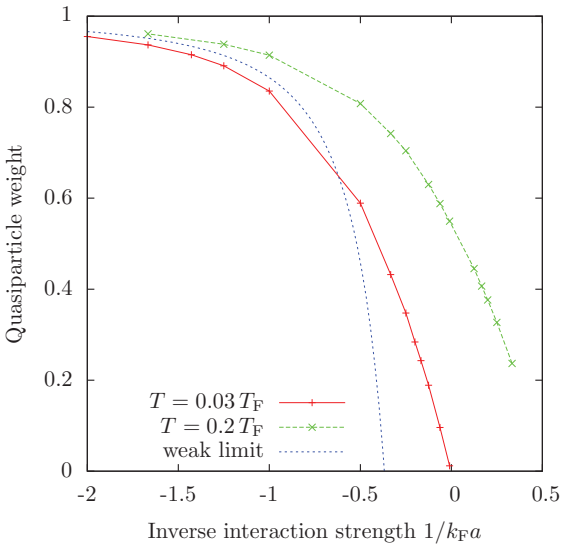


**Figure 8.3.** Quasiparticle weight as a function of the inverse interaction strength $1/k_F a$ for $T = 0.2T_F$ and $T = 0.03T_F$. For comparison, the analytical result in the weakly attractively interacting limit [88] is also shown. Figure adapted from Publication IV.

The quasiparticle weight according to the definition above vanishes slightly on the repulsive side of the crossover (for $T = 0.2T_F$), in good agreement with the experiment [166], although a different definition of $Z$ was used in the analysis of the experiment. Although the theory should not be fully trusted below the superfluid transition temperature, we also show the result for $T = 0.03T_F$, which shows a vanishing quasiparticle weight at smaller values of $1/k_F a$, suggesting that the precise point at which the Fermi liquid description breaks down is temperature dependent. In addition, on the weakly repulsive side, we find good agreement at low temperatures with the analytical zero-temperature result [88]:

$$Z_{\text{weak}} = 1 - \frac{4}{3\pi^2}(k_F a)^2. \tag{8.9}$$

In Ref. [158] it was reported that Fermi liquid behaviour is recovered throughout the crossover. However, this study also indicates that this

only applies to the coherent part of the excitation spectrum. It is precisely this coherent part that vanishes when the quasiparticle weight $Z$ goes to zero, so the difference between Refs. [158] and [166] is primarily one of emphasis.

### 8.4.3 Contact

The extended BG theory also yields the contact (see Chapter 2). We display the result in Figure 8.4, where we also compare our predictions to the measured contact [42]. In the weakly interacting limit, we also find good agreement with the exact result [87]. This is a marked improvement over BCS theory, which anomalously predicts a contact that decays exponentially for decreasing $k_F a$. Meanwhile, we find excellent agreement with previous results for the high-temperature limit [34] at unitarity using a virial expansion, with the (normalized) contact given by:

$$\frac{C}{Nk_F} = 3\pi\left(\frac{T}{T_F}\right)^2 z^2, \tag{8.10}$$

where $z = e^{-\mu/k_B T}$ is the fugacity, and $\mu$ is the chemical potential. This result can be obtained through converting Eq. (3.21) to the continuum limit and replacing the momentum distributions by the Maxwell-Boltzmann distribution.

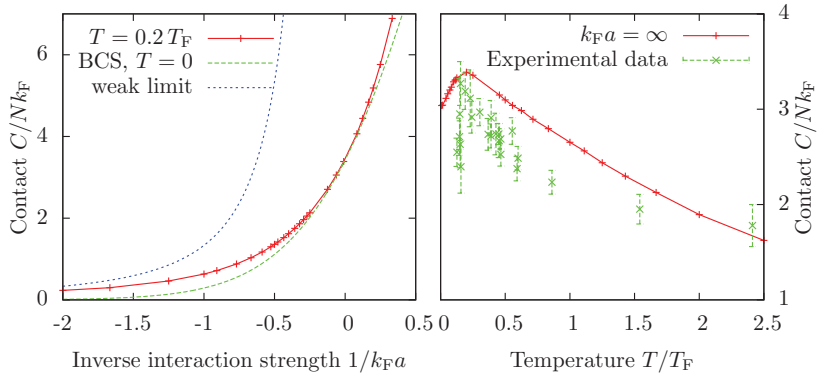


**Figure 8.4.** Left: contact as a function of inverse interaction strength $1/k_F a$. Dashed line shows the exact result in the weakly interacting limit. Right: contact as a function of temperature, compared to experimental data from Ref. [42]. Figure adapted from Publication IV.

# 9. Conclusions and Outlook

In this thesis, we have discussed various seemingly disconnected systems. However, through Tan's universal relations, we can find common themes in all of these systems, demonstrating the power of these relations.

In the highly polarized one-dimensional case (the Fermi polaron), we compute Tan's contact exactly at zero temperature, and use the T-matrix formalism to extend the analysis to finite temperature. At very high temperatures, the contact approaches a constant value, unlike in the higher-dimensional case, where the contact decays to zero as the temperature $T \to \infty$. For the case where an external trap is present, we extend Chevy's variational method to systems with an arbitrary external trap and arbitrary inter-particle interactions. This analysis shows that lattice models tend to neglect the physics related to the high-momentum asymptote, showing that one must be cautious when employing lattice models, as one might neglect some essential physics in the problem.

Extending this latter idea further, we have shown that the short-range correlations neglected in the Anderson model of disorder lead to essentially different physics if we instantaneously switch off (quench) the inter-particle interactions. In the case where spatial correlations are present in the disordered potential, Tan's relations guarantee the significant population of high-energy delocalized states, leading to delocalization after the interaction quench, dubbed *quench-induced delocalization*.

For the three-dimensional case, we extend the Brueckner-Goldstone theory, adding a perturbative extension that correctly reproduces the expected high-momentum asymptote in the momentum distribution. Furthermore, this theory reproduces the experimental result that the Fermi liquid description breaks down slightly on the repulsive side of the crossover from the Bardeen-Cooper-Schrieffer limit of weak attraction to the Bose-Einstein condensation limit of pairs of fermions.

The work in this thesis provides a starting point for further investigation. One interesting avenue is to consider the *interacting* dynamics of polarized and few-body systems. This allows the investigation of non-equilibrium properties and phenomena such as metastable states. A possible scenario involves the dynamical response of an impurity due to a collision with a many-body system, complementing studies of an impurity in a lattice system such as in Ref. [106].

Disordered systems are currently also under investigation, especially in connection to the predicted many-body localized phase [153], which was recently claimed to be found in an experiment [173]. It would be of interest to extend the investigation considered in this thesis to the interacting dynamics of disordered quantum gases in the continuum to further our understanding of disordered, interacting systems.

# Bibliography


[1] H. Kamerlingh Onnes. The resistance of pure mercury at helium temperatures. *Commun. Phys. Lab. Univ. Leiden*, 12:120, 1911.

[2] J. Bardeen, L. N. Cooper, and J. R. Schrieffer. Microscopic theory of superconductivity. *Phys. Rev.*, 106:162–164, 1957.

[3] P. Kapitza. Viscosity of liquid helium below the $\lambda$-point. *Nature*, 141:74, 1938.

[4] J. F. Allen and A. D. Misener. Flow phenomena in liquid helium II. *Nature*, 142:643–644, 1938.

[5] S. N. Bose. Plancks Gesetz und Lichtquantenhypothese. *Z. Phys.*, 26:178, 1924.

[6] A. Einstein. Quantentheorie des einatomigen idealen Gases. *Sitzungsber. Preuss. Akad. Wiss., Phys. Math. Kl. Bericht*, pages 261–267, 1924.

[7] A. Einstein. Quantentheorie des einatomigen idealen Gases. 2. Abhandlung. *Sitzungsber. Preuss. Akad. Wiss., Phys. Math. Kl. Bericht*, pages 3–14, 1925.

[8] M. H. Anderson, J. R. Ensher, M. R. Matthews, C. E. Wieman, and E. A. Cornell. Observation of Bose-Einstein condensation in a dilute atomic vapor. *Science*, 269(5221):198–201, 1995.

[9] K. B. Davis, M. O. Mewes, M. R. Andrews, N. J. van Druten, D. S. Durfee, D. M. Kurn, and W. Ketterle. Bose-Einstein condensation in a gas of sodium atoms. *Phys. Rev. Lett.*, 75:3969–3973, 1995.

[10] W. D. Phillips. Nobel Lecture: Laser cooling and trapping of neutral atoms. *Rev. Mod. Phys.*, 70:721–741, 1998.

[11] B. DeMarco and D. S. Jin. Onset of Fermi degeneracy in a trapped atomic gas. *Science*, 285(5434):1703–1706, 1999.

[12] S. J. J. M. F. Kokkelmans. Feshbach resonances in ultracold gases. In P. Törmä and K. Sengstock, editors, *Quantum gas experiments - exploring many-body states*, chapter 4. Imperial College Press, London, 2014.

[13] A. Griesmaier, J. Werner, S. Hensler, J. Stuhler, and T. Pfau. Bose-Einstein condensation of chromium. *Phys. Rev. Lett.*, 94:160401, 2005.

[14] B. Yan, S. A. Moses, B. Gadway, J. P. Covey, K. R. A. Hazzard, A. M. Rey, D. S. Jin, and J. Ye. Observation of dipolar spin-exchange interactions with lattice-confined polar molecules. *Nature*, 501:521–525, 2013.

[15] I. Bloch. Ultracold quantum gases in optical lattices. *Nature Phys.*, 1:23–30, 2005.

[16] M. Greiner, O. Mandel, T. Esslinger, T. W. Hänsch, and I. Bloch. Quantum phase transition from a superfluid to a Mott insulator in a gas of ultracold atoms. *Nature*, 415:39–44, 2012.

[17] L. Sanchez-Palencia and M. Lewenstein. Disordered quantum gases under control. *Nature Phys.*, 6:87, 2010.

[18] P. W. Anderson. Absence of diffusion in certain random lattices. *Phys. Rev.*, 109:1492–1505, 1958.

[19] J. Billy, V. Josse, Z. Zuo, A. Bernard, B. Hambrecht, P. Lugan, D. Clément, L. Sanchez-Palencia, P. Bouyer, and A. Aspect. Direct observation of Anderson localization of matter waves in a controlled disorder. *Nature*, 453:891, 2008.

[20] G. Roati, C. D'Errico, L. Fallani, M. Fattori, C. Fort, M. Zaccanti, G. Modugno, M. Modugno, and M. Inguscio. Anderson localization of a non-interacting Bose–Einstein condensate. *Nature*, 453:895, 2008.

[21] M. W. Zwierlein, A. Schirotzek, C. H. Schunck, and W. Ketterle. Fermionic superfluidity with imbalanced spin populations. *Science*, 311(5760):492–496, 2006.

[22] S. Tan. Energetics of a strongly correlated Fermi gas. *Ann. Phys.*, 323:2952, 2008.

[23] S. Tan. Large momentum part of a strongly correlated Fermi gas. *Ann. Phys.*, 323:2971, 2008.

[24] S. Tan. Generalized virial theorem and pressure relation for a strongly correlated Fermi gas. *Ann. Phys.*, 323(12):2987, 2008.

[25] S. Tan. Universal energy functional for trapped Fermi gases with short range interactions. *Phys. Rev. Lett.*, 107:145302, 2011.

[26] M. Olshanii and V. Dunjko. Short-distance correlation properties of the Lieb-Liniger system and momentum distributions of trapped one-dimensional atomic gases. *Phys. Rev. Lett.*, 91:090401, 2003.

[27] D. M. Gangardt and G. V. Shlyapnikov. Stability and phase coherence of trapped 1D Bose gases. *Phys. Rev. Lett.*, 90:010401, 2003.

[28] M. Barth and W. Zwerger. Tan relations in one dimension. *Ann. Phys.*, 326:2544–2565, 2011.

[29] M. Valiente, N. T. Zinner, and K. Mølmer. Universal relations for the two-dimensional spin-1/2 Fermi gas with contact interactions. *Phys. Rev. A*, 84:063626, Dec 2011.

[30] E. Braaten, D. Kang, and L. Platter. Universal relations for identical bosons from three-body physics. *Phys. Rev. Lett.*, 106:153005, 2011.

[31] D. H. Smith, E. Braaten, D. Kang, and L. Platter. Two-body and three-body contacts for identical bosons near unitarity. *Phys. Rev. Lett.*, 112:110402, Mar 2014.

[32] J. E. Drut, T. A. Lähde, and T. Ten. Momentum distribution and contact of the unitary Fermi gas. *Phys. Rev. Lett.*, 106:205302, 2011.

[33] Y. Yan and D. Blume. Harmonically trapped Fermi gas: Temperature dependence of the Tan contact. *Phys. Rev. A*, 88:023616, 2013.

[34] H. Hu, X.-J. Liu, and P. D. Drummond. Universal thermodynamics of a strongly interacting Fermi gas: theory versus experiment. *New J. Phys.*, 12(6):063038, 2010.

[35] X.-J. Liu. Virial expansion for a strongly correlated Fermi system and its application to ultracold atomic Fermi gases. *Phys. Rep.*, 524(2):37 – 83, 2013.

[36] E. Braaten. Universal relations for fermions with large scattering length. In W. Zwerger, editor, *The BCS-BEC Crossover and the Unitary Fermi Gas*. Springer, Heidelberg, 2012.

[37] Y.-Y. Chen, Y.-Z. Jiang, X.-W. Guan, and Q. Zhou. Critical behaviours of contact near phase transitions. *Nature Comm.*, 5:5140, 2014.

[38] M. Olshanii. Atomic scattering in the presence of an external confinement and a gas of impenetrable bosons. *Phys. Rev. Lett.*, 81:938–941, 1998.

[39] E. Haller, M. J. Mark, R. Hart, J. G. Danzl, L. Reichsöllner, V. Melezhik, P. Schmelcher, and H.-C. Nägerl. Confinement-induced resonances in low-dimensional quantum systems. *Phys. Rev. Lett.*, 104:153203, Apr 2010.

[40] J. T. Stewart, J. P. Gaebler, T. E. Drake, and D. S. Jin. Verification of universal relations in a strongly interacting Fermi gas. *Phys. Rev. Lett.*, 104:235301, 2010.

[41] E. D. Kuhnle, H. Hu, X.-J. Liu, P. Dyke, M. Mark, P. D. Drummond, P. Hannaford, and C. J. Vale. Universal behavior of pair correlations in a strongly interacting Fermi gas. *Phys. Rev. Lett.*, 105(7):070402, 2010.

[42] Y. Sagi, T. E. Drake, R. Paudel, and D. S. Jin. Measurement of the homogeneous contact of a unitary Fermi gas. *Phys. Rev. Lett.*, 109:220402, 2012.

[43] R. J. Wild, P. Makotyn, J. M. Pino, E. A. Cornell, and D. S. Jin. Measurements of Tan's contact in an atomic Bose-Einstein condensate. *Phys. Rev. Lett.*, 108:145305, 2012.

[44] A. B. Bardon, S. Beattie, C. Luciuk, W. Cairncross, D. Fine, N. S. Cheng, G. J. A. Edge, E. Taylor, S. Zhang, S. Trotzky, and J. H. Thywissen. Transverse demagnetization dynamics of a unitary Fermi gas. *Science*, 344(6185):722–724, 2014.

[45] O. Hen, L. B. Weinstein, E. Piasetzky, G. A. Miller, M. M. Sargsian, and Y. Sagi. Correlated fermion pairs in nuclei and ultracold atomic gases. *arXiv: 1407:8175*, 2014.

[46] R. Weiss, B. Bazak, and N. Barnea. Nuclear neutron-proton contact and the photoabsorption cross section. *Phys. Rev. Lett.*, 114:012501, 2015.

[47] P. Fulde and R. A. Ferrell. Superconductivity in a strong spin-exchange field. *Phys. Rev.*, 135:A550–A563, Aug 1964.

[48] A. I. Larkin and Yu. N. Ovchinnikov. *Zh. Eksp. Teor. Fiz.*, 47:1136, 1964.

[49] I. Bloch, J. Dalibard, and W. Zwerger. Many-body physics with ultracold gases. *Rev. Mod. Phys.*, 80(3):885, 2008.

[50] F. Chevy and C. Mora. Ultra-cold polarized Fermi gases. *Rep. Prog. Phys.*, 73(11):112401, 2010.

[51] P. Massignan, M. Zaccanti, and G. M Bruun. Polarons, dressed molecules and itinerant ferromagnetism in ultracold Fermi gases. *Rep. Prog. Phys.*, 77(3):034401, 2014.

[52] Z. Lan and C. Lobo. A single impurity in an ideal atomic Fermi gas: current understanding and some open problems. *J. Indian I. Sci.*, 94:179, 2014.

[53] M. Punk, P. T. Dumitrescu, and W. Zwerger. Polaron-to-molecule transition in a strongly imbalanced Fermi gas. *Phys. Rev. A*, 80(5):053605, 2009.

[54] N. Prokof'ev and B. Svistunov. Fermi-polaron problem: Diagrammatic Monte Carlo method for divergent sign-alternating series. *Phys. Rev. B*, 77(2):020408, 2008.

[55] R. Combescot, F. Alzetto, and X. Leyronas. Particle distribution tail and related energy formula. *Phys. Rev. A*, 79(5):053640, 2009.

[56] C. Mora and F. Chevy. Ground state of a tightly bound composite dimer immersed in a Fermi sea. *Phys. Rev. A*, 80:033607, Sep 2009.

[57] P. W. Anderson. Infrared catastrophe in Fermi gases with local scattering potentials. *Phys. Rev. Lett.*, 18:1049–1051, Jun 1967.

[58] F. Chevy. Universal phase diagram of a strongly interacting Fermi gas with unbalanced spin populations. *Phys. Rev. A*, 74(6):063628, 2006.

[59] M. Ku, J. Braun, and A. Schwenk. Finite-size and confinement effects in spin-polarized trapped Fermi gases. *Phys. Rev. Lett.*, 102:255301, Jun 2009.

[60] E. Anderson, Z. Bai, C. Bischof, S. Blackford, J. Demmel, J. Dongarra, J. Du Croz, A. Greenbaum, S. Hammarling, A. McKenney, and D. Sorensen. *LAPACK Users' Guide*. Society for Industrial and Applied Mathematics, Philadelphia, PA, 1999.

[61] R. Combescot, A. Recati, C. Lobo, and F. Chevy. Normal state of highly polarized Fermi gases: Simple many-body approaches. *Phys. Rev. Lett.*, 98(18):180402, 2007.

[62] S. Giraud and R. Combescot. Highly polarized Fermi gases: one-dimensional case. *Phys. Rev. A.*, 79:043615, 2009.

[63] M. M. Parish and J. Levinsen. Highly polarized Fermi gases in two dimensions. *Phys. Rev. A*, 87:033616, 2013.

[64] C. J. M. Mathy, M. M. Parish, and D. A. Huse. Trimers, molecules, and polarons in mass-imbalanced atomic Fermi gases. *Phys. Rev. Lett.*, 106:166404, Apr 2011.

[65] J. Levinsen and S. K. Baur. High-polarization limit of the quasi-two-dimensional Fermi gas. *Phys. Rev. A*, 86:041602, Oct 2012.

[66] C. Trefzger and Y. Castin. Impurity in a Fermi sea on a narrow Feshbach resonance: A variational study of the polaronic and dimeronic branches. *Phys. Rev. A*, 85:053612, May 2012.

[67] P. Massignan. Polarons and dressed molecules near narrow Feshbach resonances. *Europhys. Lett.*, 98(1):10012, 2012.

[68] J. Levinsen, P. Massignan, F. Chevy, and C. Lobo. $p$-wave polaron. *Phys. Rev. Lett.*, 109:075302, Aug 2012.

[69] P. Massignan and G. M. Bruun. Repulsive polarons and itinerant ferromagnetism in strongly polarized Fermi gases. *Eur. Phys. J. D*, 65:83, 2011.

[70] A. Schirotzek, C.-H. Wu, A. Sommer, and M. W. Zwierlein. Observation of Fermi polarons in a tunable Fermi liquid of ultracold atoms. *Phys. Rev. Lett.*, 102(23):230402, 2009.

[71] M. Koschorreck, D. Pertot, E. Vogt, B. Fröhlich, M. Feld, and M. Köhl. Attractive and repulsive Fermi polarons in two dimensions. *Nature*, 485:619, 2012.

[72] C. Kohstall, M. Zaccanti, M. Jag, A. Trenkwalder, P. Massignan, G. M. Bruun, F. Schreck, and R. Grimm. Metastability and coherence of repulsive polarons in a strongly interacting Fermi mixture. *Nature*, 485:615–618, 2012.

[73] P. Massignan, Z. Yu, and G. M. Bruun. Itinerant ferromagnetism in a polarized two-component Fermi gas. *Phys. Rev. Lett.*, 110:230401, Jun 2013.

[74] O. Goulko, F. Chevy, and C. Lobo. Collision of two spin-polarized fermionic clouds. *Phys. Rev. A*, 84:051605, Nov 2011.

[75] N. G. Nygaard and N. T. Zinner. Efimov three-body states on top of a Fermi sea. *New J. Phys.*, 16(2):023026, 2014.

[76] R. Qi and H. Zhai. Highly polarized Fermi gases across a narrow Feshbach resonance. *Phys. Rev. A*, 85:041603, Apr 2012.

[77] J. Vlietinck, J. Ryckebusch, and K. Van Houcke. Quasiparticle properties of an impurity in a Fermi gas. *Phys. Rev. B*, 87:115133, Mar 2013.

[78] Z. Lan, G. M. Bruun, and C. Lobo. Quasiparticle lifetime in ultracold fermionic mixtures with density and mass imbalance. *Phys. Rev. Lett.*, 111:145301, Oct 2013.

[79] C. Lobo, A. Recati, S. Giorgini, and S. Stringari. Normal state of a polarized Fermi gas at unitarity. *Phys. Rev. Lett.*, 97(20):200403, 2006.

[80] A. Recati, C. Lobo, and S. Stringari. Role of interactions in spin-polarized atomic Fermi gases at unitarity. *Phys. Rev. A*, 78:023633, Aug 2008.

[81] A. L. Fetter and J. D. Walecka. *Quantum theory of many-particle systems*. McGraw-Hill, New York, 1971.

[82] J. J. Kinnunen. Hartree shift in unitary Fermi gases. *Phys. Rev. A*, 85:012701, 2012.

[83] X.-W. Guan, M. T. Batchelor, and C. Lee. Fermi gases in one dimension: From Bethe ansatz to experiments. *Rev. Mod. Phys.*, 85:1633–1691, 2013.

[84] V. E. Barlette, M. M. Leite, and S. K. Adhikari. Integral equations of scattering in one dimension. *American J. Phys.*, 69(9):1010–1013, 2001.

[85] S. A. Morgan, M. D. Lee, and K. Burnett. Off-shell $t$ matrices in one, two, and three dimensions. *Phys. Rev. A*, 65:022706, 2002.

[86] T. Giamarchi. *Quantum Physics in One Dimension*. Clarendon Press, Oxford, 2003.

[87] V. A. Belyakov. The momentum distribution of particles in a dilute Fermi gas. *J. Exptl. Theoret. Phys. (U.S.S.R.)*, 40:1210–1212, 1961.

[88] R. Sartor and C. Mahaux. Self-energy, momentum distribution, and effective masses of a dilute Fermi gas. *Phys. Rev. C*, 21(4):1546, 1980.

[89] J. B. McGuire. Interacting fermions in one dimension. I. Repulsive potential. *J. Math. Phys.*, 6(3):432, 1965.

[90] J. B. McGuire. Interacting fermions in one dimension. II. Attractive potential. *J. Math. Phys.*, 7(1):123, 1966.

[91] M. Girardeau. Relationship between systems of impenetrable bosons and fermions in one dimension. *J. Math. Phys.*, 1(6):516–523, 1960.

[92] E. H. Lieb and W. Liniger. Exact analysis of an interacting Bose gas. i. The general solution and the ground state. *Phys. Rev.*, 130:1605–1616, May 1963.

[93] B. Paredes, A. Widera, V. Murg, O. Mandel, S. Fölling, I. Cirac, G. V. Shlyapnikov, T. W. Hänsch, and I. Bloch. Tonks-Girardeau gas of ultracold atoms in an optical lattice. *Nature*, 429:277–281, 2004.

[94] T. Kinoshita, T. Wenger, and D. S. Weiss. Observation of a one-dimensional Tonks-Girardeau gas. *Science*, 305(5687):1125–1128, 2004.

[95] E. Braaten and L. Platter. Exact relations for a strongly interacting Fermi gas from the operator product expansion. *Phys. Rev. Lett.*, 100:205301, May 2008.

[96] R. Combescot and S. Giraud. Normal state of highly polarized Fermi gases: Full many-body treatment. *Phys. Rev. Lett.*, 101(5):050404, 2008.

[97] M. D. Hoffman, P. Javernick, A. C. Loheac, W. J. Porter, E. R. Anderson, and J. E. Drut. Universality in one-dimensional fermions at finite temperature: density, pressure, compressibility, and contact. *preprint at: arXiv:1410.7370*, 2014.

[98] J. Voit. One-dimensional Fermi liquids. *Rep. Prog. Phys.*, 58(9):977, 1995.

[99] M. Lewenstein, A. Sanpera, V. Ahufinger, B. Damski, A. Sen(De), and U. Sen. Ultracold atomic gases in optical lattices: mimicking condensed matter physics and beyond. *Advances in Physics*, 56(2):243–379, 2007.

[100] S. E. Gharashi, X. Y. Yin, Y. Yan, and D. Blume. One-dimensional Fermi gas with a single impurity in a harmonic trap: Perturbative description of the upper branch. *Phys. Rev. A*, 91:013620, Jan 2015.

[101] M. Fisher, P. Weichman, G. Grinstein, and D. Fisher. Boson localization and the superfluid-insulator transition. *Phys. Rev. B*, 40:546–570, Jul 1989.

[102] J. Hubbard. Electron Correlations in Narrow Energy Bands. *Proc. R. Soc. London A*, 276:238–257, November 1963.

[103] G. Vidal. Efficient classical simulation of slightly entangled quantum computations. *Phys. Rev. Lett.*, 91(14):147902, 2003.

[104] U. Schollwöck. The density-matrix renormalization group in the age of matrix product states. *Ann. Phys.*, 326(1):96 – 192, 2011.

[105] J. Kajala, F. Massel, and P. Törmä. Expansion dynamics in the one-dimensional Fermi-Hubbard model. *Phys. Rev. Lett.*, 106:206401, 2011.

[106] F. Massel, A. Kantian, A. J. Daley, T. Giamarchi, and P. Törmä. Dynamics of an impurity in a one-dimensional lattice. *New J. Phys.*, 15(4):045018, 2013.

[107] A.-M. Visuri, D.-H. Kim, J. J. Kinnunen, F. Massel, and P. Törmä. Moving perturbation in a one-dimensional Fermi gas. *Phys. Rev. A*, 90:051603, Nov 2014.

[108] A. N. Wenz, G. Zürn, S. Murmann, I. Brouzos, T. Lompe, and S. Jochim. From few to many: Observing the formation of a Fermi sea one atom at a time. *Science*, 342(6157):457–460, 2013.

[109] G. E. Astrakharchik and I. Brouzos. Trapped one-dimensional ideal Fermi gas with a single impurity. *Phys. Rev. A*, 88:021602, 2013.

[110] H. P. Büchler. Microscopic derivation of Hubbard parameters for cold atomic gases. *Phys. Rev. Lett.*, 104:090402, 2010.

[111] G. Modugno. Anderson localization in Bose–Einstein condensates. *Rep. Prog. Phys.*, 73(10):102401, 2010.

[112] B. Shapiro. Cold atoms in the presence of disorder. *J. Phys. A: Math. Th.*, 45(14):143001, 2012.

[113] S. Fishman, Y. Krivolapov, and A. Soffer. The nonlinear Schrödinger equation with a random potential: results and puzzles. *Nonlinearity*, 25(4):R53, 2012.

[114] J. D. Bodyfelt, T. V. Laptyeva, G. Gligoric, D. O. Krimer, Ch. Skokos, and S. Flach. Wave interactions in localizing media — a coin with many faces. *Int. J. Bifurcation Chaos*, 21(08):2107–2124, 2011.

[115] U. Gavish and Y. Castin. Matter-wave localization in disordered cold atom lattices. *Phys. Rev. Lett.*, 95:020401, Jul 2005.

[116] P. Massignan and Y. Castin. Three-dimensional strong localization of matter waves by scattering from atoms in a lattice with a confinement-induced resonance. *Phys. Rev. A*, 74:013616, Jul 2006.

[117] S. Ospelkaus, C. Ospelkaus, O. Wille, M. Succo, P. Ernst, K. Sengstock, and K. Bongs. Localization of bosonic atoms by fermionic impurities in a three-dimensional optical lattice. *Phys. Rev. Lett.*, 96:180403, May 2006.

[118] F. Andraschko, T. Enss, and J. Sirker. Purification and many-body localization in cold atomic gases. *Phys. Rev. Lett.*, 113:217201, Nov 2014.

[119] A. F. Ioffe and A. R. Regel. Non-crystalline, amorphous and liquid electronic semiconductors. *Prog. Semicond.*, 4:237, 1960.

[120] F. M. Izrailev, S. Ruffo, and L. Tessieri. Classical representation of the one-dimensional Anderson model. *J. Phys. A: Math. Gen.*, 31(23):5263, 1998.

[121] D. S. Wiersma, P. Bartolini, A. Lagendijk, and R. Righini. Localization of light in a disordered medium. *Nature*, 390:671, 1997.

[122] F. Scheffold, R. Lenke, R. Tweer, and G. Maret. Localization or classical diffusion of light? *Nature*, 398:206, 1999.

[123] H. Hu, A. Strybulevych, J. H. Page, S. E. Skipetrov, and B. A. van Tiggelen. Localization of ultrasound in a three-dimensional elastic network. *Nature Phys.*, 4:945, 2008.

[124] F. M. Izrailev, A. A. Krokhin, and N. M. Makarov. Anomalous localization in low-dimensional systems with correlated disorder. *Phys. Rep.*, 512(3):125, 2012.

[125] A. Polkovnikov, K. Sengupta, A. Silva, and M. Vengalattore. Colloquium: Nonequilibrium dynamics of closed interacting quantum systems. *Rev. Mod. Phys.*, 83:863–883, 2011.

[126] M. Schlosshauer. Decoherence, the measurement problem, and interpretations of quantum mechanics. *Rev. Mod. Phys.*, 76:1267–1305, Feb 2005.

[127] W. J. Zurek. Quantum Darwinism. *Nature Phys.*, 5:181–188, 2009.

[128] T. Kinoshita, T. Wenger, and D. S. Weiss. A quantum Newton's cradle. *Nature*, 440:900, 2006.

[129] U. Schneider, L. Hackermüller, J. P. Ronzheimer, S. Will, S. Braun, T. Best, I. Bloch, E. Demler, S. Mandt, D. Rasch, and A. Rosch. Fermionic transport and out-of-equilibrium dynamics in a homogeneous Hubbard model with ultracold atoms. *Nature Phys.*, 8:213, 2012.

[130] M. Gring, M. Kuhnert, T. Langen, T. Kitagawa, B. Rauer, M. Schreitl, I. Mazets, D. Adu Smith, E. Demler, and J. Schmiedmayer. Relaxation and prethermalization in an isolated quantum system. *Science*, 337(6100):1318–1322, 2012.

[131] L. D. Contreras-Pulido, M. Bruderer, S. F. Huelga, and M. B. Plenio. Dephasing-assisted transport in linear triple quantum dots. *New J. Phys.*, 16(11):113061, 2014.

[132] S. Peotta, C.-C. Chien, and M. Di Ventra. Phase-induced transport in atomic gases: From superfluid to Mott insulator. *Phys. Rev. A*, 90:053615, Nov 2014.

[133] M. Rigol, V. Dunjko, and M. Olshanii. Thermalization and its mechanism for generic isolated quantum systems. *Nature*, 452:854, 2008.

[134] J.-S. Caux and F. H. L. Essler. Time evolution of local observables after quenching to an integrable model. *Phys. Rev. Lett.*, 110:257203, 2013.

[135] G. Mussardo. Infinite-time average of local fields in an integrable quantum field theory after a quantum quench. *Phys. Rev. Lett.*, 111:100401, 2013.

[136] M. Srednicki. Chaos and quantum thermalization. *Phys. Rev. E*, 50:888–901, 1994.

[137] J. M. Deutsch. Quantum statistical mechanics in a closed system. *Phys. Rev. A*, 43:2046–2049, 1991.

[138] Y.-Q. Li and J.-H. Dai. $\delta$-function spin-1/2 fermions in a one-dimensional potential well. *Phys. Rev. A*, 53:3743–3748, 1996.

[139] N. Oelkers, M. T. Batchelor, M. Bortz, and X.-W. Guan. Bethe ansatz study of one-dimensional Bose and Fermi gases with periodic and hard wall boundary conditions. *J Phys. A: Math. Gen.*, 39(5):1073, 2006.

[140] M. Valiente. Lattice two-body problem with arbitrary finite-range interactions. *Phys. Rev. A*, 81:042102, 2010.

[141] J. Y. Lee, X. W. Guan, A. del Campo, and M. T. Batchelor. Asymptotic Bethe-ansatz solution for one-dimensional SU(2) spinor bosons with finite-range Gaussian interactions. *Phys. Rev. A*, 85:013629, 2012.

[142] A. U. J. Lode, K. Sakmann, O. E. Alon, L. S. Cederbaum, and A. I. Streltsov. Numerically exact quantum dynamics of bosons with time-dependent interactions of harmonic type. *Phys. Rev. A*, 86:063606, 2012.

[143] M. Hohenadler, S. Wessel, M. Daghofer, and F. F. Assaad. Interaction-range effects for fermions in one dimension. *Phys. Rev. B*, 85:195115, 2012.

[144] D. L. Shepelyansky. Coherent propagation of two interacting particles in a random potential. *Phys. Rev. Lett.*, 73:2607–2610, 1994.

[145] D.O. Krimer, R. Khomeriki, and S. Flach. Two interacting particles in a random potential. *JETP Lett.*, 94(5):406–412, 2011.

[146] I. M. Lifshits, S. A. Gredeskui, and L. A. Pastur. *Introduction to the Theory of Disordered Systems*. Wiley, New York, 1988.

[147] M. Moratti and M. Modugno. Localization of a non interacting quantum wave packet in one-dimensional disordered potentials. *Eur. Phys. J. D*, 66(5):138, 2012.

[148] E. Lucioni, B. Deissler, L. Tanzi, G. Roati, M. Zaccanti, M. Modugno, M. Larcher, F. Dalfovo, M. Inguscio, and G. Modugno. Observation of subdiffusion in a disordered interacting system. *Phys. Rev. Lett.*, 106:230403, 2011.

[149] S. Flach, D. O. Krimer, and Ch. Skokos. Universal spreading of wave packets in disordered nonlinear systems. *Phys. Rev. Lett.*, 102:024101, 2009.

[150] M. Larcher, F. Dalfovo, and M. Modugno. Effects of interaction on the diffusion of atomic matter waves in one-dimensional quasiperiodic potentials. *Phys. Rev. A*, 80:053606, 2009.

[151] M. Larcher, T. V. Laptyeva, J. D. Bodyfelt, F. Dalfovo, M. Modugno, and S. Flach. Subdiffusion of nonlinear waves in quasiperiodic potentials. *New J. Phys.*, 14(10):103036, 2012.

[152] Ch. Skokos, I. Gkolias, and S. Flach. Nonequilibrium chaos of disordered nonlinear waves. *Phys. Rev. Lett.*, 111:064101, 2013.

[153] D.M. Basko, I.L. Aleiner, and B.L. Altshuler. Metal–insulator transition in a weakly interacting many-electron system with localized single-particle states. *Ann. Phys.*, 321(5):1126 – 1205, 2006.

[154] C. Gogolin, M. P. Müller, and J. Eisert. Absence of thermalization in nonintegrable systems. *Phys. Rev. Lett.*, 106:040401, 2011.

[155] M. Serbyn, Z. Papić, and D. A. Abanin. Local conservation laws and the structure of the many-body localized states. *Phys. Rev. Lett.*, 111:127201, 2013.

[156] V. A. Yurovsky and M. Olshanii. Memory of the initial conditions in an incompletely chaotic quantum system: Universal predictions with application to cold atoms. *Phys. Rev. Lett.*, 106:025303, 2011.

[157] S. Nascimbène, N. Navon, K. J. Jiang, F. Chevy, and C. Salomon. Exploring the thermodynamics of a universal Fermi gas. *Nature*, 463:1057, 2010.

[158] S. Nascimbène, N. Navon, S. Pilati, F. Chevy, S. Giorgini, A. Georges, and C. Salomon. Fermi-liquid behavior of the normal phase of a strongly interacting gas of cold atoms. *Phys. Rev. Lett.*, 106:215303, May 2011.

[159] M. Randeria and E. Taylor. Crossover from Bardeen-Cooper-Schrieffer to Bose-Einstein Condensation and the Unitary Fermi Gas. *Annu. Rev. Condens. Matter Phys.*, 5(1):209–232, 2014.

[160] J. E. Thomas. Unitary Fermi gases. In K. Levin, A. L. Fetter, and D. M. Stamper-Kurn, editors, *Ultracold Bosonic and Fermionic Gases*, volume 5 of *Contemporary Concepts of Condensed Matter Science*, pages 157 – 175. Elsevier, 2012.

[161] J. M. Luttinger and J. C. Ward. Ground-State Energy of a Many-Fermion System. II. *Phys. Rev.*, 118:1417–1427, June 1960.

[162] J. M. Luttinger. Fermi surface and some simple equilibrium properties of a system of interacting fermions. *Phys. Rev.*, 119:1153–1163, August 1960.

[163] J. P. Gaebler, J. T. Stewart, T. E. Drake, D. S. Jin, A. Perali, P. Pieri, and G. C. Strinati. Observation of pseudogap behaviour in a strongly interacting Fermi gas. *Nat. Phys.*, 6:569, 2010.

[164] A. Sommer, M. Ku, G. Roati, and M. W. Zwierlein. Universal spin transport in a strongly interacting Fermi gas. *Nature*, 472:201–204, 2011.

[165] G. Wlazłowski, P. Magierski, J. Drut, A. Bulgac, and K. Roche. Cooper pairing above the critical temperature in a unitary Fermi gas. *Phys. Rev. Lett.*, 110:090401, Feb 2013.

[166] Y. Sagi, T. E. Drake, R. Paudel, R. Chapurin, and D. S. Jin. Breakdown of the Fermi liquid description for strongly interacting fermions. *Phys. Rev. Lett.*, 114:075301, Feb 2015.

[167] S. B. Papp, J. M. Pino, R. J. Wild, S. Ronen, C. E. Wieman, D. S. Jin, and E. A. Cornell. Bragg spectroscopy of a strongly interacting $^{85}Rb$ Bose-Einstein condensate. *Phys. Rev. Lett.*, 101(13):135301, 2008.

[168] J. J. Kinnunen and M. J. Holland. Bragg spectroscopy of a strongly interacting Bose-Einstein condensate. *New J. Phys.*, 11:013030, 2009.

[169] M. J. Leskinen, J. Kajala, and J. J. Kinnunen. Resonant scattering effect in spectroscopies of interacting atomic gases. *New J. Phys.*, 12:083041, 2010.

[170] Q. Chen, Y. He, C.-C. Chien, and K. Levin. Theory of radio frequency spectroscopy experiments in ultracold Fermi gases and their relation to photoemission in the cuprates. *Rep. Prog. Phys.*, 72(12):122501, 2009.

[171] K. A. Brueckner and C. A. Levinson. Approximate reduction of the many-body problem for strongly interacting particles to a problem of self-consistent fields. *Phys. Rev.*, 97:1344–1352, 1955.

[172] J. Goldstone. Derivation of the Brueckner many-body theory. *Proc. R. Soc. A.*, 239(1217):267–279, 1957.

[173] M. Schreiber, S. S. Hodgman, P. Bordia, H. P. Lüschen, M. H. Fischer, R. Vosk, E. Altman, U. Schneider, and I. Bloch. Observation of many-body localization of interacting fermions in a quasi-random optical lattice. *e-print at arXiv:1501.05661*.

# Errata

### Publication I

Corrected a misprint in the title of the supplementary material.

### Publication III

Figures 3 and 4 should be reversed. The caption of Figure 3 applies to the image in Figure 4 and vice versa.

Aalto-DD 72/2015

ISBN 978-952-60-6215-0 (printed)
ISBN 978-952-60-6216-7 (pdf)
ISSN-L 1799-4934
ISSN 1799-4934 (printed)
ISSN 1799-4942 (pdf)

**Aalto University**
**School of Science**
**Department of Applied Physics**
**www.aalto.fi**

**BUSINESS + ECONOMY**

**ART + DESIGN + ARCHITECTURE**

**SCIENCE + TECHNOLOGY**

**CROSSOVER**

**DOCTORAL DISSERTATIONS**